Developmental Divergence of Tendon

A Comparison of the Fetal Development of Functionally Distinct Tendons

by

Theodore J.R. Lownie

A Thesis Submitted to
Saint Mary's University, Halifax, Nova Scotia
in Partial Fulfillment of the Requirements for
the Degree of Master of Science in Applied Science

August, 2024, Halifax, Nova Scotia, Canada

Approved: Dr. Samuel Veres [Supervisor]

Professor, Division of Engineering, Saint Mary's University
Adjunct Professor, School of Biomedical Engineering, Dalhousie University

Approved: Dr. Tamara Franz-Odendaal [Committee Member]

Professor, Department of Biology, Mount Saint Vincent University
NSERC Atlantic Chair for Women in Science and Engineering

Approved: Dr. Laurent Kreplak [Committee Member]

Professor, Department of Physics & Atmospheric Science
School of Biomedical Engineering, Dalhousie University

Approved: Dr. Sarah Wells [Committee Member]

Associate Professor, Department of Physics & Atmospheric Science
School of Biomedical Engineering, Dalhousie University
Assistant Dean, Medical Sciences, Dalhousie University

Approved: Dr. Danielle Tokarz [External Examiner]

Associate Professor, Department of Chemistry, Saint Mary's University
Adjunct Professor, School of Biomedical Engineering, Dalhousie University

Date: August 30, 2024

For Stephen & Penelope

Abstract

Developmental Divergence of Tendon

A Comparison of the Fetal Development of Functionally Distinct Tendons

Abstract: Tendinopathies cause some of the most prevalent disabilities in Canada, giving rise to both widespread suffering and socioeconomic stress. Effective treatments remain elusive, and the incidence of tendinopathy is increasing. In recent years, the implantation of artificial tendon has emerged as a possible method for restoring tendon function. However, attempts at developing implants that mimic tendon properties have been hindered by insufficient knowledge of tendon development. To improve collective understanding, the present research investigated the fetal development of two functionally distinct tendons with characteristics that, in maturity, are fine tuned for the distinct mechanical roles each class of tendon experiences in life: the bovine energy storing superficial digital flexor tendon and positional common digital extensor tendon. Functional intermolecular cross–linking and morphology were evaluated via hydrothermal isometric tension testing, transmission electron microscopy, and polarized light microscopy. Structural idiosyncrasies identified between the two functionally distinct tendons during gestation, across all three methods of analysis, suggested the combined effect of differences in other early developmental cues — rather than mechanoregulation — to be the principal catalyst for the initial divergence of multiple tendon–specific characteristics. This finding points to prenatal tendon development as a rich area for future study of the control mechanisms responsible for the structure of collagenous tissues.

August 30, 2024

Acknowledgements

Foremost thanks go to the supervisor of this work, Dr. Samuel Veres, for his academic and personal support. Thanks too to other members of the Biomedical Structure–Function Labs — Amanda Lee, Austin MacDonald, and Kelsey Gsell — for your assistance with this research. Thanks to the members of the supervisory council associated with this thesis — Dr. Tamara Franz-Odendaal, Dr. Laurent Kreplak, and Dr. Sarah Wells — for your direction and insightful comments. And thanks to members of the Bone Development Lab at Mount Saint Vincent University — Juan David Carvajal, Aveeva Herold and Paige Drake — for your assistance with RT-qPCR molecular biology analysis, along with Meghan Martin, Mr. Darren Cole, Ms. Mary Ann Trevors, and Justin D'Entremont for your various contributions.

The funding for this project was provided through a grant awarded to Dr. Samuel Veres by the Natural Sciences and Engineering Research Council of Canada ('NSERC'). Theodore Lownie extends thanks to NSERC, the Province of Nova Scotia, and Research Nova Scotia for additional financial support.

Developmental Divergence of Tendon

A Comparison of the Fetal Development of Functionally Distinct Tendons

by

Theodore Lownie

A Thesis Submitted to
Saint Mary's University, Halifax, Nova Scotia
in Partial Fulfillment of the Requirements for
the Degree of Master of Science in Applied Science
Department of Applied Science

August, 2024, Halifax, Nova Scotia, Canada

Approved: _____
Dr. Samuel Veres

Approved: _____
Dr. Tamara Franz-Odendaal

Approved: _____
Dr. Laurent Kreplak

Approved: _____
Dr. Sarah Wells

Approved: _____
Dr. Danielle Tokarz

Date: August 30, 2024

Table of Contents

Table 1: List of Abbreviations

Abbreviation	Definition
Achilles tendon	calcaneal tendon
ANCOVA	analysis of covariance test
Beta Glucuronidase	GUSB
Black 6 mice	C57BL/6 mice
bovine	cattle; *Bos taurus*
C—	carboxyl terminus
CFC	collagen fibril crimp
CFD	collagen fibril diameter
chick	*Gallus gallus domesticus*
class I SLRPs	decorin, biglycan
class II SLRPs	fibromodulin, lumican
clavicle	stylopod
cm	centimeters
COL3	type III collagen
COMP	cartilage oligomeric matrix protein
cows	female cattle; *Bos taurus*
°C	degrees Celsius
digits	autopodium
equine	horse; *Equus caballus*
esSDFT	the energy storing, superficial digital flexor tendon
ESTs	energy storing tendons
Fiji	'Fiji Is Just ImageJ'
foals	horses; *Equus caballus*, of less than one year of age
forelimb	zeugopodium
FDTs	functionally distinct tendons
fwd	forward
GDs	gestational days
Gly	glycine
GPCRs	G protein-coupled-receptors
g	gram
HHL	histidino–hydroxylysino–norleucine
HIT testing	hydrothermal isometric tension testing
Hyl	hydroxylysine
Hyl–Pyr	hydroxylysyl–pyridinoline
Hz	hertz
in vitro	Latin for"in glass"
in vivo	Latin for "within the living"
KS	Kolmogorov–Smirov
L	liter
LH	lysyl hydroxylase

Continued on next page ...

Table 1 – ... continued from previous page

Abbreviation	Definition
LOX	lysyl oxidase
Lyr-Pyr	lysyl–pyridinoline
Lys	lysine
mice	*Mus musculus*
mL	milliliter
mm	millimeter
MPa	megapascals
N—	amino
N.B.	*nota bene*; Latin for "mark well"
$NaBH_4$	sodium borohydride
nm	nanometer
OPD	optical path difference
perinatal	pertaining to the period immediately before and after birth
PLM	polarized light microscopy
pCDET	the positional, common digital extensor tendon
PTs	positional tendons
rat	*Rattus norvegicus*
rev	reverse
RI	refractive index
RT–qPCR	two–step reverse transcription real time quantitative polymerase chain reaction
Scx	scleraxis
SD	standard deviation
SLRPs	small leucine–rich proteoglycans
super–healer mice	Murphy Roths large mice
'*survived*' (*in HIT testing*)	a tendon section that failed to exhibit a decrease in generated force prior to 90°C
t (*in PLM*)	thickness of a material
$t_{1/2}$	half–time of load decay
TBP	TATA Binding Protein
T_d	denaturation temperature
TEM	transmission electron microscopy
tendinocytes	cytoplasmic processes of tenocytes
tendon cells	fibroblasts, tenoblasts, tenocytes
T_{Fmax}	temperature of maximum force generation
TGF–β1	transforming growth factor beta 1
TGF–β2	transforming growth factor beta 2
TGF–β3	transforming growth factor beta 3
thermally labile cross–links	divalent aldimine cross-links
thermally stable cross–links	divalent ketoamine, or trivalent cross-links
Tsp–3, –4 and –5	thrombospondin proteins –3, –4 and –5

Continued on next page ...

Table 1 – ... continued from previous page

Abbreviation	Definition
TRP	transient receptor potential
type XII collagen	type 12 collagen
type XIV collagen	type 14 collagen
USD	United States Dollars
VEGF	vascular endothelial growth factor
α	alpha
μm	micrometer

List of Figures

1 Essential Base Knowledge

1.1 Tendon

Tendons are dense, regular connective tissues[272,272] that connect muscle to bone.[17] The high tensile strength[15] and stiffness[19] of tendons allow for effective transmission of muscular force to bones or joints[17,272,282] and in doing so permit body movement.[27] Tendons are ubiquitous throughout the human body,[272] existing on the order of thousands.[245]

1.2 The Hierarchical Structure of Tendon

Tendons are hierarchically structured over six predominant levels.[46,218] At the macroscale, a connective tissue sheath — the 'epitenon' — encloses the whole tendon.[46,295] The tier immediately beneath that of the whole tendon belongs to the collagenous fascicles[46] (*50 to 500 micrometers ('µm') in diameter*[295]) separated from one another by a markedly less dense interfascicular matrix (*see: Figure 1*)[9,71,295] that houses accessory collagenous[31] and non–collagenous[295] proteins. A single fascicle is then comprised of multiple collagenous fibers (*10 to 50 µm diameter*) which each consist of several collagen fibrils[19,111] (*20 to 500 nanometers ('nm') diameter*[218,295]) that in turn assemble from sub or microfibrils (*2 to 10 nm diameter; Figure 1*).[46,150,218] Below the hierarchical tier of the microfibrils lies only the fundamental building block of tendon: the type I collagen molecule (*∼1 nm diameter; Figure 1*).[150,230]

1.3 The Collagen Molecule

The remarkable adaptability of tendons arises from their comprising type I collagen molecules.[63] Type I collagen molecules are approximately ∼1000 amino acid residues[91,225,265] or three hundred nanometers[41,78] in length and consist of two identical alpha–1 ('*α1*') and a third chemically

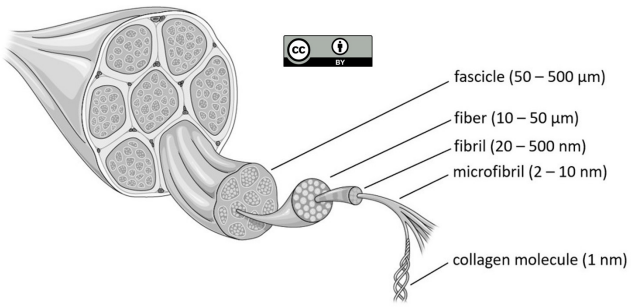

Figure 1: An illustration of the structural hierarchy of tendon from the whole tendon (*as is illustrated left most*) to the level of the type I collagen molecule (*right most*). Bracketed values signify relative structure diameters. This image was adapted from Citeroni et al. (2020) as is indicated by the Creative Commons Attribution 4.0 International License ('*CC BY 4.0*') symbol.[44] For more comprehensive copyright details regarding the adapted diagram, *see:* Appendix Section 8.4.

distinct alpha–2 ('*α2*') left handed polypeptide chains that combine together via intramolecular hydrogen bonding[111,176,224] to form the signature right handed triple helix of collagen (*see:* Figure 2).[41] The amino acids comprising each of the polypeptide *α*–chains are similarly recognizable: with the amino acid 'glycine' ('*Gly*') most typically set at every third residue and the imino acids 'proline' and 'hydroxyproline' otherwise predominating[176,265].†[41,224] Glycine — as one of the smallest amino acids due to its hydrogen side chain in place of a larger, organic one[106,160] — is nestled toward the interior of the triple helix.[176,224] This allows for tight packing of the trio of *α*–chains which ultimately enhances molecular stability.[176,224] The presence of the imino acids positioned to the exterior of the helix boost stability further: with the pyrrolidine loops of both imino acids limiting molecular flexibility,[185,225] and the highly electronegative oxygen atom of hydroxyproline stabilizing collagen via a stereoelectronic effect.[167,168,224]

Beyond the extremities of the core triple helix of type I collagen molecules and immediately previous to amino ('*N*–') and carboxyl ('*C*–') termini[6,91] lie non–helical telopeptide regions that

†*this configuration results in a repeating amino–acid–sequence of Gly–X–Y where the 'X' and 'Y' positions are often occupied by rotations of proline and hydroxyproline, respectively (Figure 2)*

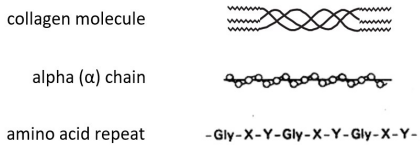

Figure 2: A representation of the structure of the type I collagen molecule (***i***) triple helix (*centered*) and (***ii***) terminal telopeptide regions (*represented at the ends*). Glycine is denoted as '*Gly*' with the subsequent amino–acid–positions (*denoted as:* 'X' *and* 'Y') most typically being occupied by proline and hydroxyproline, respectively.

are approximately ∼9 to 25 amino–acid–residues in length (*see: Figure 2*).[6,265] These regions are rich in both 'lysine' ('*Lys*') and 'hydroxylysine' ('*Hyl*') amino acids,[106] which play a critical role in mediating collagen fibrillogenesis.[265] Only in these telopeptide regions can the key cross–linking enzymes of collagen molecules, lysyl oxidases ('*LOX*', *hereafter*),[6,62,71] oxidatively deaminate (*or: 'remove an amino group from'*) resident Lys or Hyl residues (*see: Step 1 of Figure 3*) and lay the foundation for the formation of the chemical features that conjoin adjacent collagen molecules and drastically enhance the mechanical strength of tendon: enzymatic intermolecular cross–links.[62,71,230]

1.4 The Intermolecular Cross–Links of Tendon

Intermolecular cross–links between type I collagen molecules ('*intermolecular cross–links*', *hereafter*) form when telopeptide 'Lys' or 'Hyl' aldehydes that result from LOX–mediated oxidative deamination interact with the triple helix of an adjacent collagen molecule quarter–staggered in relation to the first (*see: Step 2 of Figure 3*).[6,60,71,230] In particular, formation of a Schiff base intermolecular cross–link occurs when the double–bonded oxygen atom of a telopeptide aldehyde reacts with a primary ε–amino group of a Lys or Hyl from a highly conserved 'Lys/Hyl–Gly–histidine–arginine' sequence of the triple helix (*Figure 3*).[6,109,286] During this process, variation in the identity of the amino acids supplying both: (***i***) the participating aldehyde, arising from

hydroxylation by the lysyl hydroxylase (‘*LH*’) family of enzymes) and (***ii***) ε–amino group[6] — alongside added distinctions arising from tissue maturity[60,234] — give rise to several unique species of intermolecular cross–links.[6,62]

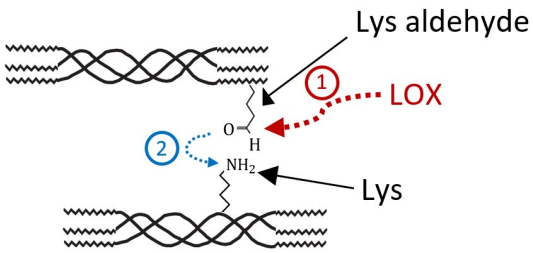

Figure 3: An illustration detailing the creation of an ‘*immature*’ (*or: ‘divalent’*) enzymatic intermolecular cross–link between two type I collagen molecules within tendon. In Step 1 (*as is illustrated in: red*), a lysyl oxidase (‘*LOX*’) enzyme converts a telopeptide lysine residue (‘*Lys*’) to a Lys–derived aldehyde. In Step 2 (*illustrated in blue*), the double bonded oxygen atom of the Lys–derived aldehyde reacts with a primary ε–amino group of a Lys resident in the triple–helical region of an adjacent molecule to form a divalent Schiff base intermolecular cross–link. Substitution of either Lys residue with a hydroxylysine residue (‘*Hyl*’) gives rise to variation in cross–link speciation.

There are eight predominant species of intermolecular cross–links in tendon.[6] These cross–links are most frequently categorized as belonging to two ‘immature’ classes, the (**i**) aldimines and (**ii**) ketoamines, and a third, more mature class (*see: Figure 4*).[6,62,286] Immature aldimine and ketoamine intermolecular cross–links are divalent in nature (*in connecting two collagen molecules*) where species of the mature class are trivalent (*in connecting three; Figure 4*).[62,286]

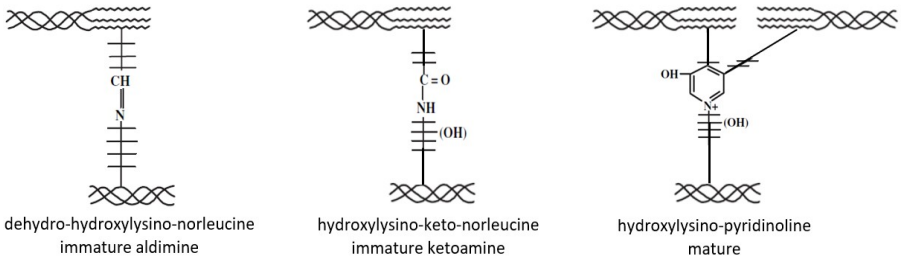

Figure 4: Depictions of representative inter-collagen cross–links from each of the three major cross–link classes: with the divalent inter-collagen cross–links: (***i***) '*dehydro–hydroxylysino–norleucine*' and (***ii***) '*hydroxylysino–keto–norleucine*' representing '*divalent*' aldimine and ketoamine cross–links, respectively, and the trivalent intermolecular cross–link: (***iii***) '*hydroxylysino–pyridinoline*' representing the '*mature*' class of cross–links. These images of intermolecular cross–links were adapted from *Collagen: Structure and Mechanics (2008)*.[6] For more comprehensive copyright details regarding the adapted diagrams, *see:* Appendix Section 8.4.

Divalent aldimine intermolecular cross–links result when a Lys–derived aldehyde finds either a Lys or Hyl residue on an adjacent triple helix, forming: (***i***) dehydro–lysino–norleucine or (***ii***) dehydro–hydroxylysino–norleucine, respectively (*see: Figure 5*).[6,62,166] Both divalent aldimine intermolecular cross–links are relatively unstable and labile to thermal degradation.[6,104] In contrast, comparatively heat stable[6,104] divalent ketoamine intermolecular cross–links[‡] emerge when an Hyl–derived aldehyde forms an intermolecular cross–link with a Lys or Hyl residue of an adjacent helix, forming: (***iii***) lysino–keto–norleucine or (***iv***) hydroxylysino–keto–norleucine, respectively (*Figure 5*).[62,166] From these divalent intermolecular cross–links derive four species of thermally–stable mature intermolecular cross–links: (***v***) histidino–hydroxylysino–norleucine (*or:* '*HHL*'), (***vi***) hydroxylysyl–pyridinoline ('*Hyl–Pyr*'), (***vii***) lysyl–pyridinoline ('*Lyr–Pyr*'), and (***viii***) lysine pyrrole — with HHL hypothesized to result from the reaction of a dehydro–hydroxylysino–norleucine and a histidine,[127,285] Hyl–Pyr from a hydroxylysino–keto–norleucine and a Hyl–derived

[‡] *divalent ketoamine cross–links are stabilized by the presence of a local amide*[5]

aldehyde,[6,62,66,127] Lys–Pyr from lysino–keto–norleucine and a Lys–derived aldehyde,[62,127] and lysine pyrrole from a hydroxylysino–keto–norleucine and a Lys–derived aldehyde (*Figure 5*).[6,134] The relative presence of each of the three classes of intermolecular cross–links is both time and tissue–dependent: with tendons accumulating a greater proportion of 'mature' intermolecular cross–links with age[6,47,62] and more repeatedly used tendons possessing greater amounts of divalent ketoamine and trivalent intermolecular cross–links.[17,104,125,242,252]

Intermolecular cross–links significantly reduce the entropy of collagen molecules by limiting their configurational freedom and drawing them closer together, displacing the water molecules that exist between them.[1,114,169] This effect is explained by the 'polymer-in-a-box' mechanism, where each collagen molecule (*the 'polymer'*) is confined by neighboring molecules (*the 'box'*).[2,170,274] The reduction in entropy decreases the overall reactivity of collagen within a tissue, as more energy is required to reach the activation threshold for reactions when molecules are tightly packed and constrained.[1] For example, in humans, the denaturation temperature of isolated collagen in solution, which is around 37°C, can increase by up to 27°C when the collagen is organized into fibers.[168] Therefore, the thermodynamic properties of a tissue can be indicative of its level of collagen cross–linking and interconnectivity.[104,114,274]

1.5 The Protein Composition of Tendon

The type I collagen molecules discussed hitherto comprise only approximately ∼60–80 percent[244,257] of the tendon proteome. The remaining ∼20–40% of the tendon proteome is predominantly made up of other collagens — and especially collagens III (*at: ∼0–10%*)[244,257] and IV (*at: ∼2%*)[244] — alongside other non–collagenous proteins.[257] Some major non-collagenous matrix proteins include: cartilage oligomeric matrix protein ('*COMP*'; *at: ∼3%*),[244] and elastin (*∼1–2%*),[43,257] alongside various proteoglycans (*∼1–5%*).[244] Variation in the extent to which

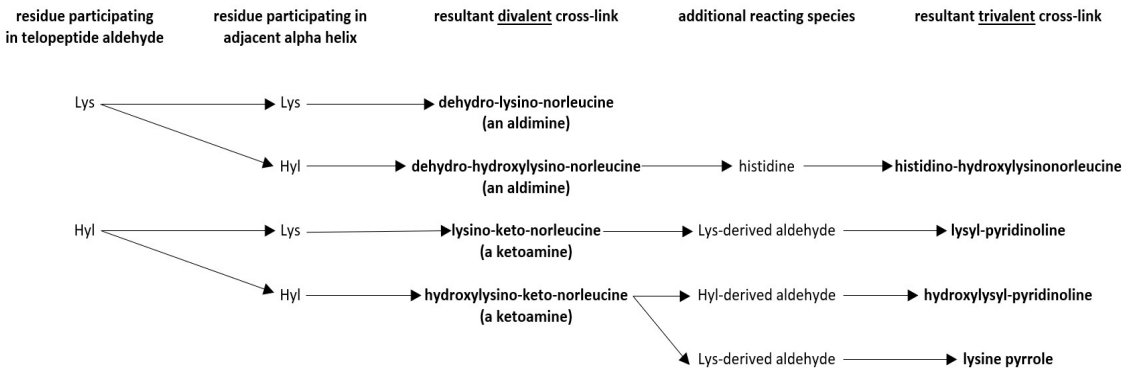

Figure 5: An illustration depicting the reacting species involved in the creation of the eight predominant intermolecular cross–links found in tendon. The amino acid lysine is abbreviated to '*Lys*' and the amino acid hydroxylysine to '*Hyl*'.

accessory proteins such as these are incorporated in different tendons can give rise to substantial inter–tendon diversity in mechanical properties.[89,184]

1.6 The Diversity of Tendons

Tendon diversity both between[26,87,101,200] and within[175,186,250] bodily regions are of benefit to elucidating the functional consequences of various forms of developmental stimuli.[179] Between regions, while cranial tendons derive from ectodermal neural crest cells, axial tendons instead arise from a somitic compartment, and limb tendons from lateral plate mesoderm.[87,101,254] These separate embryological origins could suggest the development of different tendons to be uniquely regulated[26,28,200] in alignment with the distinct mechanical responsibilities of select tendons in tissue maturity. Within limbs, two functionally distinct classes of tendons are recognized: (***i***) those that function under low load, and are primarily responsible for the precise positioning of limbs or digits (*which will collectively be referred to as positional tendons; 'PTs', hereafter*)[104,204,290] and (***ii***) those select few[188] that have the added role of repeatedly storing and releasing energy under high load to reduce the energetic cost of locomotion (*as energy storing tendons; 'ESTs'*).[43,203,250]

In humans, the former are often embodied by the positional anterior tibial,[123] and the latter by the anatomically proximate energy storing Achilles.[182,186] This contrast exists across mammalian quadrupeds,[186,231] allowing tendon diversity to be studied in animal proxies.[89,248,261]

1.7 The Physical Properties of Tendon

Tendons are often characterized by their relative: (***i***) stiffness[198] and (***ii***) strength.[13] The 'stiffness' of a tendon is the force resistance to applied extension, and is often used synonymously with modulus, the slope of the stress–strain response during elongation.[30,82] Here, 'elasticity' refers to a tendon's ability to revert from deformation to its original configuration once the applied force is removed.[30,82] In contrast, tendon 'strength' instead describes the maximum stress a tendon can accommodate before rupture.[82] In this way, both stiffness and strength are crucial to tendon functionality[82] and, resultantly, significant effort has been made to establish a correlation between the composition of a given tendon and its relative stiffness and strength (*for example, see: Birch 2007*). This work has so far largely shown PTs to be both stiffer[19,208,225,253] and stronger[184,187,232,263] than ESTs.

1.8 Bovine Energy Storing Tendons and Positional Tendons

A commonly studied EST–PT pairing is the energy storing superficial digital flexor tendon ('*esSDFT*', *hereafter*) and positional common digital extensor tendon ('*pCDET*'), found in the forelimbs of large quadrupeds such as bovines (*or: cattle*; *Bos taurus*) and equines (*or: horses; Equus caballus*). The esSDFT is located in the posterior half of the forelimb and connects the superficial digital flexor muscle at the approximate level of the carpus (*equivalent to the wrist in humans*) to the proximal phalanx (*P1*) and the lateral and medial eminences of the middle phalanx (*P2*) of the digits, enabling flexion of the digits (*think of it as 'the quadruped Achilles tendon'; see:*

Figure 6).[32,52,53] Here, as further context, parallel to but deeper from the skin than the esSDFT lies the deep digital flexor tendon ('*DDFT*'), which extends from the deep digital flexor muscle to the distal phalanx (*P3*) of the digits, and provides additional, but more fine support for digit flexion.[32,49,53] In contrast, the pCDET lies in the anterior region of the forelimb and connects the common digital extensor muscle to the extensor process of the P3, allowing extension of the digits (*'the quadruped anterior tibial tendon'; Figure 6*).[32,52] In this region, similar to the presence of the DDFT, the pCDET is accompanied by additional digital extensor tendons, the medial ('*MDET*') and lateral ('*LDET*') digital extensor tendons, which provide the digits with additional extension capabilities.[32,49] The properties of the esSDFT and pCDET have been found to differ tremendously in tissue maturity: with several distinctions in tendon: (***i***) molecular biology,[22,89] (***ii***) structure,[17,19] and (***iii***) mechanics[184,263] arising between the fully–developed esSDFT and its pCDET counterpart.

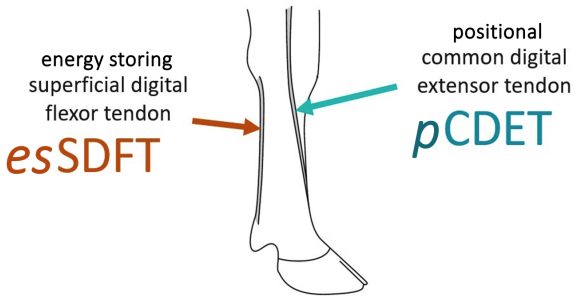

Figure 6: An illustration of the posteriorly positioned energy storing superficial digital flexor tendon ('*esSDFT*'; *shown left*) and the anteriorly positioned positional common digital extensor tendon('*pCDET*'; *right*) of the bovine (*or: cattle; Bos taurus*) forelimb. This image was adapted from Herod et al. (2016).[104] For more comprehensive copyright details regarding the figure, *see:* Appendix Section 8.4.

In bovine locomotion, the esSDFT and pCDET deploy their respective functions in digit flexion and extension.[99,179,258,277] First, the esSDFT helps lift the hoof off the ground by flexing the digits toward the posterior face of the forelimb, after which the esSDFT continues to maintain the digits in this bent position as the leg swings forward.[99,250] Thereafter, as the hoof descends back toward the ground, the pCDET extends the digits of the hoof toward the anterior face of the forelimb, returning the foot to a parallel position with the ground and straightening the digits to

support weight effectively.[258,277] During this landing process, the esSDFT stretches and, as its name implies, absorbs energy like a spring as the pCDET extends and the hoof makes contact with the ground.[179,250] This stored energy is then used to help propel the limb forward when the hoof is next lifted.[99,179,250]

1.9 The Developmental Divergence of Tendon

The energy storing nature of the esSDFT is reflected in multiple measures of its *in vivo* mechanical loading conditions and behaviour, including: its comparatively high (***i***) stress level under physiological load,[126] (***ii***) strain experienced during normal function,[22,236,253] and (***iii***) predisposition to injury, relative to the pCDET.[43,128,188,289] First, the ordinary stress experienced by the bovine esSDFT has been estimated to be approximately seven times greater (*at: ∼70 megapascals*; '*MPa*') than that experienced by the pCDET (*at: ∼10 MPa*).[126] This is mirrored by the relative strains experienced by the two tendons:[253] in equines, strains of up to 16% have been recorded in the esSDFT[29,236,253] whereas the maximum strain of the pCDET has been estimated at only approximately ∼2.5%.[22,253] Finally, the higher stress and strain experienced by the esSDFT relative to the pCDET have been found to culminate in a greater incidence of macroscopic failure in the EST than in the PT,[43,128,188,289] attributable exclusively to the relatively high use of the esSDFT over the pCDET rather than a higher damage susceptibility in the esSDFT.[10,89,104,253] Among other factors, these characteristics have highlighted a clear difference in the mechanical stimulation of the two functionally distinct tendons ('*FDTs*', *hereafter*) *in vivo*;[43,126,253] prompting many to ponder just how imperative the role of mechanical influence is in shaping the unique attributes of the esSDFT and pCDET.[182,243,290] Indeed, though both: (***i***) internal regulatory mechanisms and (***ii***) environmental factors undoubtedly play a part in shaping class specific characteristics as they appear in tissue maturity,[43] which of the two serves as the primary driving

force responsible for the initial segregation of esSDFT and pCDET properties (*and those of ESTs and PTs more broadly*) during their developmental timeline remains unanswered. In essence: is the initial divergence of the intricacies of ESTs and PTs a product of each tendon's nature... or of their nurture?

1.10 The Argument for Mechanically Mediated Divergence

The properties of a tissue attributed to 'mechanoregulation' refer to those properties that result from the reaction of the tissue's cells to the physical forces present in the cell's surroundings.[182,270] In mechanoregulation, many types of cells come equipped with 'mechanosensory' features that are capable of recognizing and translating mechanical stimuli into molecular signalling pathways.[14,137] These pathways can induce a variety of cellular responses, which occur concurrently during development.[137] As development progresses, these responses may manifest as multiple interconnected changes, including (***i***) morphological alterations,[164] (***ii***) behavioural adaptations,[193] and (***iii***) modulation of gene expression (*via adjustments of epigenetic modifiers*[51] *or manipulation of transcription factors*[137]). Such mechanosensory features are widespread in the cells resident to tendon[137] (*commonly referred to as 'tenocytes', 'tenoblasts', or, more generally, as 'fibroblasts'**), and include: (***i***) 'mechanoreceptors' such as integrin complexes or G protein-coupled receptors ('*GPCRs*')[158] and also (***ii***) 'mechano-activated channels' like Piezo and transient receptor potential ('*TRP*') channels,[55] to name a few (*for more detail on mechanosensation and mechanotransduction in tendon, see: Lavagnino et al. 2015*). These 'mechanosensory features' confer tendon with remarkable adaptability in its handling of forces like tensile loading and compression.[138] This

**while 'tenocytes' are mature, elongated tendon cells with cytoplasmic processes, 'tenoblasts' are highly metabolically–active, immature precursors to tenocytes, and 'fibroblasts' are a broader cell type generally responsible for extracellular matrix synthesis in a variety of tissues in addition to tendon*[146]

adaptability is made most evident, perhaps, in consideration of those tendons that are functionally distinct from one another (*see: The Diversity of Tendons*).[175,186,250]

To address the previously mentioned adjustments with examples in the context of the FDTs under present study, with respect for morphological alterations: tenocytes have been found: (***i***) to become more elongated when subject to cyclic loading,[110] and (***ii***) to also exhibit both shortened and less highly branched cytoplasmic processes (*or: 'tendinocytes'; see:* Figure 7) upon an onset of muscle paralysis[240] — together suggesting these features to be more pronounced among the cells of (*the comparatively highly loaded*) ESTs in relation to those of their PT counterparts. Next, in consideration of cell behavioural adaptations, tenocytes have also been shown to proliferate under repeated loading[294] and, resultantly, to be more prevalent in more frequently loaded tendons like fully–developed ESTs compared to their paired PTs.[10,17,20] Lastly, regarding possible modulation of gene expression: tendon cells have also been found to upregulate their expression of elastin associated genes in response to cyclic loading[117] — culminating, presently, in a distinctly high presence of elastic fibers in fully–developed ESTs over fully–developed PTs, among other effects.[17,89] With these various mechanoregulatory mechanisms in mind, it becomes clear, then, why the mechanical stimulation of a given tendon has been so highly regarded for its evident role in modifying key tendon characteristics.[182,243,290] However, widespread marvel for the impressive versatility tendons show in accommodating their varying functional demands[138] may thus far have resulted in a preemptive conclusion[290] that any variation that should arise between the FDTs during their development is primarily a product of the distinct mechanical stimuli experienced by different tendons.

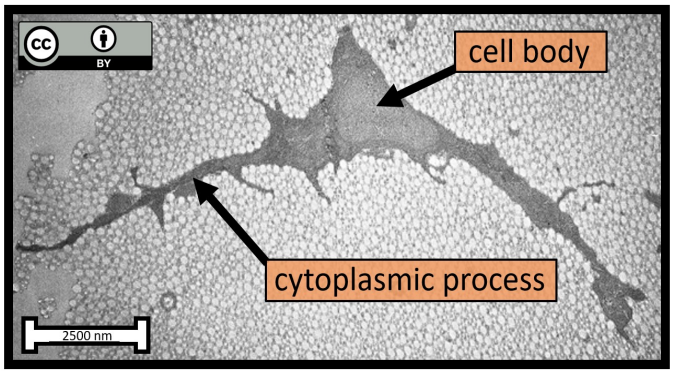

Figure 7: A transmission electron microscopy (‘*TEM*’) image of a cross section of a tendon cell (*commonly referred to as a ‘tenocyte’, ‘tenoblast’, or, more generally, a ‘fibroblast’*) from the Achilles (*or:* ‘*calcaneal*’) tendon of a rat (*Rattus norvegicus*) to depict its elongated cell body and branched cytoplasmic processes (*or:* ‘*tendinocytes*’). The tendon cell is pictured as the darker (*or: more* ‘*electron dense*’) entity in the middle of the image while the remainder of the image is largely comprised of collagen fibrils of approximately ∼75 nanometers (‘*nm*’) diameter. A scale bar approximating ∼2500 nm (*or: ∼2.5 micrometers;* ‘*µm*’) is provided. This image was adapted from Franchi et al. (2007)[78] as is indicated by the Creative Commons Attribution 3.0 International License (‘*CC BY 3.0*’) symbol. For more comprehensive copyright details regarding the adapted image, *see:* Appendix Section 8.4.

1.11 The Argument for Non–Mechanically Mediated Divergence

In contrast to the notion that the distinctions between FDTs arise principally as a result of postnatal mechanoregulation, there may alternatively be good reason to speculate that certain attributes of ESTs and PTs instead diverge as a result of differences in other early developmental factors between the two classes of FDTs.[58,92,200,231] Take, for example, a study[92] that showed tenoblasts that originated from the esSDFTs of equine fetuses to synthesize “*extremely large amounts*” of cartilage oligomeric matrix protein (‘*COMP*’, *hereafter*) upon cytokine stimulation *in vitro* in comparison to to tenoblasts instead sourced from pCDETs.[92] As further support, consider the recent finding[81] that, at two months post–operation, tendon allografts from Murphy Roths large “super–healer” mice (*Mus musculus*) outperformed autografts in treating the patellar tendon injuries of Black 6 (*or:* ‘*C57BL/6*’) mice — a result that served to highlight innate variation between tenocytes and their local environments as playing a significant role in the determination

of tendon properties under the otherwise equal conditions of: (***i***) equivalent mechanoregulation, and (***ii***) no variation in systemic and hormonal factors.[81] However, it becomes challenging to decipher whether a specific characteristic of ESTs and PTs initially becomes distinct *in vivo* due to differences in: (***i***) other early developmental factors[92] or (***ii***) mechanical stimuli.[290] Indeed, how can one truly discern which of: (***i***) disparate developmental factors or (***ii***) mechanoregulation confers an inter–tendon difference in a particular property given the mutual perpetuity and interdependent nature of these two factors throughout natural life?

Previous research has attempted to tackle this challenge using various methods.[110,120,192] For instance, certain studies have investigated the impact of modifying the mechanical stimulation of tenocytes *in vitro*.[72,92,110,294] However, even the most sophisticated of artificial emulations fall short in their attempt to capture the complexity of intracorporeal biology.[94] Alternative research approaches, such as inducing limb (***i***) hyper-mobility[120,182,264] or (***ii***) paralysis,[157,192,238] also present challenges, as artificially altering muscle activity may introduce confounding effects alongside the intended variation in mechanical stimulation. In light of this, a better approach may lie in evaluating ESTs and PTs during the brief period of their existence in which the effects of innate programming can be studied in isolation from effects stemming from mechanoregulation, *or:* the relative quiescence of gestation.[28,177,178] Specifically, though some movement of the fetus undoubtedly occurs during prenatal development,[154] the unique role for which the properties of ESTs have been proposed to be finely tuned[17,184] (*in offsetting the metabolic cost of strenuous or repetitive physical activity to a greater extent than do PTs*[43,203,250]) most certainly does not apply within the confines associated with fetal development. Accordingly, as an environment devoid of the diverse mechanical stimuli encountered by different tissues (*or*: tendons) in postnatal life[126,188,236], gestation can provide insight into how the tenocytes of the two FDTs organize their surrounding environment without the influence of varied mechanoregulation. Based on the existing

literature, the conclusion one would draw is, at the very least, that the tenocytes within the two FDTs would behave "similarly" to one another in their orchestration of tendon extracellular matrix[182,243,290].

1.12 Bovine Gestation

Bovines offer a suitable model for exploring the possibility of differences in the properties of the esSDFT and pCDET during fetal development. As large mammals, bovines possess gestational windows of comparable duration to that of humans[118] at approximately ∼283 days (*or: ∼40 weeks*).[194,196,280] Forelimb buds are first seen in the developing embryo at approximately ∼24 gestational days ('*GDs*', *hereafter*).[174] Thereafter, ossification of the forelimb begins at the fetal stage with the proximal stylopod (*or: the clavicle*) at approximately ∼41 GDs[174] and extends distally (*to the humerus*) at ∼50 GDs.[174] The bones of the zeugopodium (*or: forelimb; at ∼64 GDs*)[174] and autopodium (*digits; at*: *∼78 GDs*)[174,280] soon follow — together providing both the insertion points[32] and a substantial portion of the chemical signalling[247,291] necessary for forelimb tendon formation. Forelimbs subsequently grow from a length of 1.6 centimeters ('*cm*') at the time point of autopod ossification to over 23cm perinatally[280] during which time the esSDFT and pCDET scale proportionately.

2 The Current Investigation

2.1 Research Context

Tendinopathy is the pain and swelling associated with tendon damage.[43,206,246] In North America, tendinopathies currently afflict one in four adults and make up about half of all musculoskeletal injuries.[11,56,101] They are most prevalent among active individuals,[16] with elite athletes at fifty–six percent risk of incurring injury to their calcaneal ('*Achilles*') tendons over their careers.[43,250] The high incidence of tendinopathies may stem from a lack of effective preventative measures and treatments for tendon degeneration.[147,178,287] Presently, even the most successful medical interventions cannot fully restore the properties of damaged tendons.[202,212,287] This gap signals a need for novel treatments with the potential to improve tissue regeneration.

Tendinopathies are already a major source of socioeconomic stress[43,206,287] and the incidence of tendinopathies is increasing in developed nations with aging populations.[145,206,246,283] Tendon pathology has recently accounted for approximately seven percent of healthcare appointments[228] and culminated in annual healthcare costs estimated between $8.3 and 15.4 million U.S. Dollars ('*USD*') per one hundred thousand citizens (*as inferred from American*[206,267] *and European*[287] *data, respectively*). Worse yet, this range belies the actual cost of tendinopathies[16,283] as tendon–related disabilities have plagued workforces.[56,64] The occurrence of shoulder tendinopathy has been as high as nineteen percent in manual laborers[227] and musculoskeletal damage has accounted for up to sixty–three percent of all lost time claims.[56,281] This has increased worker's compensation payouts,[64,140] amplified unrealized economic production,[16,281] and brought additional costs associated with worker overtime, replacement, and training.[233] Because of these the full economic burden of

musculoskeletal injuries and tendinopathies remains unclear.

The implantation of artificial tendon tissue has recently emerged as a potential means of regaining tendon function after injury.[214,256,287] Though early efforts at tendon construction are promising,[3,219,259] attempts have yet to generate replacement tissue of comparable mechanical function to natural tendon. This failure might be due to a lack of understanding of native tendon development[28,144,147] as the mechanisms driving natural tendon maturation remain unclear.[26,35,87,192] Thus, novel strategies of tissue engineering may await an improved understanding of the elaboration of tendon structure, molecular biology, and mechanics during development.[28,144,177,178]

Fully–developed ESTs and PTs differ molecularly,[22,89] structurally,[17,19] and mechanically,[184,263] with each class highly specialized to meet distinct physiological demands. Together, the superior fatigue resistance of ESTs[253] and the notable strength of PTs[223] have given rise to the notion of trade–offs during tendon development.[104] In contrast to class divergence in tissue maturity, the attributes of unloaded tendons of the two functionally distinct classes in the fetal stage of development have been proposed to be similar.[43,191,243] In fact, variance in functional loading during the early postnatal development of precocial mammals has been held to be key in the regulation of the class–specific properties of their FDTs (*as in 'mechanoregulation', see: The Argument for Mechanically...*)*.[235,288,290] However, several differences in structure[231,235,290] and molecular biology[58,92,175,191,200] have been documented between developing ESTs and PTs of mammalian fetuses and, of added interest, many of these prenatal differences intuitively align with mature

precocial mammals, like the cattle under present examination (and also horses, sheep, and rabbits) differ from altricial mammals (and particularly, humans) in moving independently almost immediately following birth, which should be kept in mind in assessing the transferability of the current work to human development

class characteristics.[17,89,243] For precocial mammals, these differences might suggest the functional divergence of their FDTs to occur during fetal rather than postnatal development.[43,92,175] Critically, the partial establishment of class phenotypes by birth would imply divergence to result from differences in other early developmental cues rather than being mechanically mediated.[231] Yet, the possibility for gestational divergence of ESTs and PTs is insufficiently studied,[161] and so studies that have suggested alternative mechanisms in regulating divergence[58,92,200,231] remain contested by those that have instead cited postnatal mechanoregulation.[182,243,290]

2.2 Existing Knowledge Relevant to Research

2.2.1 Properties of FDTs Known to Be Distinct During Gestation

2.2.1.1 Inter–Tendon Disparity in Intermolecular Cross–Linking

Structural differences associated with the characteristics of the intermolecular cross–links native to each tendon class have been uncovered.[231] In particular, in tests of tendons from bovine fetuses aged between GDs 114 and 229 (*of: ∼283 GDs at full term*), the esSDFT was shown to have a greater presence of functional intermolecular cross–links than its pCDET counterpart.[231] Further, the esSDFT was also found to possess a greater presence of thermally stable (*or: 'divalent ketoamine–'; or: 'trivalent'*) intermolecular cross–links than the pCDET during fetal development.[231] These findings align with the intermolecular cross–linking characteristics of the two tendons in tissue maturity.[19,104] That is, fully–developed ESTs have previously been shown to have: (***i***) a greater total presence of inter-collagen cross–links[19,40,104] and (***ii***) a greater presence of thermally stable intermolecular cross–links[17,104] than PTs. These characteristics are well documented to alter tendon mechanics.[45,62,178,203]

A comparatively extensive intermolecular cross–link network in the esSDFT (*over the pCDET*) at the fetal stage of gestation[231] could result from: (***i***) relatively high cellularity[235,290] or (***ii***) low collagen turnover[7,22,129,252] in the EST relative to its PT counterpart during gestation. First, relatively high cellularity in a developing EST over a developing PT[235,290] during fetal development could give rise to an elevated expression of the lysyl oxidase ('*LOX*') enzymes that are necessary to initiate the formation of intermolecular cross–links in tendon.[62,67,162,251] Second, a comparatively low rate of collagen turnover in a developing EST relative to its PT counterpart[22,89,252] may allow for longer interactions between the LOX enzymes and collagen molecules in the EST[129] during gestation and thereby assist the formation of intermolecular cross–links.[2,7,129] In support of these

theories, the relatively low presence of inter-collagen cross–links found in fully–developed PTs compared to their fully–developed EST counterparts[19,40,104] has been shown to be accompanied by: (***i***) comparatively low cellularity[10,20] and (***ii***) relatively rapid collagen turnover in fully–developed PTs compared to in fully–developed ESTs.[22,89,184,252]

2.2.2 Properties of FDTs Plausibly Distinct During Gestation

2.2.2.1 The High Potential for Inter–Tendon Protein Disparity

The strongest untapped argument for divergence of the two FDT classes during fetal development may come from evidence of distinct molecular profiles prior to birth.[58,92,175,191,200] First, in tendon locales of developing chick (*Gallus gallus domesticus*) limbs, several tendon–associated proteins were found to be expressed earlier in the development of chick posterior (*energy storing*) flexor tendons versus anterior (*positional*) extensor tendons.[26,58,180,284] The earlier expression of these proteins (*including receptors,*[58] *transcription factors,*[26,180,284] *and structural proteins*[58]) collectively suggested the development of energy storing flexor tendons to begin earlier than the development of their positional extensor counterparts in the *ultra*–precocial chick model under study.[50] However, with respect for less–immediately–mobile and altricial animals, earlier development of ESTs than PTs would also be intuitive given the added biological complexity associated with their: (***i***) high cellularity[10,17,20] or (***ii***) rich proteomes[10,17,248] relative to PTs when fully mature.

Additional evidence of disparity between the FDTs at the fetal stage has been found in disparate expression of three members of the thrombospondin family of proteins (*thrombospondin–3, –4, and –5; or: 'Tsp–3', '–4', and '–5', hereafter*) together often referred to as cartilage oligomeric matrix protein ('*COMP*').[92,107,295] Namely, in *in vitro* investigations of equine esSDFTs and pCDETs during gestation, cells isolated from esSDFTs were found to produce more COMP in

response to exogenously applied transforming growth factor beta–1 or –3 (‘*TGF–β1*’ *or* ‘*–β3*’) than did cells isolated from pCDETs.[43,92] This might have suggested a greater capacity for COMP production in the cells of esSDFTs over those of pCDETs during gestation[92] — which would be in alignment with the relatively high expression of COMP in the esSDFT over the pCDET seen in tissue maturity.[21,229] From this, the possibility of comparatively high COMP expression in both prenatal and postnatal esSDFTs is intriguing. High COMP expression in ESTs during fetal development could be of significance given its roles in: type I collagen recruitment,[295] collagen fibrillogenesis,[239] and myotendinous junction assembly.[107] Moreover, genetic studies conducted on mice have suggested Tsp–4 to be involved in restricting the lateral growth of collagen fibrils.[83] Thus, high COMP in ESTs during gestation[21,92,229] may contribute to the comparatively small mean collagen fibril diameter (‘*CFD*’, *hereafter*) seen in fully–developed ESTs relative to that in fully–developed PTs.[19,243]

A second protein implicated in regulating the lateral growth of the type I collagen fibrils is type III collagen (‘*COL3*’, *hereafter*).[4,78,133,151,152] Specifically, depletion of COL3 has been documented to increase the mean thickness of type I collagen fibrils[84,268] such that the diameter of any given fibril may be proportional to its type I collagen/COL3 molar ratio (*or: high COL3 → low mean collagen fibril diameter*).[4,124] Resultantly, a greater presence of COL3 has been proposed to result in: (***i***) a decrease of tissue strength[65] and (***ii***) an increase of tissue damage susceptibility.[18] These effects have been held to stem from the structural similarity between COL3 and its type I counterpart: namely, COL3 is able to colocalize with type I collagen in the formation of type I microfibrils[4,6,268] and thereby directly participate in lateral fibril expansion.[152,237] However, COL3 has been hypothesized to join type I microfibrils with lower efficiency than does type I collagen[73,148,152] and so the intrusion of a COL3 molecule into a type I microfibril has been proposed to result in a lackluster foundation for subsequent collagen accretion, and eventual

inhibition of lateral fibril growth.[4,23,152,268] Accordingly, the concentration of COL3 has generally been found to be greater in tissues with functions that demand high elasticity,[31,132,226,295] like fully–developed ESTs over fully–developed PTs.[21,295] Further, this relationship may also extend to developing tendons, as tenocytes isolated from the esSDFTs of eight month old 'foals' (*or: equines of less than one year of age*) have been found to produce more COL3 in response to TGF–β1 stimulation than do tenocytes instead isolated from match–paired pCDETs.[92] Thus, high expression of COL3 in ESTs during gestation could serve as an alternative explanation (*to COMP*) for the relatively small mean diameter of collagen fibrils within ESTs relative to that metric within PTs in tissue maturity.[19,243]

Another protein that may function differently between the FDTs is the class I basic helix–loop–helix[11,101,239] transcription factor scleraxis ('*Scx*').[175] Scleraxis is the earliest known tendon marker[25,48,87,271] and has been associated with both the recruitment of tenoblasts into tendon tissue[108,175] and the upregulation of various tenogenic factors including: COMP,[11,246] tenomodulin,[26,239,254] and type XIV (*or: 14*) collagen.[87,144,178] In mice, while Scx knockout mutation was found to result in near complete disruption of forelimb flexor tendons, Scx mutation was instead identified as having a comparatively negligible effect on neighbouring extensor tendons.[175] This plausibly indicated Scx function to be instrumental in the development of forelimb ESTs but not in that of PTs.[26,108] Thus, prolonged Scx function in ESTs may increase tenocyte recruitment and contribute to the high cellularity of ESTs over PTs in tissue maturity.[10,17,20] Further, both (***i***) tenomodulin[107,178] and (***ii***) type XIV collagen[35,87] have been proposed to take part in restraining the lateral growth of collagen fibrils during development, so a high presence of tenomodulin and type XIV collagen as a result of prolonged Scx expression in developing ESTs could be partially responsible for the relatively small mean CFD of fully–developed ESTs compared to their PT

counterparts.[19,96,243]

An additional protein found to be divergent between the FDTs during fetal development is the angiogenic vascular endothelial growth factor ('*VEGF*', *hereafter*).[191,246,254] While Petersen et al. (2002)[191] found VEGF expression to stay ubiquitous throughout the human fetal period (*from: 0–40 weeks*) in the energy storing Achilles tendon, VEGF expression was instead found to start decreasing mid–term (*at approximately ∼20–24 weeks*) in the positional tibialis posterior tendon.[89,191] Depletion of VEGF in PTs by the latter stages of fetal development may relate to the finding of relatively poor vascularization in select PTs compared to ESTs by birth.[149,191,212] Though, drawing such a connection between VEGF expression and vascularization remains speculative. However, one might also speculate that comparatively poor vascularization in PTs relative to ESTs perinatally could be of detriment to the subsequent ability of PTs to regenerate damaged tissue[8,149,216] and sustain tenocyte populations[57,119] — which would align with the relatively low damage resistance[10,89,253] and cellularity[10,17,20] of PTs compared to ESTs in tissue maturity. In support of the notion that these tissue characteristics in maturity could stem from disparate VEGF expression, the comparatively low cellularity of fully–developed PTs[10,17,20] relative to their EST counterparts has been documented in mid[290] and late term[235] equine fetuses (*shortly after the alleged decrease of VEGF*[191]).

Vascular endothelial growth factor has also been implicated as an upregulator of TGF–β1[133] which has, in turn, been reported to: (***i***) induce other tenogenic factors,[87,101,246] (***ii***) increase tendon mechanical strength,[254] and (***iii***) supplement tendon healing ability.[69,133] Resultantly, variance in expression of VEGF may catalyze additional differences between FDTs via VEGF's induction of signaling cascades. In alignment with the previously mentioned results of Petersen et al. (2002),[191] TGF–β1 expression has been found to increase from 3 to 6 months post–birth in the

esSDFTs of equines while no such surge has been identified in pCDETs.[290] Thus, the potential for an innate divergence of VEGF expression during the gestational development of the FDTs merits further investigation.

A final protein that might function differently in the development of ESTs and PTs is another isoform of the TGF superfamily: transforming growth factor beta 2 ('*TGF–β2*').[200] In mice, opposite to findings related to Scx,[175] TGF–β2 knockout mutation was found to result in the near complete loss of developing forelimb (*positional*) extensor tendons while the development of the proximal flexor (*energy storing*) tendons remained comparatively undisturbed.[200] This may have suggested TGF–β2 to play a critical role in the development of PTs but not in that of ESTs.[200] Establishing such a relation would be of great interest as the role of TGF–β2 in tendon development is currently unknown.[246] Although some research has associated TGF–β2 with altered expression of: (***i***) collagen types I, XII (*or 12*), and XIV (*or 14*),[59] (***ii***) Scx,[26,87,178] and (***iii***) tenomodulin,[246] the function of TGF–β2 —— and to what extent its function may differ from its sister –β1 and –β3 isoforms —— remains a mystery.

2.2.2.2 Unknowns About the Growth of Collagen Fibril Diameter

Multiple structural features that differ between the FDTs in tissue maturity but remain insufficiently characterized at the fetal stage may offer additional evidence that ESTs and PTs begin to become distinct from one another during fetal development.[121,142,192] A first example of such a feature is the disparity in the mean diameter of collagen fibrils within each of the FDTs.[121,192,293] In particular, fully–developed PTs have been found to possess collagen fibrils of larger mean diameter than do fully–developed ESTs.[19,104,203,243] The comparatively large mean CFD of fully–developed PTs relative to fully–developed ESTs has been proposed to contribute to the notable: (***i***) stiffness[19,208,225,253] and (***ii***) strength[104,187] of PTs over their EST counterparts.

Conversely, the relatively small mean CFD of fully–developed ESTs compared to their PT counterparts has been held to play a role in the notable: (***i***) elasticity[78,187] and (***ii***) creep resistance[78,208] exhibited by fully–developed ESTs over fully–developed PTs. These associations have made the diameter distributions of collagen fibril populations of particular interest to the study of tendon functional divergence.

The growth of CFD in prenatal tendon is well characterized.[9,68,121] A population of immature collagen fibrils unimodally distributed about ∼40 nanometers ('*nm*') has first been found to arise at the approximate midpoint of fetal development[24,105] and to persist at that size for the majority of gestation.[24,105,121] Then, in the weeks leading up to and following birth, the lateral fusion of neighbouring fibrils[9,199,293] has been proposed to spur a period of rapid lateral fibril growth.[24,192] This, in turn, has been held to culminate in a rapid increase in the number of larger diameter collagen fibrils perinatally (*of: up to ∼400 nm*[90]); and ultimately result in a CFD distribution bimodal about ∼40 and ∼100 nm.[68,121,292] Thus, it is reasonable to hypothesize that the mean diameter of collagen fibrils within each of the FDT classes first diverges perinatally,[24,192] with the collagen fibrils of PTs more readily engaging in lateral fusion with one another than do the collagen fibrils within ESTs.[68,121,199] This hypothesis would project a greater proportion of larger diameter (*∼100 nm*) collagen fibrils in PTs than in ESTs as fetal development nears its end.[19,203,243] However, this relationship remains unsubstantiated between any studied EST–PT pairing. So, finding the precise developmental timepoint at which mean CFD diverges between an EST and PT pairing would add to the literature. Further, identifying the exact moment of mean CFD divergence in one such EST and PT pairing could also bear the potential to assist in resolving additional unknowns about fibril development. For example, an exhaustingly large, nonexclusive list of proteins — from small leucine–rich proteoglycans ('*SLRPs*') of both class I (*like: decorin and biglycan*)[178,256,292] and class II (*fibromodulin and lumican*),[39,68,116] to COMP,[9,83] to collagen

types III and XIV (*or: 14*)[133,295] — have all been put forward as potential regulators of lateral collagen fibril development; together suggesting a need for increased research aimed at identifying the factor(s) truly responsible for the mediation of lateral fibril growth. To that effect, monitoring protein expression at developmental time points of substantial collagen fibril expansion could prove very informative.

2.2.2.3 Unknowns About the Formation of Collagen Fibril Crimp

Another structural feature that has previously been found to differ between select pairings of FDTs in tissue maturity is the wavy, undulating pattern that often extends longitudinally down collagen fibrils: most commonly referred to as 'crimp' ('*collagen fibril crimp*'& '*CFC*' *hereafter*).[102,142] CFC has been held to serve primarily as a protective buffer during the first stages of elongation[75,78,98] but may also contribute to tendon elasticity.[21,75,142] Accordingly, CFC has been indicated to be *tighter* (*or: of shorter mean wavelength or larger crimp angle*) in tendons that experience repeated mechanical strain than in tendons of paralyzed limbs.[115] Reflecting this, the collagen fibrils of (*the notably elastic*) fully–developed ESTs have been found to possess tighter crimp[76,232] — that is, shorter crimp length[21] and larger crimp angle[249] — than the fibrils of their PT counterparts. However, this relationship has seldom been studied at the fetal stage (*but see: Zamboulis et al. 2020*[290]).

The factors responsible for determining the characteristics of CFC are unclear[142] — stemming, at least in part, from an uncertainty of when crimp originates during development.[75,121,215] Though 'crimp–like patterning' has been identified in gestational collagen fibrils,[189,215,220,290] the absence of multiple characteristics of the crimp of mature fibrils in these structural undulations[121,215] have made the relationship of the (***i***) fibril undulations seen during gestation to (***ii***) the crimp seen among the collagen fibrils of fully–developed tissue, obscure. For example, the 'crimp' present in

fibrils of embryonic tendon has been shown to lack the distinct knots often associated with the crimp visualized in fully–developed tendon.[75] Accordingly, to better assess the relatedness of these two structures, recent theories that: (***i***) CFC originates from cooperative tenocyte contraction[102] mediated by extensive intercellular actin networks,[178,215] and that (***ii***) the propensity of a given fibril to 'crimp' is inversely related to its fibril stiffness[102] may be of use. In particular, because theory ('***i***') postulates a positive correlation between the tightness of fibril crimp and cell density,[102,142,273] identifying a relationship between prenatal 'crimp–like patterning' and cellularity at the fetal stage could help establish the gestational undulations as a legitimate precursor of the crimp present in the collagen fibrils of fully–developed tendons. Similarly, with respect for the second hypothesis ('***ii***'), establishing a relationship between: (***i***) the degree of prenatal 'crimp–like patterning' in a given tendon during gestation, and (***ii***) that tendon's fibril stiffness, could serve to further reinforce findings.[102] While the phenotypes of the FDTs align with these theories in tissue maturity,[§] whether this relationship extends prenatally as a result of alleged high cellularity in perinatal ESTs[235,290] is in need of further exploration.

[§] *Namely, with: tighter fibril crimp,*[76,104,249] *higher cellularity,*[10,20] *and lesser fibril stiffness*[19,253] *in fully–developed ESTs than in fully–developed PTs*

2.3 Research Aims

This research aimed to better characterize the divergence of a FDT pairing that occurs during development.[43] Clear differences exist between ESTs and PTs in tissue maturity[10,17,248] and, among other traits, these differences confer unequal susceptibility to tendinopathy.[10,89,104,253] Therefore, elucidating the details surrounding the process by which ESTs and PTs differentiate during development has the potential to deepen collective understanding of the factors underlying the properties that make certain tendons more prone to tendinopathy than others.

This investigation challenged the notion that variance in postnatal functional loading is critical for tendon divergence (*or 'mechanoregulation', see: The Argument for Mechanically...*).[288] Instead, this research looked to expand on the possibility[92,231,290] that the differences between functionally distinct tendons ('*FDTs*', *hereafter*) arise innately during fetal development.[42,182,192] Confirming the hypotheses that follow in the subsequent section could: (***i***) aid in the understanding of how tendon development relates to eventual susceptibility to tendinopathy; (***ii***) strengthen the selection of autograft tissue sources; (***iii***) improve the ability to engineer effective replacement tendon; and (***iv***) help in the evaluation of tailored therapeutics for individuals with tendon related disabilities.

2.4 Research Hypotheses

2.4.1 Greater Intermolecular Cross–Linking in esSDFTs Compared to Match–Paired pCDETs During Prenatal Development?

→ *That esSDFTs will come to have higher: (**i**) denaturation temperature ('T_d', hereafter), (**ii**) temperature of maximum force generation ('T_{Fmax}'), and (**iii**) half–time of load decay ('$t_{1/2}$') values by the end of gestation in relation to their pCDET counterparts.*

Higher T_d values in esSDFTs than in pCDETs prenatally will be indicative of relatively dense molecular packing in esSDFTs gestationally.[114,141] Notably dense molecular packing in esSDFTs will potentially be brought about by a greater presence of intermolecular cross–links in esSDFTs than in pCDETs during fetal development.[231] Additionally, higher T_{Fmax} values in esSDFTs than in pCDETs during fetal development may suggest esSDFTs to possess a greater presence of thermally stable (*or: 'divalent ketoamine–'; or: 'trivalent'*) intermolecular cross–links than their match–paired pCDETs.[104] Finally, higher $t_{1/2}$ values in esSDFTs than in their match–paired pCDETs during gestation both: (***i***) before and (***ii***) after stabilization treatment via sodium borohydride ('$NaBH_4$') might signal the collagen molecules within esSDFTs to be conjoined (*as in: '**i**'*) with a greater presence of thermally stable intermolecular cross–links[262] and (*in: '**ii**'*) with a greater presence of intermolecular cross–links than those within pCDETs,[2] respectively. Relatively high T_d and T_{Fmax} values in esSDFTs over pCDETs during gestation will reinforce the results of an earlier study[231] conducted on bovine (*or: cattle*; *Bos taurus*) fetuses. Additionally, a comparatively high presence of intermolecular cross–links and a greater presence of thermally stable

intermolecular cross–links in a given esSDFT over its match–paired pCDET during fetal development could result from abundant LOX catalysis[7] — plausibly enabled by high cellularity[290] or low collagen turnover[129,252] — in esSDFTs relative to in match–paired pCDET gestationally.

2.4.2 Smaller Mean Collagen Fibril Diameter in esSDFTs Than in pCDETs Perinatally?

→ *That disparity in the mean diameter of the collagen fibrils within the FDTs will first arise toward the end of gestation, with the mean diameter of collagen fibrils within esSDFTs maturing to be smaller than that of the collagen fibrils within pCDETs.*

This will align with the comparatively small mean collagen fibril diameter ('*CFD*', *hereafter*) within the fully–developed esSDFT relative to that reported for the fully–developed pCDET.[19,203,243] Divergence of mean CFD between the two FDTs will occur toward the end of gestation, as this perinatal period is marked by extensive lateral fusion of immature collagen fibrils and an abrupt increase of mean CFD.[68,121,292] During this time, the frequency at which collagen fibrils laterally fuse with one another will be lower in perinatal esSDFTs than in their match–paired pCDETs.

2.4.3 Finer Collagen Fibril Crimp in esSDFTs Than in pCDETs During Gestation?

→ *That 'crimp–like patterning' will become identifiable in collagen fibrils during fetal development and will mature to be tighter[76,232] (or: of shorter mean crimp wavelength[21] or larger crimp angle[104,249]) in esSDFTs than in pCDETs by the end of gestation.*

Comparatively tight fibril crimp in esSDFTs relative to in pCDETs during gestation will align with the tight collagen fibril crimp seen in fully–developed ESTs relative to

that seen in fully–developed PTs,[21,76,104,249] and will result from comparatively high cellularity in the esSDFT over the pCDET gestationally.[10,20]

3 Methods

3.1 The Bovine esSDFT and pCDET

Tendons were acquired from the forelimbs of fetuses present in pregnant adult (*24 to 36 month old*) cows (*or: female cattle*; *Bos taurus*) freshly killed for food at multiple local abattoirs. A spectrum of fetuses halted at various stages of development were studied with '*crown–to–rump length*' serving as an index of gestational maturity (*in which fetuses measured ∼100 centimeters at full term or ∼278–290 gestational days; 'GDs', hereafter*[194,196]). [231] Following a well established proxy of human tendons, [104] comparative tests were done on match–paired esSDFTs and pCDETs from the forelimbs of each fetus as archetypes of ESTs and PTs, respectively. [89,186,222] Tendons were preserved within double–bagged forelimbs and stored at –86 degrees Celsius ('*°C*', *hereafter*) for a maximum of six months until testing. [104] Prior to testing, forelimbs were thawed at room temperature in sealed bags.

3.2 Structural Assessments

3.2.1 Hydrothermal Isometric Tension ('HIT') Testing

For the full protocol associated with HIT testing, *see:* Appendix Section 8.1.

Hydrothermal isometric tension ('*HIT*') testing was used to evaluate the molecular stability [114,276] and functional intermolecular cross–link characteristics [104,136,195] of tendons from twenty–three distinct fetuses. In HIT testing, thawed tendons were first sectioned to approximately ∼1.5 millimeters ('*mm*') in width and ∼7 mm in length. A given tendon section was then isometrically constrained by clamping ∼2.5 mm of tendon tissue from each end of the section into steel grips and mounting the section vertically between: (***i***) a load cell and (***ii***) fixed support (*see: Figure 8*). The system was then submerged in room temperature distilled, deionized water

(*Figure 8*). Following submersion, a tensile preload of approximately ∼15 grams (*∼0.15 newtons*) was applied to each section immediately before a 10–minute relaxation window. The temperature of the system was then brought to 90°C (*at: 1.5°C per minute to 75°C and 0.7°C per minute thereafter*) using a computer–controlled hotplate, during which time temperature–time–load data was continuously catalogued at 0.2 hertz ('*Hz*') using load cells (*as has previously been done; see: Herod et al. 2016*[104]).[262] The resulting force–temperature data was then evaluated using Microsoft Excel.[104,262]

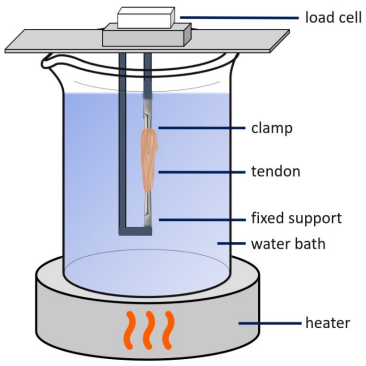

Figure 8: An illustration depicting the hydrothermal isometric tension ('*HIT*') testing apparatus that was used in the determination of (***i***) collagen molecular stability and (***ii***) intermolecular cross–linking characteristics. The diagram illustrates a tendon section isometrically constrained between (***i***) a load cell (*depicted toward the top*) and (***ii***) a fixed support (*toward the bottom*) submerged in water held in a 4–liter glass beaker.

3.2.1.1 Denaturation Temperature ('T_d')

In HIT testing, a tendon section first heated to its denaturation temperature ('T_d'; *see: Figure 9*).[2] At this temperature, the intra–helical hydrogen bonds responsible for maintaining the structure of the collagen molecules within a tendon section have gained sufficient kinetic energy to begin to hydrolyze.[141,275,296] This hydrolysis then causes substantial helix unwinding and sees affected collagen molecules undergo an entropically driven helix–to–coil transition in which collagen alpha–helices seek to longitudinally contract.[114,141] However, the presence of more thermo–resistant intermolecular cross–links prevents such a transition from occurring and instead translates the contractive force of affected molecules into a larger scale, section wide phenomenon.[2,104,114,141] While this would typically drive the entire section to contract,[114,190]

isometric constraints placed at the longitudinal extremities of the section prevent it from doing so and instead translate its desire to contract into a sharp increase in tension [104,261,276] (*represented by an 'elbow'*[2] *on a load–temperature plot; see: Figure 9*). Thereby, the onset of load generation at a relatively high temperature (*or: a relatively high T_d value*) signifies a comparatively high resistance of collagen molecule triple helices to water solvation [114,141] — potentially attributable to greater cross–link induced molecular packing, [231] among other factors. [2,33] Specifically, a greater presence of intermolecular cross–links may increase a section's T_d by limiting the number of configurations its collagen molecules are able to achieve[2] and thereby lowering the section's overall entropy.

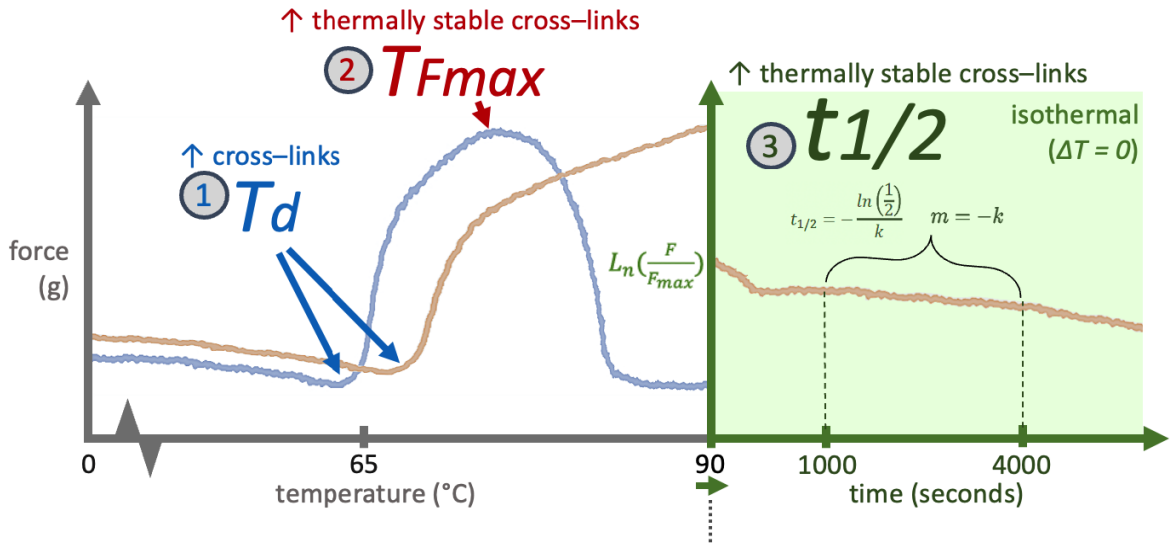

Figure 9: A representation of the force generated (*in grams*, '*g*') by two tendon sections evaluated via hydrothermal isometric tension ('*HIT*') testing analysis. Each section first heated to its section–specific denaturation temperature ('T_d'; *in degrees Celsius*, '°*C*') followed by its section–specific temperature of maximum force generation ('T_{Fmax}'). A subsequent isothermal period then allowed for extrapolation of section–specific half–time of load decay ('$t_{1/2}$', '°*C*') through the construction of a '*time*' (*in seconds*) ***vs.*** '$L_n(\frac{Force}{Maximum\ Force})$' (*or:* '$L_n(\frac{F}{F_{max}})$') plot and an analysis of the slope of the data generated therein (*with: slope* '–*k*' *in* '$t_{1/2} = -\frac{ln(1/2)}{k}$'). The green shaded ('*isothermal*') region serves to represent a halt in the system's temperature increase.

3.2.1.2 Temperature of Maximum Force Generation ('T_{Fmax}')

In addition to information gleaned from denaturation temperature, whether the temperature of maximum force generation ('T_{Fmax}') of a section transpires: (***i***) during the temperature ramp of its surrounding water to 90°C, or (***ii***) in the midst of the 90°C isotherm that occurs thereafter can provide information about the functional absence or presence of thermally stable intermolecular cross–links within the section (*see: Figure 9*).[104] In particular, following the onset of the production of tension that is marked by a section's denaturation temperature ('T_d'), the tension generated by the then denatured, gelatinous collagen within the section continues to increase in proportion to the collagen's absolute temperature,[74,114] exhibiting behaviour consistent with the theory of rubber elasticity.[114,139] This behaviour arises from the similarity between (***i***) the newly randomly–coiled polymer chains of collagen still interconnected by a portion of its original intermolecular cross–links, and (***ii***) a rubber–like polymer network.[2,114,139] In greater detail: as the thermal energy bestowed upon each collagen molecule within the section continues to increase beyond that energy associated with T_d, the gyrating, newly randomly–coiled collagen molecules experience a gradually–intensifying entropic force to contract longitudinally with further heating, in a manner analogous to the behavior exhibited by cross–linked rubber polymers (*Figure 9*).[2,114,141]

The behavior of a network of collagen molecules under heat stress, however, is further complicated by the varying thermal stability of the intermolecular cross–links that conjoin them.[104,274] In particular, these cross–links play a crucial role in translating the contractive forces of denatured collagen molecules to the macroscale, but can be susceptible to hydrolysis under elevated temperatures.[1,6] Accordingly, when a significant portion of the intermolecular cross–links within a sample are cleaved, it creates a discordance between the degree of denaturation of a given sample and the tension it reports.[70,104,274] This phenomenon occurs because the affected collagen

molecules, either individually or as aggregates, may be made free to contract longitudinally without contributing to the overall tension measured at the macroscale in the event of cross–link hydrolysis. So, as the rate of cross–link hydrolysis increases, it can outpace the tension generated by the remaining intact network, leading to a plateau and eventual decrease in tension (*as is seen in Figure 9*).[74,104,114,261] This process manifests as a peak in the load-temperature plot, corresponding to the section's 'T_{Fmax}' (*Figure 9*).[261] In tendon, thermally stable intermolecular cross–links (*or: 'divalent ketoamine'; or: 'trivalent' cross–links*) are able to resist being cleaved at temperatures between T_d and 90°C, and can thereby effectively maintain a network of denaturing collagen molecules ramping up to that temperature.[2,70,104] In contrast, their thermally labile (*or: 'divalent aldimine' cross–link*) counterparts are more susceptible to hydrolysis and, in HIT testing, can plausibly compromise collagen interconnectedness prior to 90°C.[2,70] Accordingly, a T_{Fmax} value of less than 90°C is suggestive of a comparative functional absence of thermally stable intermolecular cross–links within a section; while no sign of a T_{Fmax} value prior to 90°C instead signifies a relative abundance of thermally stable intermolecular cross–links.[104]

3.2.1.3 Half–Time of Load Decay ('$t_{1/2}$')

Following the temperature ramp to 90°C, holding a section at 90°C for a prolonged period can cause progressive hydrolysis of the peptide bonds that give structure to each of the three alpha–chains within each collagen molecule present in the section (*see: Figure 2*).[262] This hydrolysis of peptide bonds ultimately results in the collapse of alpha–chains and slippage of adjacent collagen fragments.[274] Similar to the unrestricted molecular coiling that can occur upon the hydrolysis of intermolecular cross–links,[70,274] this slippage can give rise to Maxwellian decay (*see: Figure 9*) that is quantifiable via a section's half–time of load decay ('$t_{1/2}$', '*°C*').[104] More specifically, section–specific half–time of load decay can be extrapolated through the construction of a '*time*' (*in seconds*) ***vs.*** '$L_n(\frac{Force}{Maximum\ Force})$' (*or:* '$L_n(\frac{F}{F_{max}})$') plot and an analysis of the slope of the data

generated therein (*with: slope* '$-k$' *in* '$t_{1/2} = -\frac{ln(1/2)}{k}$'). At this point of denaturation, this gradual decrease in tension during the 90°C isotherm is slowed only by the effort of present intermolecular cross–links in maintaining the molecular order of collagen molecules[2] —– that is, the networking afforded by the still functional thermally stable intermolecular cross–links between collagen.[104] For this reason, the $t_{1/2}$ of a section (*like its* T_{Fmax}) is positively correlated with the presence of thermally stable intermolecular cross–links in a tissue.[262] Put differently, a relatively slow load decay suggests a greater presence of divalent ketoamine or trivalent intermolecular cross–links within a given tendon section.[104]

3.2.1.4 Sodium Borohydride ('$NaBH_4$') Treatment

The present research also deployed the gradual tensile load decay of isometrically constrained tendon during a 90°C isotherm to: (***i***) assess intermolecular cross–link speciation, and (***ii***) give a better estimate of the presence of functional intermolecular cross–links within a section than could be determined from relative T_d value alone.[2,104,194] This was done in sections from six distinct fetuses and involved the chemical reduction of thermally labile intermolecular cross–links into a thermally stable form via the deployment of sodium borohydride ('$NaBH_4$') as a mild reducing agent[2,104] prior to HIT testing. In subsequent HIT testing, a comparison of the $t_{1/2}$ values of replicates of a tendon section assessed: (***i***) with, or (***ii***) without $NaBH_4$ stabilization treatment provided information about the section's proportion of divalent aldimine intermolecular cross–links.[70,104,194] In particular, gradual tensile decay can be markedly slowed (*and* $t_{1/2}$ *value correspondingly increased*) following the $NaBH_4$ stabilization of a section that bears a substantial population of divalent aldimine cross–links.[104,194] Further, because $NaBH_4$ treatment converts all thermally labile intermolecular cross–links within a given section to a thermally stable form, the rate of tensile load decay post–reduction provides information about the total presence of functional intermolecular cross–links in one $NaBH_4$–stabilized section relative to another.[2,104]

Specifically, a section with a greater presence of cross–linking should exhibit a slower tensile decay (*and a greater* $t_{1/2}$ *value*) than a less highly cross–linked counterpart following $NaBH_4$ treatment.[2,104]

3.2.2 Transmission Electron Microscopy ('TEM') Analysis

For the full protocol associated with TEM analysis, *see:* Appendix Section 8.2.

Transmission electron microscopy ('*TEM*') was used to evaluate the progression of collagen fibril diameter ('*CFD*', *hereafter*)[95,121,279] at intervals of approximately 10–20 GDs throughout the 2nd and 3rd trimesters of gestation in a total of fifteen fetuses. TEM has become a common tool for the visualization of developing tendons[12,36,131] and has previously been deployed[121] to assess CFD at a single embryonic time point in a non–load–bearing tendon.[121] TEM is often used to evaluate minute structures such as collagen fibrils because a standard transmission electron microscope can achieve a resolution that is over one hundred times greater than a standard light microscope (*of approximately: one nanometer ('nm') and 200 to 300 nm, respectively*).[80,93,278] The reason for TEM's superior resolution to light microscopy lies in the comparatively short *de Broglie* wavelength of an electron within an electron beam in relation to that of a photon within light.[61] In the present research, tendons were cut into transverse sections that were approximately 100 nanometers thick (*see: Appendix 8.2*). These ultra–thin sections served as two–dimensional planes of tissue, containing regions that were either electron–dense (*absorbing many of the incident electrons*) or electron–sparse, with electron–dense regions corresponding to areas of substantial collagen content. In the visualization of each sample, a beam of high–energy electrons was first generated by heating a lanthanum hexaboride ('*LaB6*') crystal and accelerating its thermionically–emitted electrons down a column at 80 kV.[135] When electrons within this high–energy electron beam encountered the plane of our ultra–thin tendon section, electron–atom interactions resulted in a

portion of the incident electrons being completely absorbed, while the direction of other electrons became scattered, and the pathing of the remaining electrons continued through unchanged.[80,278] The altered beam then eventually reached a scintillator, which served to convert the signals from the incident electrons into photons.[113] These photons were subsequently transformed into computer–processable electrical signals by the charge–coupled device ('*CCD*') within a specialized digital camera,[93,113] from which the resulting digital image was displayed and analyzed on a computer monitor.

3.2.3 Polarized Light Microscopy ('PLM') Analysis

For the full protocol associated with PLM, *see:* Appendix Section 8.3.

Polarized light microscopy ('*PLM*') was used to characterize any 'crimp–like patterning' present in sections representative of early (*of approximately GD ∼100*), mid (*GD ∼140*), and late (*GD ∼245*) gestation in a total of four fetuses.[102,232] Polarized light microscopy allowed for high contrast analysis of sections[197] in deploying two polarizing filters[79,102,195] oriented perpendicularly to one another on either side of a light microscope's specimen plane.[79,232] The first of these polarizers (the '*polarizer*') was situated between the microscope's light source and condenser lens and the second (the '*analyzer*') between the objective lens and eyepiece.[197] A polarizer takes incoming white light — that under normal circumstances vibrates omnidirectionally at right angles to its path with equal probability[79] — and polarizes it to vibrate unidirectionally in a plane parallel to its filter.[79,172,197] In this way, crossed polars oriented at right angles to one another block any incident light from reaching the microscope's eyepiece in a blank setup.[79,172,197,232] This blockage also holds true during the analysis of an 'isotropic material' that possesses a single 'refractive index' (*or: 'RI'; a measure of how fast light can pass through a medium*)[79] and thereby exhibits identical optical properties when probed with light incident from any direction.[197] In contrast, an image

arises when an 'anisotrophic material' instead exhibits 'instrinsic birefringence' in possessing two or three different refractive indices.[79,197,232] This is the case in 90% of all solid materials,[197] including collagen.[130,232] In these materials, multiple refractive indices give rise to double (*or: even triple*) diffraction of incident light into distinct wavefronts[130,197] with differing velocities:[79] most typically a faster 'ordinary ray' travelling in a direction with a lower RI and a slower 'extraordinary ray' in the direction with a higher RI.[232] In addition, intrinsic birefringence often occurs in combination with 'form birefringence'.[232] In form birefringence, the spatial arrangement of substructures within a material further alters the phase difference between exiting wavefronts.[232] Accordingly, both intrinsic (*as: 'RI'*) and form birefringence (*as: 't'*) are acknowledged in the equation for optical path difference ('*OPD'; Equation 1*).[197] Finally, following their propagation through a material, out of phase wavefronts are forced to recombine at the microscope's analyzer (*or: second 'polarizer'*)[79,197] which results in constructive or destructive interference that is reported as a specific color.[37,79] In the present analysis of collagen fibrils, the intrinsic birefringence of collagen saw all collagen fibrils made visible against their (*less birefringent*) surrounding matrix,[130] and the form birefringence of undulating fibrils distinguished areas of crimp from flatter regions.[232] The tightness of the 'crimp–like patterning' was then quantified via a mean measurement of 'crimp wavelength', which represented the peak to peak measurement of each discernible crimp peak.[195]

Equation (1): $\mathrm{OPD} = \Delta RI \times t$

where ΔRI is: the change in refractive index as light enters a material

and t is: the thickness of the material

3.3 Statistics

Statistical tests were conducted using R (*version 4.2.2*). Data were presented as mean ± standard error unless otherwise specified (*as: standard deviation*). While one–way 'analysis of

covariance' tests ('*ANCOVAs*') were used to identify differences over gestational time, paired two–sample t–tests were used to compare gestational means, and Kolmogorov–Smirov ('KS') tests to assess for statistical differences between distributions. In temperature of maximum force generation ('T_{Fmax}') investigations, any tendon section that "survived" the temperature ramp to 90 degrees Celsius ('*°C*'; *in failing to exhibit a decrease in generated force prior to 90°C*) was omitted from calculation of mean–T_{Fmax}–value and further statistical analysis.[§] In all tests a p–value of less than 0.05 ($p < 0.05$) was taken as being significant.

[§] *(see: the treatment of subsamples within each of the three samples comprising each tendon–trimester treatment grouping in sub–figures '***a.***' and '***b.***' of Figure 13)*

4 Results

Data were presented as mean ± standard deviation (*unless otherwise specified as standard error*).

4.1 Samples Assessed

Thirty–four fetuses were assessed (*see: Figure 10*). Fetuses ranged in age from gestational day ('*GD*', *hereafter*) 86 to GD 247 (*with: GD ~283 representing full term*). The majority of fetuses assessed were within the GD range represented by the 2nd or 3rd trimesters of fetal development (*with: 55.8% and 41.2% of all fetuses, respectively*). Only one fetus (*2.9% of all fetuses assessed*) was aged to the 1st trimester.

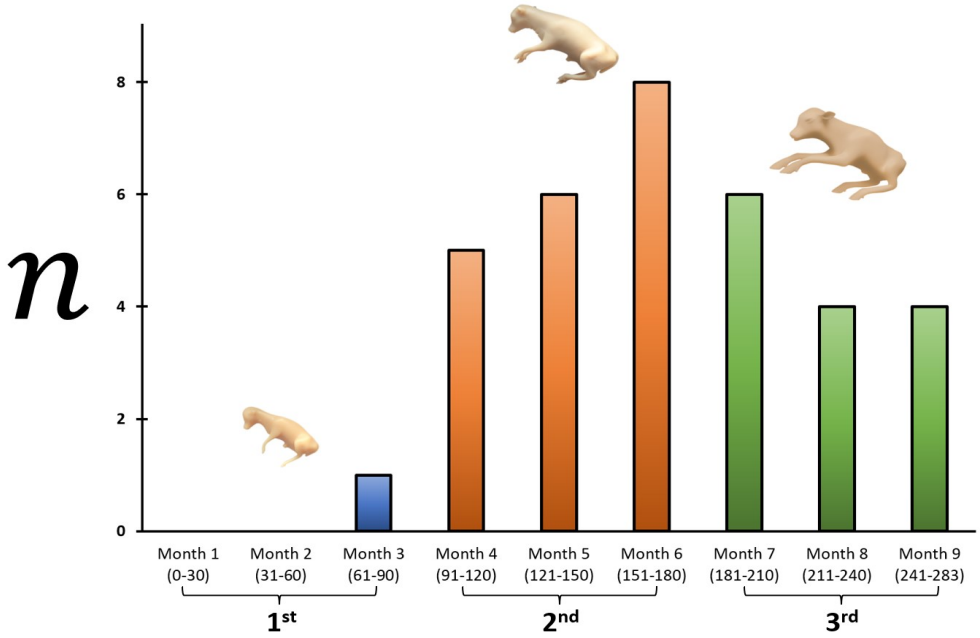

Figure 10: A histogram of fetuses assessed categorized by month and trimester. The 1st, 2nd, and 3rd trimesters served to comprise gestational days ('*GDs*') 0 through 90, 91 through 180, and 181 through 283, respectively. Fetuses were collected between June 19th, 2022 and March 7th, 2023. Each count (*as represented on the y–axis; by* '*n*') represented a distinct fetus.

4.2 Results Associated With HIT Analysis

4.2.1 T_d Increased at a Faster Rate in the esSDFT Than in the pCDET During Gestation?

Tendon pairings from fourteen distinct fetuses were subjected to denaturation temperature (*or:* 'T_d') analysis. Results showed signs of tendon specific changes in T_d during gestational development (*see: Figure 11.a*). While T_d values of match–paired esSDFTs and pCDETs initially appeared similar in sections from fetuses younger than GD 190 ($n_{SDFT} = 7$, $n_{CDET} = 6$), sections from fetuses of or older than GD 190 exhibited consistently higher T_d values in esSDFTs than in match–paired pCDETs ($n_{SDFT} = 7$, $n_{CDET} = 7$; *Figure 11.a*). Resultantly, the rate of increase of T_d during gestation appeared to be greater in the esSDFT than in the pCDET (*Figure 11.a*). This trend may have suggested a structural difference that conferred a discrepancy between the relative T_d values of the esSDFT and the pCDET to have arisen toward the beginning of the 3rd trimester of fetal development.

A one–way ANCOVA was conducted (*using R; version 4.2.2*) to determine whether a statistically significant difference existed between the T_d values of the esSDFT and pCDET whilst controlling for gestational age. Gestational age was found to have a significant impact on T_d (*Figure 11.a; $p \leq 0.001$, $n_{SDFT} = 14$, $n_{CDET} = 13$*) and the rate of increase of T_d with increasing age was found to be significantly higher in the esSDFT than in the pCDET ($p = 0.009$, $n_{SDFT} = 14$, $n_{CDET} = 13$). In contrast, the mean–T_d–values of all esSDFTs (*at: 66.38°C ± 0.32*) and pCDETs (*66.05°C ± 0.19*) analyzed were not found to significantly differ (*Figure 11.b; t = -0.87, $p = 0.39$, $n_{SDFT} = 14$, $n_{CDET} = 13$*).

4.2.2 A Higher Mean–T_{Fmax}–Value Among esSDFTs Than pCDETs Prenatally?

Similar to T_d analysis, tendon pairings from fourteen distinct fetuses were subjected to temperature of maximum force generation (*or:* 'T_{Fmax}') assessment. Unlike T_d, T_{Fmax} analysis generated results with less indication of tendon–specific changes; with data appearing inconsistently scattered throughout the duration of gestation (*see: Figure 12.a*). However, fetuses of or older than GD 200 largely exhibited consistently higher T_{Fmax} values in esSDFTs than in match–paired pCDETs ($n_{SDFT} = 5$, $n_{CDET} = 6$; *Figure 12.a*). Like trends seen among the relative T_d values of each tendon (*see: Figure 11*), this may have suggested a structural difference altering the relative T_{Fmax} values of the esSDFT and pCDET to have arisen toward the beginning of the 3rd trimester of development.

A one–way ANCOVA was conducted (*using R; version 4.2.2*) to determine whether a statistically significant difference existed between the T_{Fmax} values of the esSDFT and pCDET whilst controlling for gestational age. Gestational age was not found to have a significant impact on T_{Fmax} (*Figure 12.a; $p = 0.57$, $n_{SDFT} = 13$, $n_{CDET} = 14$*) and the rate of change in T_{Fmax} with increasing age was not found to significantly differ between the esSDFT and pCDET (*$p = 0.099$, $n_{SDFT} = 13$, $n_{CDET} = 14$*). However, the mean T_{Fmax} value of all esSDFTs (*at: 77.5°C ± 1.8*) was found to be significantly higher than that of all pCDETs (*72.5°C ± 1.5; Figure 12.b; $t = -2.11$, $p = 0.04$, $n_{SDFT} = 13$, $n_{CDET} = 14$*)

4.2.3 $NaBH_4$–Mediated Stabilization Treatment Increased the Mean T_{Fmax} and $t_{1/2}$ Values of Both the esSDFT and the pCDET Throughout the 2nd and 3rd Trimesters of Gestation

The tendon pairings of six fetuses were subjected to intermolecular cross–link stabilization treatment via sodium borohydride (*or: '$NaBH_4$'*) treatment. All tendons exhibited an increase

in their mean T_{Fmax} and $t_{1/2}$ values following $NaBH_4$ treatment (*see: Figure 13*), irrespective of tendon (*being esSDFT or pCDET*) and developmental trimester (*2nd nor 3rd*). The greatest increases in mean–T_{Fmax}–values following $NaBH_4$–mediated stabilization treatment belonged to the 2nd and 3rd trimester pCDET groupings, which exhibited increases in mean–T_{Fmax}–values from: 74.1°C ± 4.4 and 72.4°C ± 2.8 (*in the two control groupings*) to 89.1°C ± 1.4 and 87.3°C ± 2.5 following $NaBH_4$ treatment of the 2nd and 3rd trimester groupings, respectively (*paired two–sample t–tests: '2nd & 3rd'; t = -5.56 & -6.85, p = 0.02 & < 0.01, n = 3 & 3; Figure 13.a&b*). Similarly, $t_{1/2}$ saw its largest magnitude increase in the 3rd trimester pCDET grouping, which exhibited a non–significant increase from: 0.22 hours ± 0.13 in the control grouping to 3.28 hours ± 1.68 after stabilization treatment (*t = -3.15, p = 0.09, n = 3; Figure 13.d*). Moreover, pCDETs generally showed a greater increase in $t_{1/2}$ values than did esSDFTs, with the second largest increase mean–$t_{1/2}$–value following stabilization belonging to the 2nd trimester pCDET grouping, which increased from 0.32 hours ± 0.29 to 2.80 hours ± 0.77 following stabilization treatment (*t = -5.20, p = 0.02, n = 3; Figure 13.c*). In sum, $NaBH_4$ stabilization treatment largely appeared to convert pCDET tendons aged to both the 2nd and 3rd trimesters — which under natural conditions possessed relatively low mean–T_{Fmax}–values and often uninterpretable $t_{1/2}$ values (*as was the case in 7/16 cases*) — to tissues that not only 'survived' their temperature ramps to 90°C but also exhibited equivalent (*if not marginally higher*) $t_{1/2}$ values to their stabilized esSDFT counterparts (*the 2nd trimester mean–$t_{1/2}$–values for the pCDET versus esSDFT were: 2.80 hours ± 0.77 vs. 2.55 hours ± 0.77, respectively, and for the 3rd: 3.28 hours ± 1.68 vs. 3.01 hours ± 0.54; see: Figure 13.c&d*).

A series of paired two–sample t–tests revealed statistical significance among several additional findings to those described in the T_{Fmax} and $t_{1/2}$ values of 2nd and 3rd trimester pCDET groupings. First, t–tests showed the mean–T_{Fmax}–values of non–stabilized 2nd and 3rd trimester esSDFT–

groupings (*at: 83.8°C ± 2.8 & 88.5°C ± 1.4, respectively*) to naturally be significantly higher than those of their 2nd and 3rd trimester pCDET counterparts (*at: 74.1°C ± 4.4 & 72.4°C ± 2.8; paired two–sample t–tests: '2nd & 3rd' trimester pCDET groupings; t = 3.17 & 8.95, p = 0.04 & < 0.01, n = 3 & 3; Figure 13.a&b, as denoted in black*). Second, the mean–$t_{1/2}$–values of the esSDFT groupings were also shown to naturally increase from: (***i***) 0.56 hours ± 0.06 in the 2nd to (***ii***) 1.34 hours ± 0.14 in the 3rd trimester grouping (*t = -8.72, p = ≤ 0.01, n = 3; Figure 13.c→d, as denoted in purple*) while no such temporal increase was identified between pCDET groupings (*with pCDET groupings, from '2nd → 3rd', exhibiting: 0.32 hours ± 0.29 → 0.22 hours ± 0.13, t = 0.57, p = 0.61, n = 3; Figure 13.c→d*). Finally, the non–stabilized esSDFT grouping of the 3rd trimester was found to have a significantly larger mean–$t_{1/2}$–value under natural conditions (*at: 1.34 hours ± 0.14*) than its pCDET grouping counterpart (*at: 0.22 hours ± 0.13; t = 10.25, p ≤ 0.01, n = 3; Figure 13.d, denoted in black*).

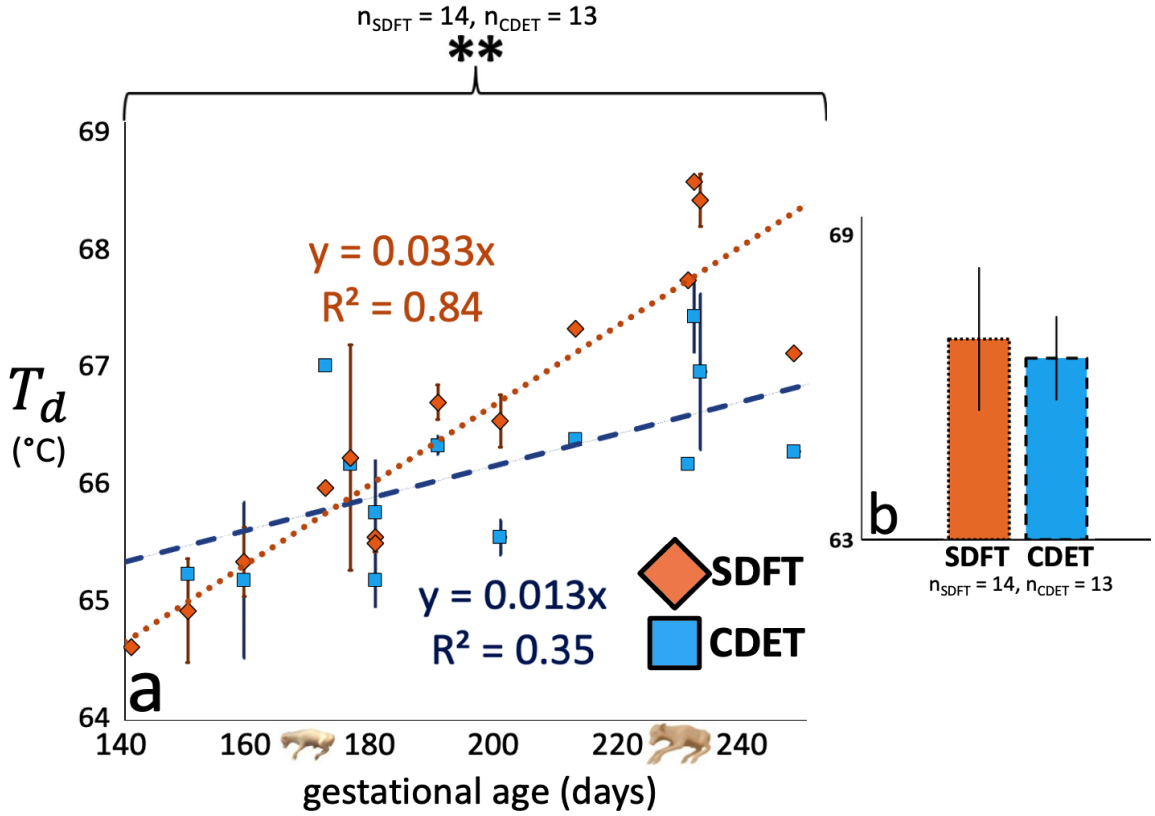

Figure 11: (**a**) The progression of denaturation temperature ('T_d') values (*in degrees Celsius;* '*°C*') of the energy storing superficial digital flexor tendon ('*esSDFT*') and positional common digital extensor tendon ('*pCDET*') during the 2nd and 3rd trimesters of development. Trendlines were based on data obtained from fourteen fetuses that were aged between gestational days ('*GDs*') 141 and 247. The $y = mx$ equation and R^2 value of each trendline were provided to two significant digits. A one–way ANCOVA revealed gestational age to have a significant impact on T_d ($p \leq 0.001$, $n_{SDFT} = 14$, $n_{CDET} = 13$) and the rate of T_d increase with age to be significantly higher in the esSDFT than in the pCDET ($p = 0.009$, $n_{SDFT} = 14$, $n_{CDET} = 13$) (**b**) The mean esSDFT and pCDET T_d values (*in °C*) of all tendons analyzed with no significant difference identified between the two groups (*paired two–sample t–test;* $t = -0.87$, $p = 0.39$, $n_{SDFT} = 14$, $n_{CDET} = 13$). Error bars represented ± standard deviation, indicating the variance among multiple subsamples (*from the opposite forelimb*) of the same fetus.

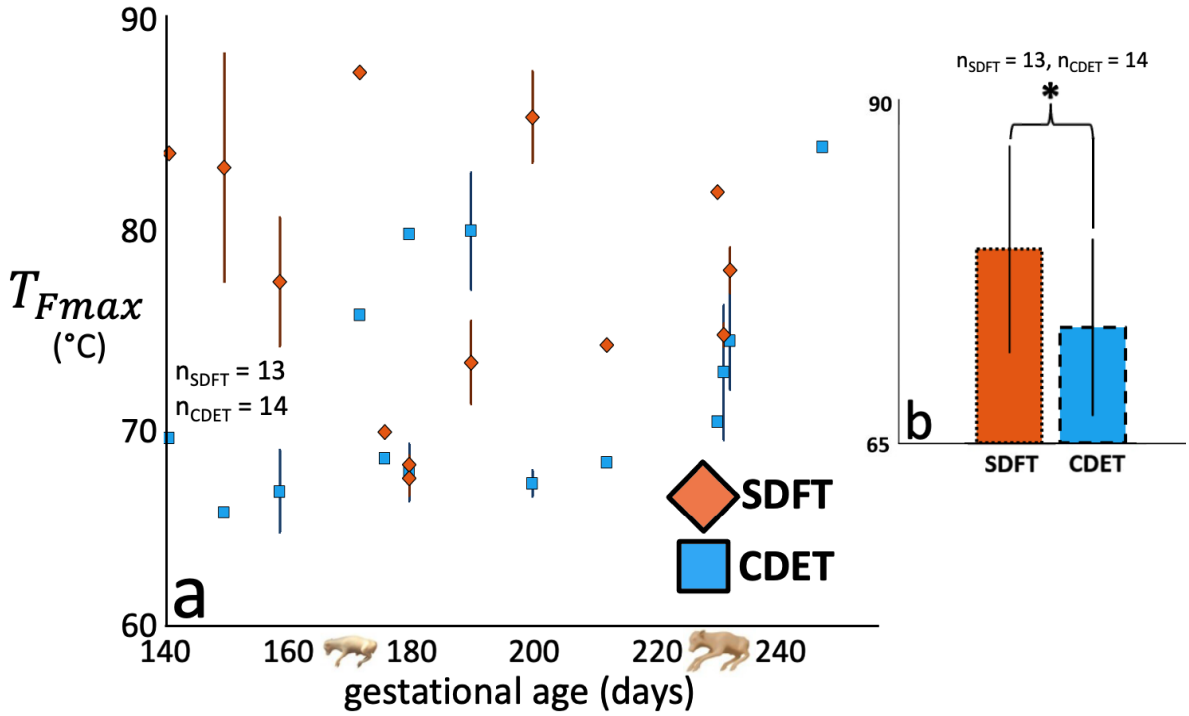

Figure 12: (**a**) The progression of temperature of maximum force generation ('T_{Fmax}') values (*in degrees Celsius;* '*°C*') of the energy storing superficial digital flexor tendon ('*esSDFT*') and positional common digital extensor tendon ('*pCDET*') during the 2nd and 3rd trimesters of development. A one–way ANCOVA revealed gestational age to not have a significant impact on T_{Fmax} ($p = 0.57$, $n_{SDFT} = 13$, $n_{CDET} = 14$) and the rate of T_{Fmax} increase to not significantly differ between the esSDFT and pCDET ($p = 0.099$, $n_{SDFT} = 13$, $n_{CDET} = 14$). (**b**) The mean esSDFT and pCDET T_{Fmax} values (*in* °C) of all tendons analyzed with a significant difference identified between the two groups (*paired two–sample t–test;* $t = -2.11$, $p = 0.04$, $n_{SDFT} = 13$, $n_{CDET} = 14$). Error bars represented ± standard deviation, indicating the variance among multiple subsamples (*from the opposite forelimb*) of the same fetus.

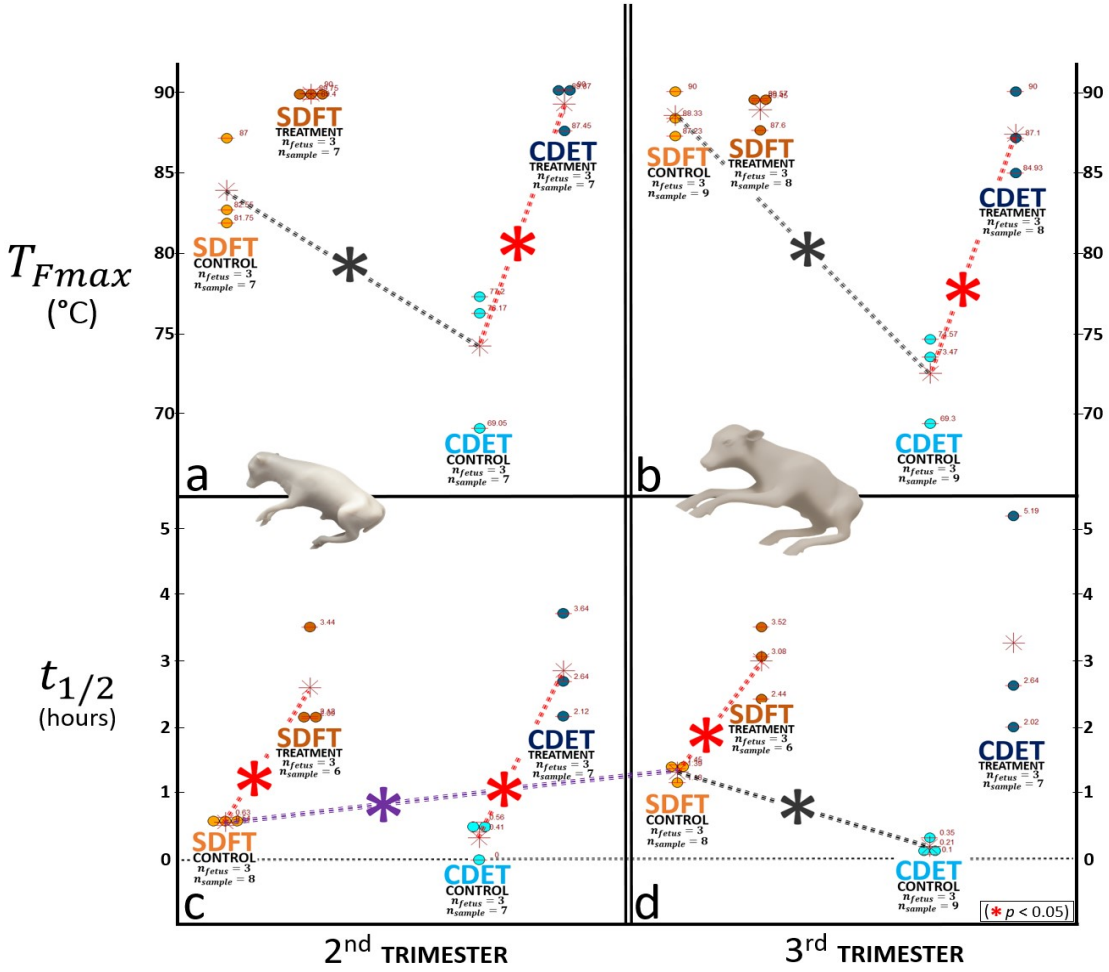

Figure 13: Dotplots of the: (***i***) temperature of maximum force generation– ('T_{Fmax}'; *in degrees Celsius;* '*°C*') and (***ii***) half–time of load decay ('$t_{1/2}$'; *in* '*hours*') values yielded: (***i***) before (*denoted as: 'CONTROL'; left-most in each trimester–tendon pairing*) and (***ii***) after (*as: 'TREATMENT'; right–most*) cross–link stabilization treatment via sodium borohydride ('$NaBH_4$') of the energy storing superficial digital flexor tendon ('*esSDFT*') and positional common digital extensor tendon ('*pCDET*') during the 2nd (*assigned to sub–figures* '**a.**' *and* '**c.**') and 3rd (*to sub–figures* '**b.**' *and* '**d.**') trimesters of fetal development. The central asterisks were deployed to denote significant differences between: (***i***) CONTROL and TREATMENT groupings within each tendon–trimester coupling under study (*as was signified in red*), (***ii***) the same treatment condition (*CONTROL or TREATMENT*) in the other functionally distinct tendon ('*FDT*', *hereafter*) within the same trimester grouping (*in black*), and (***iii***) the mirrored tendon–treatment grouping in the other trimester under study (*in purple*; *all of which were taken as being significant at:* $p \leq 0.05$). The sample size pertaining to each dataset was given below its corresponding boxplot: with 'n_{fetus}' representing the number of distinct fetuses that contributed to the data associated with a given boxplot, and 'n_{sample}' the number of cumulative subsamples from all fetuses. Data was comprised of the tendons of six distinct fetuses that were aged to: gestational day ('*GD*', *hereafter*) 150, GD 163, and GD 180 (*mean:* ***164 GDs***) for the 2nd trimester, and: GD 196, GD 202, and GD 204 for the 3rd (*mean:* ***201 GDs****; with GD ~283 representing full term*).

4.3 Mean Collagen Fibril Diameter was Lower in the esSDFT Than in the pCDET Throughout Gestation

Collagen fibril diameter ('*CFD*', *hereafter*) was analyzed in fourteen fetal specimens of eleven distinct gestational ages. These included eight samples from fetuses that were aged to the 2nd trimester of gestation and six samples from fetuses that were aged to the 3rd trimester. All collagen fibril distributions appeared unimodal irrespective of gestational age or tendon class (*see: Figures 14, 15 & 16*). Further, mean CFD was found to be lower in esSDFTs than in match–paired pCDETs across all eleven gestational ages that were analyzed (*see: Figure 18*).

Two–sample Kolmogorov–Smirov ('KS') tests were conducted to assess for statistical differences between the CFD distributions of the energy storing esSDFT and pCDET pairings at each gestational age that was analyzed (*see: Figure 16*). KS tests revealed statistically significant differences between the esSDFT and pCDET CFD distributions in all fourteen specimens studied (*Figure 16; $D = 0.112 - 0.824$, $p = \leq 0.001$*).

Results also suggested the rate of CFD increase to be lesser in the esSDFT than in the pCDET during the 2nd and 3rd trimesters of gestation (*see: Figure 18*). This was indicated by the lesser slope of the trendline that was associated with results from analysis of the esSDFT than pCDET samples (*Figure 18*). A one–way ANCOVA was conducted (*using R; version 4.2.2*) to determine whether a statistically significant difference existed between the mean CFD values of the esSDFTs and pCDETs analyzed whilst controlling for gestational age. Gestational age was found to have a significant impact on mean CFD (*Figure 18; $p \leq 0.001$, $n = 14$*) but the rate of change of mean CFD with increasing age was not found to significantly differ between the esSDFT and pCDET ($p = 0.319$, $n = 14$).

The standard deviation ('*SD*') values of esSDFT and pCDET samples analyzed were also

considered as measures of CFD variation. In all but one sample pairing (*being: the sample aged to GD 100; with: esSDFT SD = 3.51 nanometers ('nm') and pCDET SD = 3.15 nm*) the esSDFTs consistently exhibited lower SD values than did their match–paired pCDETs (*see: Figure 19; n = 14*). This plausibly suggested the diameter of collagen fibrils to be more highly regulated in esSDFTs than in pCDETs during gestational development. In further investigation, a one–way ANCOVA was conducted (*using R; version 4.2.2*) to determine whether a statistically significant difference existed between the SD values of the esSDFT and pCDET samples whilst controlling for gestational age. Gestational age was found to have a significant impact on SD (*Figure 19; $p \leq 0.001$, $n = 14$*) but the rate of change of SD with increasing age was not found to significantly differ between the esSDFT and pCDET ($p = 0.094$, $n = 14$).

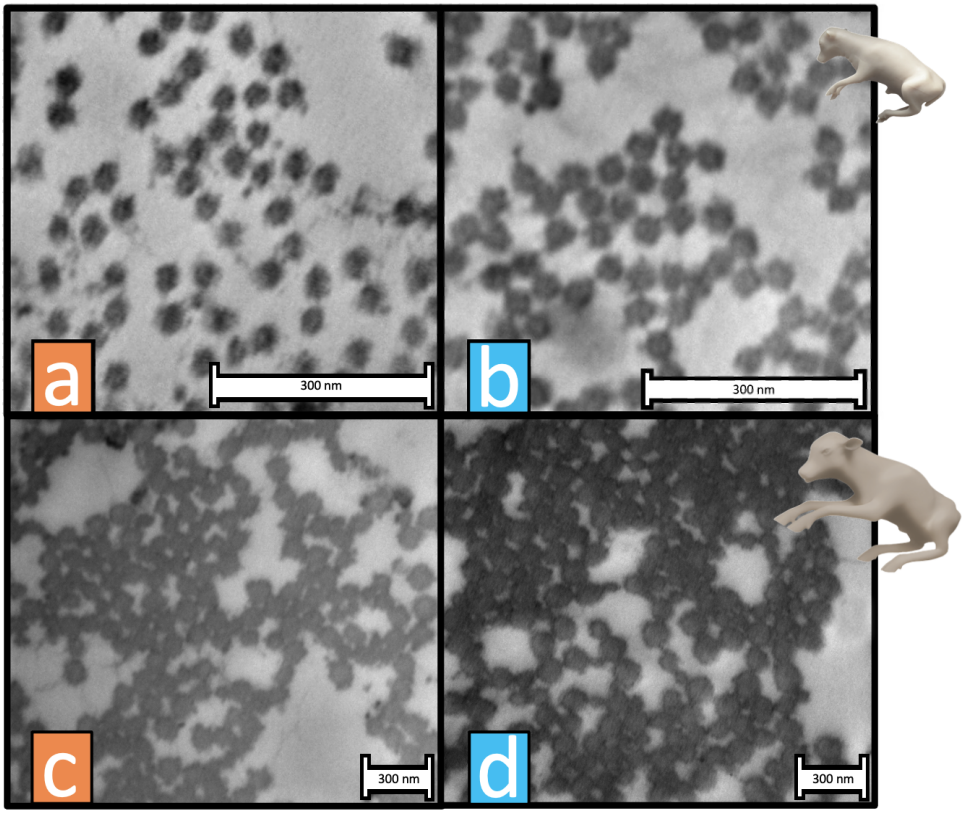

Figure 14: Representative transmission electron microscopy ('*TEM*') images that were used in the generation of fibril diameter distributions and calculation of mean collagen fibril diameter ('*CFD*', *hereafter*). Images marked in orange correspond to those obtained from energy storing superficial digital flexor tendons ('*esSDFTs*') while those marked in blue were obtained from positional common digital extensor tendons ('*pCDETs*'). Images '***a***' and '***b***' are of a fetus that was aged to gestational day ('*GD*', *hereafter*) 100, while images '***c***' and '***d***' were obtained from a GD 232 fetus. Scale bars approximating 300 nanometers ('*nm*') are provided within each image.

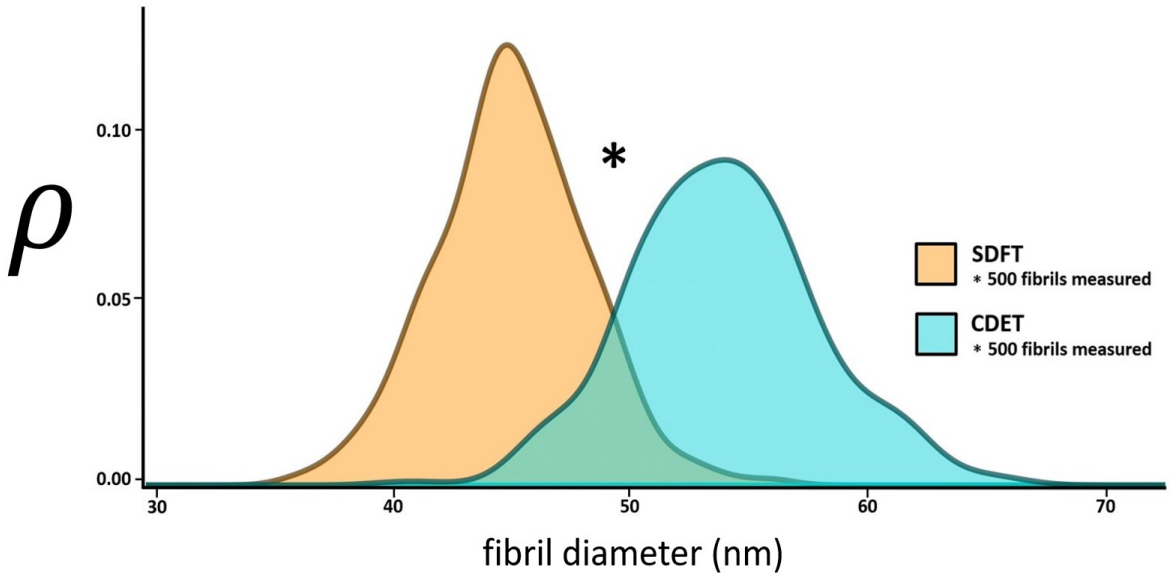

Figure 15: A representative pair of collagen fibril diameter ('*CFD*', *hereafter*) distributions (*with: density* ('ρ') *on the y-axis*) corresponding to a fetus that was aged to gestational day ('*GD*', *hereafter*) 180 (*with: GD ∼283 representing full term*). CFDs were obtained via transmission electron microscopy ('*TEM*') analysis of tendons at 100,000× magnification and five hundred fibrils were considered per tendon. The orange shaded distribution represented collagen fibrils measured from the energy storing superficial digital flexor tendon ('*esSDFT*') while the blue shaded distribution represented fibrils measured from the positional common digital extensor tendon ('*pCDET*'). The central asterisk denoted the significant result of a Kolmogorov–Smirov ('*KS*') test ($p \leq 0.001$).

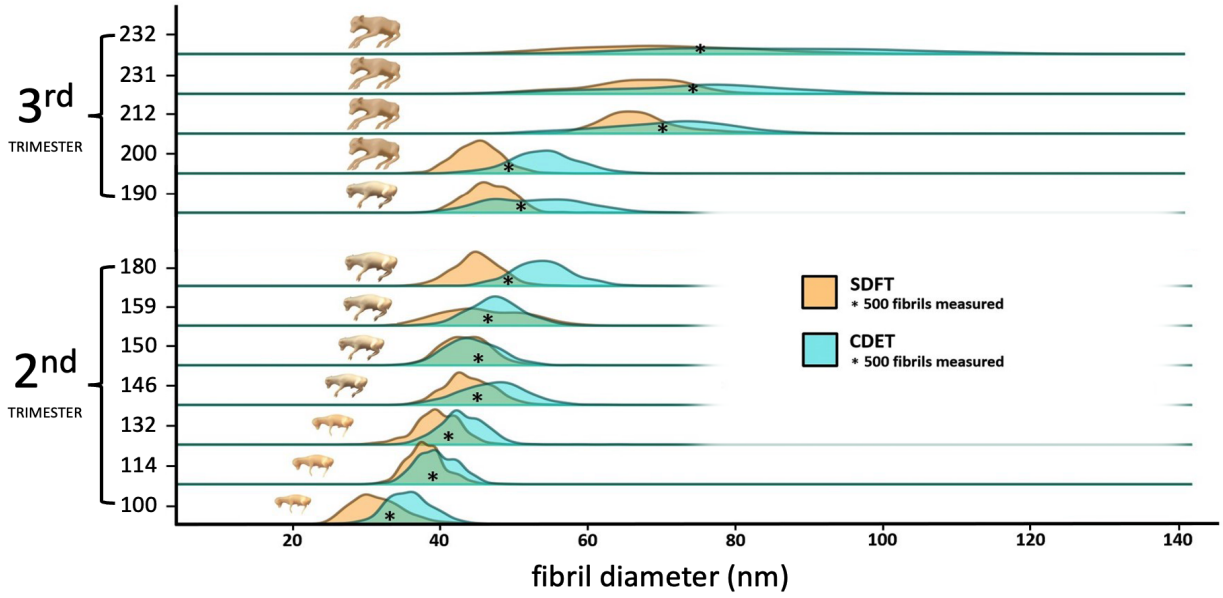

Figure 16: The collagen fibril diameter (‘*CFD*’, *hereafter*) distributions of the energy storing superficial digital flexor tendon (‘*esSDFT*’*; shaded in orange*) and positional common digital extensor tendon (‘*pCDET*’; *blue shaded*) corresponding to twelve distinct fetuses aged to: gestational day (‘*GD*’, *hereafter*) 100, GD 114, GD 132, GD 146, GD 150, GD 159, GD 180, GD 190, GD 200, GD 212, GD 231, and GD 232 (*with: GD ∼283 representing full term*). CFDs were obtained via transmission electron microscopy (‘*TEM*’) analysis of tendons at 10,000× to 150,000× magnification and five hundred fibrils were considered per tendon per gestational age. Analyses of two additional fetuses aged to: GD 180 and GD 231 were omitted from this plot to aid in visual clarity. The central asterisks were deployed to denote significant results of Kolmogorov–Smirov (‘*KS*’) tests (*all of which yielded* $p \leq 0.001$*;* $D = 0.112 - 0.824$).

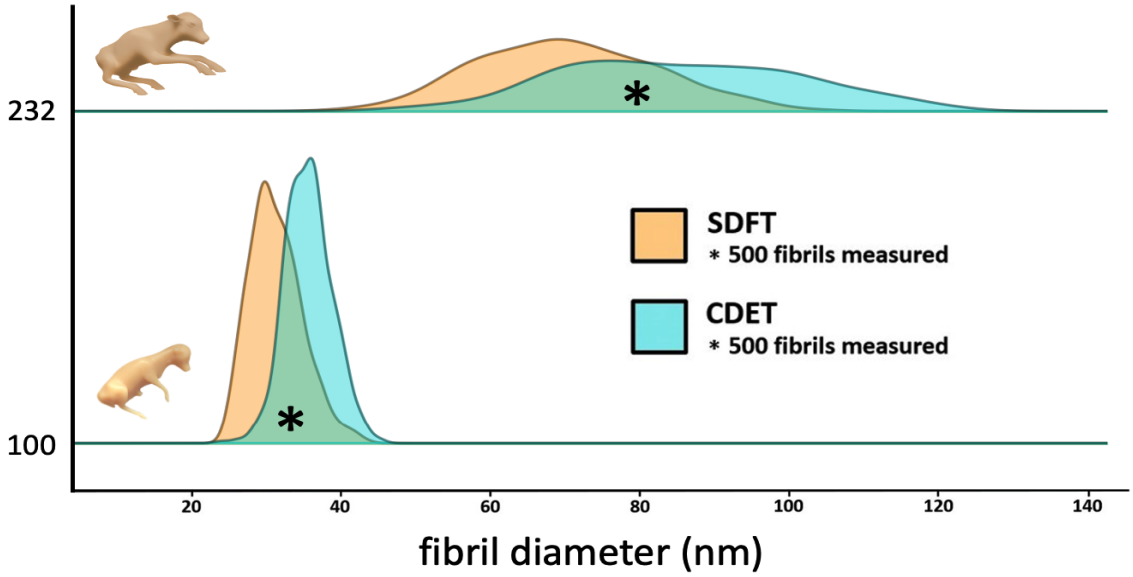

Figure 17: The collagen fibril diameter ('*CFD*', *hereafter*) distributions of the energy storing superficial digital flexor tendon ('*esSDFT*'*; shaded in orange*) and positional common digital extensor tendon ('*pCDET*'; *blue shaded*) corresponding to tendons from the youngest (aged to: gestational day ('*GD*', *hereafter*) 100) and eldest (*GD 232*) fetuses analyzed (*with: GD ∼283 representing full term*). CFDs were obtained via transmission electron microscopy ('*TEM*') analysis of tendons at 10,000× to 150,000× magnification and five hundred fibrils were considered per tendon per gestational age. The central asterisks were deployed to denote significant results of Kolmogorov–Smirov ('*KS*') tests (*both of which yielded* $p \leq 0.001$).

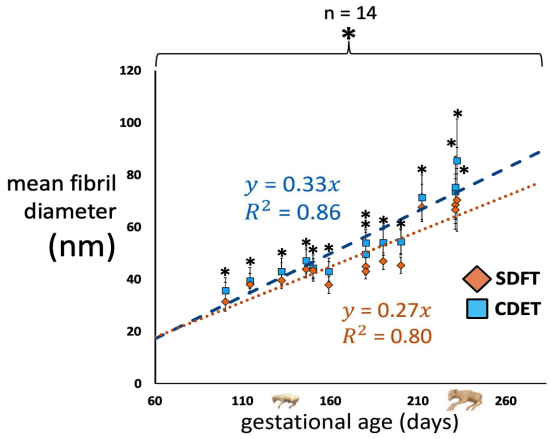

Figure 18: The progression of mean collagen fibril diameter ('*CFD*', *hereafter*; *in nanometers;* '*nm*') of the energy storing superficial digital flexor tendon ('*esSDFT*') and positional common digital extensor tendon ('*pCDET*') during the 2nd and 3rd trimesters of fetal development. Trendlines were based on data obtained from fourteen samples of each FDT that were aged between gestational days ('*GD*') 100 and 232. CFDs were obtained via transmission electron microscopy ('*TEM*') analysis of tendons at 10,000× to 150,000× magnification and five hundred fibrils were considered per tendon per gestational age. The $y = mx$ equation and R^2 value of each trendline were provided to two significant digits. A one–way ANCOVA revealed gestational age to have a significant impact on mean CFD ($p \leq 0.001$, $n = 14$) but the rate of mean CFD increase to not significantly differ between the esSDFT and pCDET ($p = 0.319$, $n = 14$). The central asterisks were deployed to denote significant results of paired two–sample t–tests between tendons (*all of which yielded* $p \leq 0.001$, $n = 14$). Error bars were ± standard deviation.

Figure 19: The progression of standard deviation ('*SD*', *in nanometers;* 'nm') of CFD distributions of the energy storing superficial digital flexor tendon ('*esSDFT*'*; represented in orange*) and positional common digital extensor tendon ('*pCDET*'*; in blue*) during the 2nd and 3rd trimesters of development. Trendlines were based on data obtained from fourteen samples of each FDT that were aged between gestational days ('*GD*') 100 and 232. CFDs were obtained via transmission electron microscopy ('*TEM*') analysis of tendons at 10,000× to 150,000× magnification and five hundred fibrils were considered per tendon per gestational age. The $y = mx$ equation and R^2 value of each trendline were provided to two significant digits. A one–way ANCOVA revealed gestational age to have a significant impact on the standard deviation of CFD ($p \leq 0.001$, $n = 14$) but the rate of increase of standard deviation of CFD to not significantly differ between the esSDFT and pCDET ($p = 0.094$, $n = 14$). Error bars were ± standard deviation.

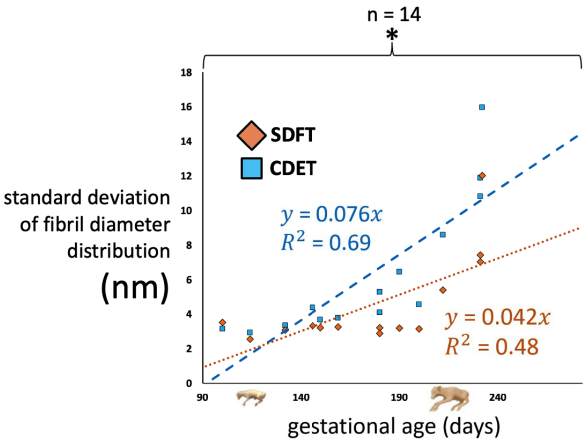

4.4 Collagen Fibril Crimp Became Better Ordered and More Regular in the esSDFT Than in the pCDET Toward the End of Gestation

Collagen fibril crimp (‘*CFC*’ *hereafter*) was investigated between the FDTs in four fetuses that were sampled from three distinct gestational ages. These four fetuses included two that were aged to the 2nd trimester (*of: GDs: 106 and 141*) and two aged to the 3rd (*GDs: 245 and 247; see Figure 22*). A longer mean CFC wavelength was found in esSDFTs (*at: a mean of 52.81 micrometers (‘µm’) ± 23.61 standard deviation; ‘SD’*) than in pCDETs (*averaging 41.91 µm ± 19.72 SD; see: Figures 20 & 22.b; n = 4*). However, visualized undulations generally appeared to be both better ordered and more regular within the 3rd trimester esSDFTs relative to in their match–paired pCDETs (*see: Figure 21*).

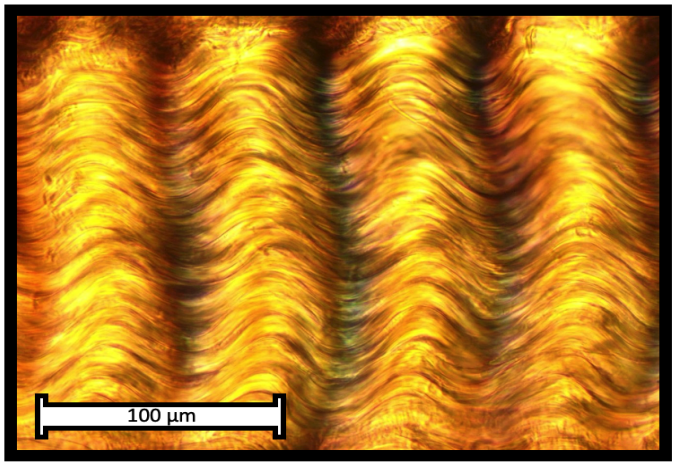

Figure 20: The longitudinal undulations (*and perhaps: ‘crimp’*) that were visualized in the collagen fibrils of an energy storing superficial digital flexor tendon (‘*esSDFT*’) from a fetus that was aged to gestational day (‘*GD*’) 247. This esSDFT was sectioned to 30 micrometers (‘µm’) and was visualized using polarized light microscopy (‘*PLM*’) at 10× magnification.

A one–way ANCOVA was conducted (*using R; version 4.2.2*) to determine whether a statistically significant difference existed between the mean CFC wavelength values of the esSDFT and pCDET samples while controlling for gestational age. Gestational age was found to have a significant

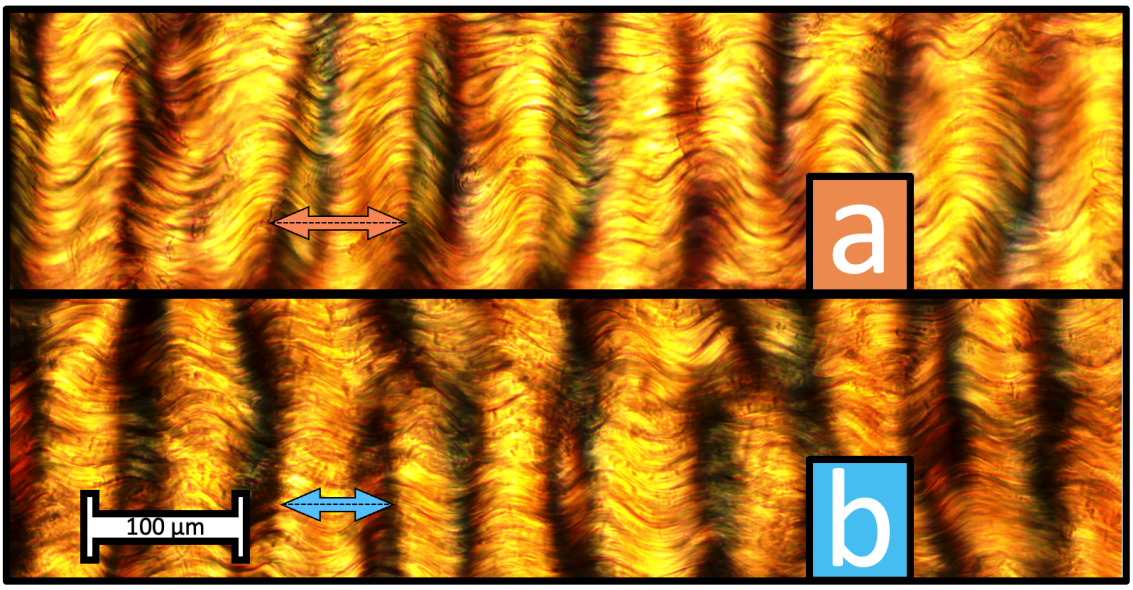

Figure 21: The collagen fibril crimp ('*CFC*', *hereafter*) that was visualized in the: (**a**) energy storing superficial digital flexor tendon ('*esSDFT*') and (**b**) positional common digital extensor tendon ('*pCDET*') of a female fetus that was aged to gestational day ('*GD*') 247. These images were obtained via polarized light microscopy ('*PLM*') evaluation at 10× magnification. Two representative measurements of CFC wavelength were given by the tips of two arrows within the sub–figures (*an orange arrow pertaining to the esSDFT, and a blue arrow to the pCDET*). A scale bar approximating 100 micrometers ('*µm*'; *applying to both images*) was provided.

impact on mean CFC wavelength (*Figure 22.a; $p \leq 0.001$, $n = 4$*) but the rate of change of mean CFC wavelength with increasing age was not found to significantly differ between the esSDFT and pCDET ($p = 0.27$, $n = 4$). Similarly, the mean CFC wavelength values of all esSDFTs (*at: 52.81 µm ± 23.61 SD*) and pCDETs (*41.91 µm ± 19.72 SD*) analyzed were not found to significantly differ (*Figure 22.b; $t = -0.71$, $p = 0.51$, $n = 4$*).

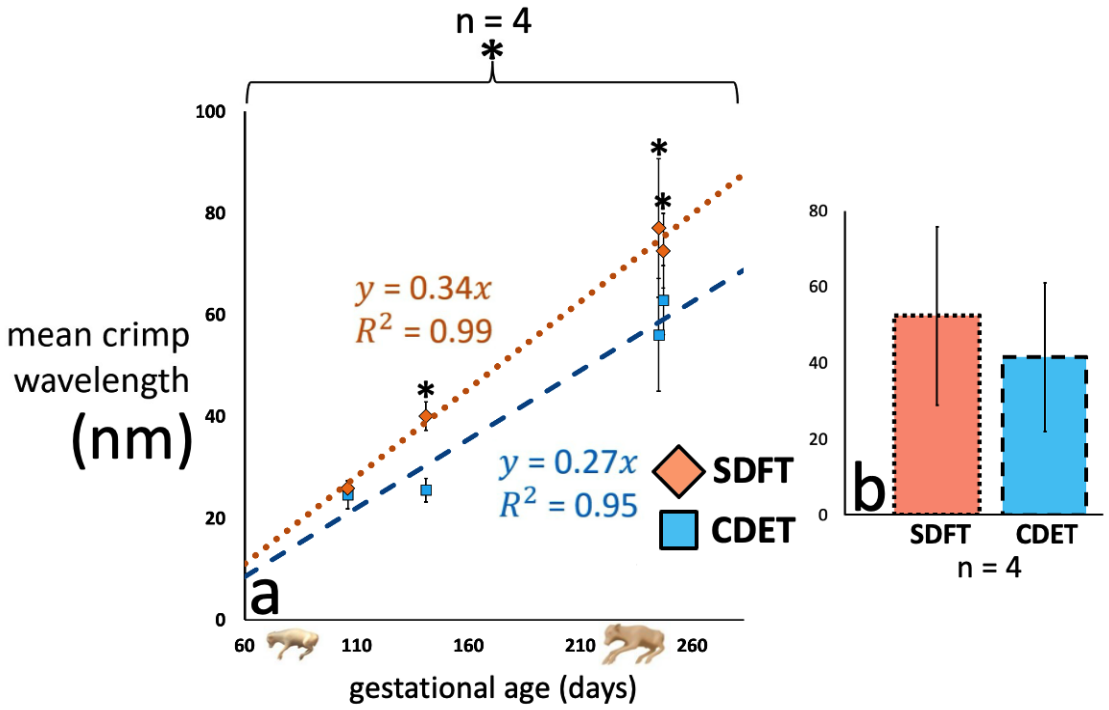

Figure 22: (**a**) The progression of mean collagen fibril crimp ('*CFC*', *hereafter*) wavelength values (*in micrometers*; '*µm*') of the energy storing superficial digital flexor tendon ('*esSDFT*'; *represented in orange*) and positional common digital extensor tendon ('*pCDET*'; *in blue*) during the 2nd and 3rd trimesters of fetal development. Trendlines were based on data obtained from four fetuses that were aged between gestational days ('*GDs*') 106 and 247. The $y = mx$ equation and R^2 value of each trendline were provided to two significant digits. A one–way ANCOVA revealed gestational age to have a significant impact on mean CFC wavelength ($p \leq 0.001$, $n = 4$) but the rate of increase of mean CFC wavelength to not significantly differ between the esSDFT and pCDET ($p = 0.27$, $n = 4$). The central asterisks were deployed to denote significant results of paired two–sample t–tests between tendons ($p \leq 0.05$). (**b**) The mean esSDFT and pCDET CFC wavelength values (*in* '*µm*') of all tendons analyzed with no significant difference identified between the two groupings (*paired two–sample t–test;* $t = -0.71$, $p = 0.51$, $n = 4$). Tendons were visualized at 10× magnification under polarized light microscopy ('*PLM*') and approximately two hundred measurements of CFC wavelength were made per tendon. Error bars were ± standard deviation, and in subfigure (**a**) served to represent the variance in mean CFC wavelength values that was seen between triplicate samplings of the same tendon from an individual animal.

5 Discussion

5.1 Discussion Associated with Intermolecular Cross–Linking

5.1.1 T_d Results May Signal a Higher Rate of Intermolecular Cross–Link Deposition in the esSDFT Than in the pCDET as Gestation Progresses

Rising denaturation temperature (*or: 'T_d'*) values during gestation in both the energy storing esSDFT and pCDET may signal increasingly dense molecular packing[114,141] brought about by rising populations of intermolecular cross–links between the collagen molecules within each tendon[2] as fetal development progresses (*see: Figure 11.a; for more on the biomechanics underlying this conclusion, see the section: Methods: Structural Assessment; or: 'M:SA', hereafter*).[114,231] Additionally, the relatively high T_d values of the esSDFT samples belonging to the 3rd trimester over those of their match–paired pCDET samples might suggest a comparatively high presence of intermolecular cross–links within esSDFT samples relative to within pCDET samples to have first emerged toward the midpoint of gestation (*Figure 11.a; M:SA*).[114,231] Generally, the result that disparity in T_d arises between the functionally distinct tendons ('*FDTs*', *hereafter*) during gestation corroborates the findings of a past study,[231] and also aligns with the relatively high presence of intermolecular cross–links in the esSDFT over that seen in the pCDET in tissue maturity.[19,40,104,231] Taken together, these findings may indicate the: (***i***) comparatively high cellularity[235,290] or (***ii***) low collagen turnover[7,22,89,129,252] of fully–developed esSDFTs in relation to their pCDET counterparts to also apply prenatally.

An increasing presence of intermolecular cross–links in both the esSDFT and pCDET as prenatal development proceeds seems logical.[62,230] The lysyl oxidase ('LOX') enzymes (*lysyl oxidase–like '1' to '4', included*) that are imperative to intermolecular cross–link formation[6] may have greater opportunity to affix a larger proportion of neighbouring collagen molecules to one

another as gestation progresses.[6,62,71] In turn, this reaction could serve to hinder the conformational entropy of each affixed collagen molecule[6,169] and raise overall sample T_d.[6,114] Moreover, in consideration of the even greater restriction on molecular entropy trivalent intermolecular cross–links may impose by reducing the conformational freedom of a third participating collagen molecule (*see: Figure 4*),[6,62] the entropy of each molecule may be further decreased (*and T_d further increased*) by the potential maturation of some divalent (*or: 'immature'*) intermolecular cross–links into their mature ('*trivalent*') successors during the 2nd and 3rd trimesters of fetal development (*see: Figure 5*).[60,234]

An increase in the presence of intermolecular cross–links over gestational time may also confer parallel increases in tendon: (***i***) elastic modulus,[162,182] (***ii***) strength,[100,201] and (***iii***) resilience.[71] The mechanical properties of tendons have been found to increase dramatically during gestation,[161] and multiple studies have shown this elaboration to be hindered in the event of LOX enzyme inhibition.[162,182] Similarly, an absence of LOX enzymes has been found to halt the developmental progress of *in–vitro* tendon–like constructs: resulting in weaker materials comprised of highly disorganized collagen.[103]

While literature on the progression of intermolecular cross–linking during gestation is limited, the notion of a steady increase in enzymatic intermolecular cross–links until birth (*see: Figure 11.a*; *M:SA*) has been both supported[6,230,275] but also refuted[210,213] by previous postnatal research. In fact, the overall population of intermolecular cross–links in a given tendon may actually *decrease* in early postnatal life[210,234] and so the assumption that the presence of intermolecular cross–links should increase linearly throughout the 2nd and 3rd trimesters of fetal development (*in parallel with T_d*) may be unwarranted (*Figure 11.a*). In support of a possible decrease in the presence of intermolecular cross–links postnatally, the mean–T_d–values of each tendon in the 3rd trimester of

gestation in the present study — *at* approximately: ∼67.1 °C ± 0.3 and ∼66.1 °C ± 0.2 in the esSDFT and pCDET, respectively (*see:* Figure 11) — are marginally higher than those values (*of: 65.4 °C ± 0.7 and 62.7 °C ± 0.4*) that have previously been reported for each of the FDTs in bovine (*or: cattle*; *Bos taurus*) maturity.[104] This finding supports the notion that some of the late term fetal tendons under present study may indeed have possessed a greater presence of intermolecular cross–links than their fully–developed counterparts (*in alignment with Stammers et al. 2020*[234]).

A greater rate of intermolecular cross–link deposition in the esSDFT than in the pCDET during gestation may serve to assist in preparing the esSDFT[54,173,201] for the particularly substantial loading the EST experiences throughout postnatal life (*see:* Figure 11).[22,236,251] Indeed, a high degree of intermolecular cross–linking has previously been held to result in a more cohesive tissue that is better able to draw on the mechanical contributions afforded by all of its constituent molecules,[54] without as much risk of damage originating from molecular slippage.[6,173,201] In light of this, a greater presence of intermolecular cross–links within the esSDFT than in the pCDET could play a role in the high fatigue resistance of the esSDFT over the pCDET in tissue maturity.[10,89,104,253] However, discordance exists between: (***i***) some of the other mechanical properties that have been proposed to be conferred by a relatively high degree of intermolecular cross–linking,[60] and (***ii***) the well documented mechanical properties of the fully–developed esSDFT relative to those of the fully–developed pCDET.[19,104] For example, a greater presence of intermolecular cross–links in tendon has also previously been shown to increase both collagen fibril: (***i***) stiffness[60] and (***ii***) strength[98] — making the notion of more extensive intermolecular cross–linking in the esSDFT than in the pCDET (Figure 11)[19,40,104] curious, given the relatively low: (***i***) elastic modulus[19,208,225,253] and (***ii***) failure stress[104,187] of the fully–developed esSDFT compared to its pCDET counterpart. This discrepancy may serve to highlight the substantial role

other structural features aside from intermolecular cross–links (*such as collagen fibril diameter; 'CFD', hereafter*[187,253]) can play in the determination of select mechanical properties of the two classes of FDTs.

The indication of a notably high presence of intermolecular cross–links in the esSDFT over the pCDET toward the end of gestation (*see: Figure 11.a*), could be the result of a comparatively large mean surface–area–to–volume ratio of collagen fibrils within the esSDFT relative to within the pCDET throughout the 2nd and 3rd trimesters of gestation.[62,143] Particularly, a large mean fibril surface–area–to–volume ratio within the developing fetal esSDFT could plausibly result from comparatively inhibited lateral fibril growth within the fetal esSDFT relative to within its pCDET counterpart.[19,243] Indeed, should the mean CFD of each tendon at the fetal stage mirror that relationship previously documented in tissue maturity* (*as indicated presently; see: Figure 16*), a greater proportion of the collagen molecules that comprise each fibril of the developing esSDFT may be made available for chemical interaction with the LOX enzymes imperative to intermolecular cross–link formation than that proportion made available in the pCDET.[62,143] As such, recent findings from Leighton et al. (2021)[143] suggest LOX enzymes to be too large (*at approximately ∼7.4 nm in diameter*) to diffuse into the only very slight pores found between collagen molecules that have been organized into collagen fibrils (*at ∼2 nm*[62]) and so LOX enzymes may only be able to function toward the periphery of a given fibril as it grows.[62,143,255] Accordingly, a relatively large mean surface–area–to–volume ratio of collagen fibrils within the developing esSDFT over that of those within its neighbouring pCDET arising from a comparatively slow accretion of collagen molecules to the surface of each fibril in the esSDFT may be more conducive

in tissue maturity, the collagen fibrils within the esSDFT are well documented to be of smaller mean diameter than in the fully developed pCDET[19,104,203,243]

to the formation of intermolecular cross–links[62,143] and give rise to the notably high T_d values seen among the developing esSDFTs under present evaluation (*see: Figure 11.a*).

Previous research that has attempted to associate the degree of enzymatic intermolecular cross–linking in a given tendon with its macroscale mechanical properties has often come up short of drawing strong correlations,[22,47,251] and so the presence of confounding effects on T_d should also be considered.[208] Perhaps the most likely alternative explanation for the higher rate of increase in T_d seen in the esSDFT than in the pCDET during gestation is the potential presence of non–enzymatic inter–fibril cross–links that instead originate from a greater presence of other, non–collagenous–molecules in the esSDFT over the pCDET (*see: Figure 11.a*).[161,163,211] In particular, the glycosaminoglycan side chains of small leucine–rich proteoglycans ('*SLRPs*') are held to be able to cross–link the molecules of adjacent collagen fibrils[112,217] and, in doing so, can serve to: (***i***) reduce the entropy of the collagen molecules the SLRPs interact with, and (***ii***) increase the denaturation temperature of each participating collagen molecule, in the same manner as enzymatic intermolecular cross–links under present study.[6,114] In alignment with this, glycosaminoglycan content has previously been indicated to be greater in the esSDFT than in the pCDET in tissue maturity,[10,248,252] and so a potential contribution of non–collagenous molecules in mediating the relative T_d values seen presently may merit further investigation (*Figure 11.a*).

5.1.2 T_{Fmax} Results Suggest a Greater Presence of Thermally Stable Intermolecular Cross–Links in the esSDFT Than in the pCDET During Gestation

The result that the T_{Fmax} values of esSDFT samples and pCDET samples remain similar throughout the 2nd and 3rd trimesters of fetal development may suggest a steady presence of thermally stable (*or: 'divalent ketoamine–'; or: 'trivalent'*) intermolecular cross–links in both of

the FDTs throughout gestation (*see: Figure 12.a; M:SA*)†.[104,231] Additionally, the finding of a higher mean–T_{Fmax}–value among esSDFT samples than among their pCDET counterparts might indicate a greater presence of thermally stable intermolecular cross–links in the esSDFT than in the pCDET during fetal development (*see: Figure 12.b; M:SA*).[231] This result would further reinforce the findings of the previous study of bovine fetuses,[231] that — in addition to commenting on gestational disparity in T_d — also presented the finding that esSDFT samples possessed a greater presence of thermally stable intermolecular cross–links than their pCDET counterparts throughout the 2nd and 3rd trimesters of gestation.[231] This result may also suggest the relatively high presence of thermally stable intermolecular cross–links previously reported in the esSDFT over the pCDET in tissue maturity[17,104] to first arise prenatally. A more substantial presence of thermally stable intermolecular cross–links in the esSDFT than in the pCDET during fetal development could result from the same characteristics theorized to give rise to relatively high T_d: (***i***) high cellularity[235,290] or (***ii***) low collagen turnover[7,22,89,129,252] in the esSDFT relative to in the pCDET, gestationally.

The apparent absence of any significant increase in the T_{Fmax} values of the two FDTs during fetal development (*see: Figure 12.a*) may signal: (***i***) little, if any, increase in the presence of divalent ketoamine intermolecular cross–links, or (***ii***) maturation of divalent inter-collagen cross–links into their thermally–stable ('*trivalent*') successors in either tendon during gestation (*see: Figure 5; and M:SA*).[70,104,274] However, a steady presence of divalent ketoamine intermolecular cross–links (*as in* '***i***') would, at least initially, appear to defy other results from the earlier T_d analysis (*see: Figure 11*). Indeed, rising T_d values in both the esSDFT and pCDET over the 2nd and 3rd trimesters of

†*though a slight increase in T_{Fmax} values over gestational time may actually have existed (see: Figure 12.a)*

fetal development were previously taken to signal an increase in the presence of intermolecular cross–links during gestation, for which an increase in divalent ketoamine intermolecular cross–links would intuitively be partly responsible (*see: Figure 11.a; 'T_d Results May Signal...'*).[2,104,114,141] Applied presently, an increased presence of divalent ketoamine intermolecular cross–links over gestational time could be responsible for the slight indication of an increase (*albeit non–significant*) in the T_{Fmax} values exhibited over the 2nd and 3rd trimesters of development (*Figure 11.a; M:SA*). Conversely, little indication of maturation of divalent intermolecular cross–links into trivalent cross–links during gestation (*or '**ii**'*) may accurately reflect the complex, multi–step chemical processes that give rise to trivalent cross–link species[6] (*see: Figure 5*) to be unachievable during the limited time frame afforded by gestation. In support of the idea of a functional absence of '*mature*' cross–links in the fetal tendons under present study, the presence of select species of mature (*or: 'trivalent'*) intermolecular cross–links have previously been reported to be negligible at birth compared to at tissue maturity.[85,165,234]

There may be good reason to speculate that the indication of an increasing presence of intermolecular cross–links in both tendons throughout the 2nd and 3rd trimesters of gestation‡ is predominantly a result of a formation of divalent aldimine rather than divalent ketoamine cross–links (*see: Figure 5*).[6,62,104] In particular, the sole formation of divalent aldimine intermolecular cross–links during the gestational development of the two FDTs might occur because enzymes of the lysyl hydroxylase ('*LH*') family may have limited opportunity to hydroxylate the collagen molecules participating in cross–links[6,62] prior to the formation of any intermolecular cross–links during fetal development. Here, the creation of the two major thermally labile divalent aldimine

‡*an increasing presence of intermolecular cross–links in both tendons during gestation was suggested by rising T_d values (see: Figure 11.a and M:SA)*

cross–links found in tendon are unique in requiring either: (***i***) minimal (*in the case of dehydro–hydroxylysino–norleucine*) or (***ii***) no (*with respect for dehydro–lysino–norleucine*) prior lysine hydroxylation of the telopeptide or alpha helix residues that participate in their formation (*Figure 5*).[62,166] This trait most likely makes the two divalent aldimine cross–links those cross–links that require the least amount of chemical modulation to the tendon tissue's native collagen structure in their formation,[6,62,166] and so the two aldimine cross–links may be the most easily formed and prevailing cross–links in new, prenatal tendon tissue. In contrast to the straightforward formation of the aldimines, the creation of the two major divalent ketoamine intermolecular cross–links found in tendon, being: (***i***) *lysino–keto–norleucine and (**ii**) hydroxylysino–keto–norleucine*, require earlier lysine hydroxylation of at least one of their cross–link–participating telopeptide or alpha helix residues (*Figure 5*).[62,166] Accordingly, this prerequisite could increase the complexity of the formation of the two ketoamine cross–links, and perhaps decrease their presence in developing tendon tissue. Thus, the notion of an increasing presence of intermolecular cross–links over gestational time stemming primarily from the prenatal formation of divalent aldimine rather than divalent ketoamine or trivalent cross–links could align with the results of the current T_d and T_{Fmax} analyses (*see: Figure 11; Figure 12; M:SA*).

The mean–T_{Fmax}–values of developing esSDFTs (*at: 77.5°C ± 1.8*) and developing pCDETs (*72.5°C ± 1.5*) may serve as additional evidence that any increase in the presence of intermolecular cross–links that occurs during gestation should be attributed principally to the formation of divalent aldimine intermolecular cross–links (*see: Figure 12.b; Figure 5*).[2,70] In particular, the mean–T_{Fmax}–values of the fully developed esSDFT and pCDET were previously reported to be >90°C and 75.1°C ± 2.7 SD, respectively,[104] and the relatively high mean–T_{Fmax}–value of the fully–developed esSDFT was proposed to be afforded by a comparatively high presence of divalent ketoamine or trivalent intermolecular cross–links in the fully–developed esSDFT over

the fully–developed pCDET (*see: M:SA*).[104,231] In contrast to the tendon's high T_{Fmax} value in maturity (*of >90°C*), the mean–T_{Fmax}–value of the present fetal esSDFT samples (*at: 76.6°C ± 1.6*) was more comparable to that value found in both prenatal (*72.6°C ± 1.4*) and mature (*75.1°C ± 2.7 SD*[104]) pCDET samples (*Figure 12.b*), and may signify a functional lack of thermally stable intermolecular cross–links within the developing esSDFT relative to within its fully–developed counterpart.

However marginal, the discrepancy between the mean–T_{Fmax}–values of the two FDTs during the 2nd and 3rd trimesters of fetal development (*at: 76.6°C ± 1.6 and 72.6°C ± 1.4 in the esSDFT and pCDET, respectively; Figure 12.b*) may alternatively signal a minor but still statistically–significant presence of divalent ketoamine or trivalent intermolecular cross–links within the esSDFT relative to within its pCDET counterpart, gestationally (*see: M:SA*).[104,231] A greater presence of divalent ketoamine cross–links in the developing fetal esSDFT could arise from a high degree of lysine hydroxylation in the esSDFT relative to in its pCDET counterpart.[6,62] Consistent with this, relatively high cellularity in the esSDFT during gestation[§] could result in a more ubiquitous presence of the LH enzymes necessary for the later formation of divalent ketoamine cross–links.[6,62,290] Alternatively, a slower rate of collagen turnover in the esSDFT than in the pCDET prenatally[¶] could instead provide preexisting divalent intermolecular cross–links with more adequate opportunity to begin to mature into their trivalent successors in the esSDFT than in the pCDET during gestation (*see: Figure 5*).[6,62]

[§] *comparatively high cellularity within the esSDFT gestationally would be in alignment with the relatively high cellularity of the esSDFT over the pCDET in tissue maturity*[10,17,20]

[¶] *a slower rate of collagen turn over in the esSDFT would also be in alignment with the relative characteristics of the FDTs in maturity*[22,89,252]

5.1.3 $NaBH_4$ Analysis Indicate a Substantial Presence of Thermally Labile Cross-Links in Both the esSDFT and pCDET Throughout the 2nd and 3rd Trimesters of Gestation, Along With Little Difference in Total Cross-Link Presence Between the Two Functionally Distinct Tendons

The findings associated with sodium borohydride (*or:* '$NaBH_4$') mediated stabilization treatment serve to reinforce the results of the previous: (***i***) denaturation temperature ('T_d') and (***ii***) temperature of maximum force generation ('T_{Fmax}') analyses (*see: Figure 13*).[231] To better explain this first with respect to the other findings related to the prior T_d analysis (*see: Figure 11*): consider that the mean half–time of load decay ('$t_{1/2}$') value of the non–stabilized esSDFT grouping of this $NaBH_4$–related analysis was found to increase from the 2nd (*at: 0.56 hours ± 0.06*) to 3rd trimesters (*1.34 hours ± 0.14*) of gestation (*see: Figure 13.c→d*). Similar to the results of the prior T_d analysis, this increase in $t_{1/2}$ suggests a rise in the presence of thermally stable intermolecular cross–links in the non–stabilized EST as fetal development progresses (*see: M:SA; Figure 13*). This conclusion aligns with those conclusions inferred from the previous T_d analysis of the esSDFT (*see: 'T_d Results May Signal...'*), and namely the notions of: (***i***) a rising population of intermolecular cross–links over gestational time, and (***ii***) a greater rate of cross–link deposition in the esSDFT than in the pCDET (*see: Figure 11.a*). Indeed, by comparison, the pCDET exhibited no such indication of a temporal increase in mean–$t_{1/2}$–value during gestation (*Figure 13.c→d*)‖.[114,141,231]

In reflection of another past conclusion, this time drawn from the earlier T_{Fmax} investigation (*see: T_{Fmax} Results Suggest a...*), disparity in the rate of cross–link deposition between the two

‖*the mean–$t_{1/2}$–value of the pCDET actually may have exhibited a slight decrease over gestational time, with 2nd trimester → 3rd: 0.32 hours ± 0.29 → 0.22 hours ± 0.13, $p = 0.61$ (Figure 13.c→d)*

FDTs was ultimately found to culminate in a higher mean–$t_{1/2}$–value among the non–stabilized 3rd trimester esSDFT samples under study (*at: 1.34 hours ± 0.14*) than that mean that was identified for their non–stabilized pCDET counterparts (*0.22 hours ± 0.13; $p \leq 0.01$; Figure 13*). This finding suggests the emergence of a greater presence of thermally stable cross–links in the esSDFT than in the pCDET in the 3rd gestational trimester (*M:SA*).[104,231] In this way, the non–stabilized, control groupings of this stabilization treatment analysis reaffirm the current work's prior conclusions that: (***i***) an increase in intermolecular cross–linking occurs over gestational time, and especially so in the esSDFT,** and (***ii***) that this increase is brought about, at least in part, by a functionally significant deposition of thermally stable cross–links (*Figure 13*).††

The inferences drawn from the previous temperature of maximum force generation ('T_{Fmax}') analysis were further reinforced by the relative T_{Fmax} values of the non–stabilized groupings for each of the four tendon–trimester pairings under $NaBH_4$–related study (*see: 'T_{Fmax} Results Suggest a...'; Figure 13.a&b*). Most conspicuously, the mean–T_{Fmax}–values of the non–stabilized esSDFT groupings pertaining to the 2nd (*at: 83.8°C ± 2.8*) and 3rd trimesters (*88.5°C ± 1.4*) were both identified as being greater than those of their 2nd (*74.1°C ± 4.4, $p = 0.04$*) and 3rd trimester (*72.4°C ± 2.8, $p \leq 0.01$*) pCDET counterparts (*Figure 13.a&b*). These findings support the results of the prior T_{Fmax} analysis (*'T_{Fmax} Results Suggest a...'*), in indicating a consistently higher presence of thermally stable intermolecular cross–links in the esSDFT than in the pCDET groupings (*see: Figure 12.b; M:SA*).[17,104,231] Of added interest, while mean–T_{Fmax}–value was found to differ little between the 2nd and 3rd trimester non–stabilized pCDET groupings (*at:*

**the result that suggests a temporal increase in mean–$t_{1/2}$–value over gestational time served to reinforce the findings of the prior T_d analysis*

††*the result that indicates a greater presence of thermally stable cross–links within the esSDFT than in the pCDET during the 3rd trimester served to reinforce the findings of the prior T_{Fmax} investigation*

74.1°C ± 4.4 & 72.4°C ± 2.8, respectively, $p = 0.61$; Figure 13.a&b), the mean–T_{Fmax}–values of the non–stabilized esSDFT groupings were found to exhibit a marked increase (*at: +4.7°C, $p = 0.06$*) from the 2nd (*at: 83.8°C ± 2.8*) to 3rd trimester (*88.5°C ± 1.4; Figure 13.a&b*).‡‡ This is perhaps in further reflection of an increase in thermally stable intermolecular cross–linking within the esSDFT over gestational time (*M:SA*). Accordingly, while the $t_{1/2}$ and T_{Fmax} values associated with the non–stabilized tendon–trimester groupings of the $NaBH_4$–related analysis lend little credence to the notion of an increasing presence of thermally stable cross–links in the pCDET as fetal development progresses (*as: Figure 13.c→d, 13.a→b, respectively*), an increase in both: (***i***) mean–$t_{1/2}$–value* and (***ii***) mean–T_{Fmax}–value† between the samples comprising the 2nd and 3rd trimester esSDFT groupings together hint at a growing network of thermally–stable cross–links in the energy storing tendon as fetal development progresses.

In addition to the corroboration of past findings that are afforded by a comparison between the non–stabilized groupings of the four tendon–trimester pairings under study, the universal increases in: (***i***) mean–T_{Fmax}–values (*see: Figure 13.a&b*), and (***ii***) mean–$t_{1/2}$–values (*Figure 13.c&d*) that were seen within each of the four tendon–trimester groupings following cross–link stabilization treatment also served to elucidate much about the speciation of cross–links present in the esSDFT and pCDET at multiple gestational timepoints of each tendon's development. To start this discussion with respect to the esSDFT evaluations of both the 2nd and 3rd trimesters,

‡‡*the increase in the mean–T_{Fmax}–value of the esSDFT from the 2nd trimester to 3rd trimester was likely made just slightly non–significant (at: $p = 0.06$) by the hard cap of the T_{Fmax} metric at 90°C*

**of: +0.78 hours, $p \leq 0.01$*

†*of: +4.7°C, $p = 0.06$*

the stabilization effect that was afforded by sodium borohydride treatment‡ was first made evident by the increases in T_{Fmax} values that were seen following stabilization treatment (*Figure 13.a&b*). In particular, cross–link stabilization treatment appeared to result in increases of T_{Fmax} values such that the mean–T_{Fmax}–values of the stabilized groupings exhibited little deviation from the ultimate 90°C of the metric (*Figure 13.a&b*).§ Most notably, stabilization treatment saw an increase in mean–T_{Fmax}–value from 83.8°C ± 2.8 to 89.7°C ± 0.3 ($p = 0.07$; *N.B. the metric's limitation*) among the samples that comprised the 2nd trimester esSDFT grouping (*Figure 13.a→b*). This result is suggestive of a particularly functionally significant presence of thermally labile cross–links (*or: 'divalent aldimine'*) in the esSDFT at the approximate midpoint of the 2nd gestational trimester (*see: M:SA*).

The changes effected by cross–link stabilization treatment of the esSDFT, and what those changes communicate about the nature of the network of intermolecular cross–linking present within the EST at various stages of its gestational maturation, are made even more clear through a comparison of the relative mean–$t_{1/2}$–values obtained within each of the two tendon–trimester groupings pertaining to the esSDFT. In particular, the marked increases in mean–$t_{1/2}$–values seen following stabilization treatment of the 2nd and 3rd trimester esSDFT groupings (*see: Figure 13.c&d*)¶ further substantiate the notion that there exists a substantial presence of thermally

‡*sodium borohydride (or: '$NaBH_4$') treatment stabilizes native intermolecular cross–links in tendon via the reduction of the thermally labile divalent aldimine cross–links: (**i**) dehydro–lysino–norleucine and (**ii**) dehydro–hydroxylysino–norleucine into a more thermally stable form (as is detailed in M:SA)*

§*that is, aside from that random deviation that should be expected given the incorporation of multiple samples of each tendon within each grouping; with mean–T_{Fmax}–values of: 89.7°C ± 0.3 and 88.5°C ± 0.3 in the 2nd and 3rd trimesters following $NaBH_4$–mediated stabilization treatment, respectively*

¶*from: 0.56 hours ± 0.06 to 2.55 hours ± 0.77, $p = 0.05$ in the 2nd trimester and 1.34 hours ± 0.14 to 3.01 hours ± 0.54, $p = 0.03$ in the 3rd trimester*

labile cross–links in the EST during the 2nd and 3rd of fetal development. Indeed, in terms of the present work, divalent aldimine cross–links present within the developing esSDFT serve as willing participants in the process of $NaBH_4$–mediated cross–link stabilization treatment that in turn confers higher mean–$t_{1/2}$–values in each trimester under study (*see: M:SA*).

Any indication of a functionally significant presence of thermally labile cross–links in the developing esSDFT is second to that presence suggested to exist within the esSDFT's pCDET counterpart (*see: Figure 13*). While $NaBH_4$–mediated cross–link stabilization treatment appeared to prompt similar increases in the mean–T_{Fmax}–values of the 2nd and 3rd trimester pCDET groupings to those that pertained to the esSDFT groupings, the increases seen among the pCDET groupings were considerably larger‖ in addition to being statistically significant (*Figure 13.a&b*). This suggests an even greater presence of thermally labile cross–links (*primed for stabilization via* $NaBH_4$) to have existed in each of the pCDET groupings than that presence comparatively made interpretable in each grouping's esSDFT counterpart (*see: M:SA*). Indeed, the notion of a particularly substantial presence of thermally labile cross–links in the developing pCDET is further supported by the remarkable increases in mean–$t_{1/2}$–values seen within the 2nd and 3rd trimester pCDET groupings following $NaBH_4$–mediated cross–link stabilization treatment (*Figure 13.c&d*).**

The comparable mean–$t_{1/2}$–values seen between the FDT groupings both: (***i***) within each

‖*the increases seen in the two pCDET groupings were 2nd:* ***+15.0°C*** *± 4.6, p = 0.02 & 3rd:* ***+14.9*** *± 3.8, p ≤ 0.01; relative to those values of* ***+5.9*** *± 2.8 &* ***0.0*** *± 1.4 in the 2nd and 3rd trimester esSDFT groupings, respectively*

******the increases in the mean–$t_{1/2}$–values of the 2nd and 3rd trimester pCDET groupings were ***+2.48*** *± 0.8, textitp ≤ 0.02 &* ***+3.06*** *± 1.68, p = 0.09, respectively — relative to those comparatively small values of* ***+1.99*** *± 0.77 &* ***+1.67*** *± 0.56 identified for their esSDFT counterparts*

trimester[††] and (***ii***) between trimesters following cross–link stabilization treatment seemingly defy the expectations that would have aligned with the results of the prior T_d analysis (*see: Figure 13.c&d; Figure 11*). Specifically, because $t_{1/2}$ value following $NaBH_4$–mediated cross–link stabilization treatment is reflective of the total presence of cross–links in a given tissue (*see: M:SA*), the tendons comprising the four stabilized tendon–trimester groupings under study were all indicated to possess reasonably similar populations of cross–links (*Figure 13.c&d*). For the esSDFT, this suggests a dramatic difference in cross–link deposition between prenatal and postnatal development.[104] Indeed, the only very slight increases in the mean–$t_{1/2}$–values seen gestationally[‡‡] suggest, at most, a marginal and largely inconsequential deposition of intermolecular cross–links within each tendon during the 2nd and 3rd trimesters of gestation (*Figure 13.c→d; M:SA*). This finding seemingly keeps in fitting with what is already known about the pCDET: the fully–developed pCDET was previously found to exhibit a mean–$t_{1/2}$–value of only 3.5 hours ± 1.0 following $NaBH_4$–mediated cross–link stabilization treatment,[104] and so a predominantly postnatal increase of 0.22 hours ± 1.96 from that value that was identified for the 3rd trimester in the present work seems reasonable, being consistent with the suggestion of a slow and methodical deposition of cross–links throughout the development of the positional tendon until it reaches maturity (*Figure 13.d*).

In stark contrast to the notion of a consistent and slow rate of intermolecular cross–link deposition in the developing pCDET is the apparent rapid deposition of cross–links that was

[††] *the mean–$t_{1/2}$–values in the 2nd trimester were 2.55 hours ± 0.77 & 2.80 hours ± 0.77, $p = 0.71$ for the esSDFT and pCDET groupings, respectively, whereas the mean–$t_{1/2}$–values in the 3rd trimester were 3.01 hours ± 0.54 & 3.28 hours ± 1.68, $p = 0.81$*

[‡‡] *while the mean–$t_{1/2}$–value of the stabilized groupings of the esSDFT from the 2nd to 3rd trimesters was found to increase by 0.46 hours ± 0.94 ($p = 0.44$), that increase of the pCDET was identified to be 0.48 hours ± 1.85 ($p = 0.67$)*

signalled to occur* during the postnatal development of the esSDFT (*Figure 13.d*). More specifically, unlike the only modest increase† in the mean–$t_{1/2}$–value of the pCDET that was suggested to take place from the approximate midpoint of the 3rd trimester until tissue maturity, the comparatively massive mean–$t_{1/2}$–value that was previously identified for the fully–developed bovine esSDFT following $NaBH_4$–mediated stabilization treatment (*of 11.5 hours ± 1.9*[104]) represents a nearly four fold increase§ in mean–$t_{1/2}$–value from that value found to pertain to the 3rd trimester (*Figure 13.d*).[104] In deviating from the relatively similar presence of intermolecular cross–links suggested to exist in the pCDET between late gestation and maturity (*Figure 13.d*), this +8.49–hour increase¶ hints at the influence of a potent catalyst that is exclusive to post but not prenatal development, that bears the potential to enact remarkable change to the reticulum of intermolecular cross–links within the esSDFT. For this, the esSDFT's repeated storing and releasing of energy under high load[43,203,250] and the proliferative effect such repetitions have been shown to have on tenocytes[294] alongside the cross–linking associated enzymes tenocytes output[159,182] (*as in: 'mechanoregulation'*) could serve as an intuitive explanation.

an apparent rapid deposition of intermolecular cross–links was suggested to occur postnatally by the ballooning of the mean–$t_{1/2}$–value of the esSDFT after birth[104]

†*the pCDET was indicated to exhibit a predominantly postnatal increase in mean–$t_{1/2}$–value of +0.22 hours ± 1.96*

§*or: a +8.49–hour ± 1.98 increase from the mean–$t_{1/2}$–value of 3.01 hours ± 0.54 that was identified in the 3rd trimester by the present work*

¶*...and the concomitant deposition of intermolecular cross–links this +8.49–hour increase, at least in theory, implies; (see: M:SA)*

5.2 The Disparate Mean Collagen Fibril Diameter Between the esSDFT and pCDET Arises Before a Differing Propensity for Lateral Fibril Fusion Could Be Principally Responsible

The relatively small mean CFD seen within the esSDFT relative to within the pCDET throughout the 2nd and 3rd trimesters of gestation defies initial expectations[192] but remains consistent with the comparatively small mean fibril diameter that was previously identified within the esSDFT when compared with the pCDET in tissue maturity (*see: Figure 18*).‖ [19,203,243] In contrast to the current findings, the results of previous studies were taken to suggest that the mean CFD within each of the FDTs to first diverge perinatally,[24,192] with the collagen fibrils of the esSDFT less readily engaging in lateral fusion than do the fibrils of the pCDET toward the final days of fetal development (*see: Unknowns About the Growth...*). Instead, the present data suggests a gradual increase in mean CFD throughout gestation and substantial disparity between the mean fibril diameters of the two FDTs apparent even in the youngest sample analyzed (*see: Figure 16*).** These findings may discredit the previously accepted notion that a tendon based difference in the tendency of collagen fibrils to fuse laterally is critical to the divergence of mean fibril diameter between the two classes of FDTs (*Unknowns About the Growth...*).

The consistency between: (***i***) the relatively small mean CFD identified within the developing esSDFT relative to that within the developing pCDET in the present work (*Figure 18*), and

‖ *at: 80 nanometers ('nm') ± 7 standard deviation ('SD') and 134 nm ± 5 SD in the esSDFT and pCDET, respectively*[104]

** *the youngest sample analyzed was aged to GD 100, and exhibited mean CFDs of 31 nm ± 4 SD and 36 nm ± 3 SD in the esSDFT and pCDET, respectively (see: Figure 18)*

(***ii***) the lower mean fibril diameter that was previously documented within the fully–developed esSDFT when compared to the fully–developed pCDET,[19,104,203,243] could be taken to indicate that the mechanical properties proposed to be conferred by the relative mean fibril diameters of the FDTs in tissue maturity also apply during fetal development (*see: Unknowns About the Growth...*). That is, the comparatively small mean CFD seen within the esSDFT relative to within the pCDET throughout the 2nd and 3rd trimesters of gestation could make the developing esSDFT both: (***i***) notably elastic[78,187] and (***ii***) creep resistant[78,208] in relation to its developing pCDET counterpart (*Figure 16*). Conversely, the comparatively large mean CFD seen presently within the pCDET over that found within the esSDFT during the 2nd and 3rd trimesters may make the developing pCDET both: (***i***) stiffer[19,208,225,253] and (***ii***) stronger[104,187] than its esSDFT counterpart throughout the second half of gestation (*Figure 16*). To date, only one study has contrasted the mechanical properties of an esSDFT and pCDET during fetal development (*in an equine, or: horse; Equus caballus, model*).[290] There were no significant mechanical differences identified between the two developing equine tendons, though the elastic modulus of the equine esSDFT appeared to trend lower than that of the equine pCDET (*see: Zamboulis et al. 2020*[290]).

The mean CFD values of each of the FDTs under study identified toward the end of gestation are strikingly similar to those values that have previously been reported in tissue maturity (*see: Figure 18*).[104] Indeed, the mean CFD values of the esSDFT and pCDET in the eldest sample assessed†† were found to be: 70 nanometers ('*nm*') ± 12 SD and 85 nm ± 16 SD, respectively (*Figure 18*). Most remarkably, this translates to a postnatal increase of only ten nanometers to reach the mean CFD of 80 nm ± 7 SD that was previously reported in the esSDFT in tissue

†† *the eldest sample assessed was aged to GD 232*

maturity (*Figure 18*).‡‡[104] This similarity suggests the collagen fibrils of the esSDFT to have largely achieved their mature diameter by the end of gestation. This finding is consistent with but more dramatic than the results of past studies that investigated CFD within the FDTs of other large mammalian species.[17,207] For example, mean CFD was reported as being approximately: ∼105 nm ± ∼30 SD among the esSDFTs of newborn equines,[207] in relation to that value of 169 nm ± 19 SD found in the same tendon in its maturity (*representing a postnatal–increase of: ∼64 nm ± ∼35.5 SD*).[17]

Opposite the apparent similarity in mean CFD between gestational and fully–developed tissue, the most glaring disparity between the: (***i***) fibril diameter distributions of either of the two FDTs during gestation and (***ii***) those of their fully–developed counterparts is the lack of a bimodal fibril diameter distribution in the esSDFT at any point of fetal development (*Figure 18; Figure 16*).[68,171] In contrast to the distributions compiled in the present work, the fully–developed esSDFT has previously been documented to be distinct from its pCDET counterpart in possessing a bimodal CFD distribution in tissue maturity.[21,181,189,207] The presence of this bimodal distribution is held to be advantageous for the esSDFT:[181,183,207] while relatively small collagen fibrils are alleged to assist in counteracting interfibril slippage,[183] larger collagen fibrils are instead proposed to serve in increasing tendon tensile strength.[104,187] These supposedly distinct functions of collagen fibrils of different sizes have also led to models wherein fibrils of differing diameter ranges are proposed to have varying: (***i***) load bearing responsibilities and (***ii***) degrees of influence on tendon mechanics at different strains[90] — which, in turn, is alleged to aid in the preservation of the structural integrity of highly stressed tissues over long periods.[183] In this way, the lack of any

‡‡*and of 49 nanometers ('nm') to reach the 134 nm ± 5 SD of the fully–developed pCDET*[104]

discernible bimodal fibril diameter distribution in the developing fetal esSDFTs in the present work may have aligned with the previously mentioned past finding[290] of comparable mechanical properties between the esSDFT and pCDET during the 2nd and 3rd trimesters of fetal development (*see: Figure 23; Figure 16*).[290] The absence of any bimodal distribution may also suggest the two distinct subpopulations of collagen fibrils previously seen in the fully–developed esSDFT in tissue maturity[104,207,253] to first arise postnatally, perhaps as an adaptation to the notably high mechanical stress experienced by the tendon.[43,203,250]

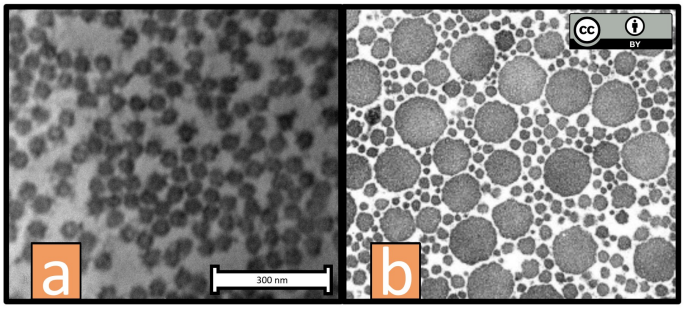

Figure 23: Transmission electron microscopy (‘*TEM*’) images of cross sections of (**a**) an energy storing superficial digital flexor tendon (‘*esSDFT*’) of a male fetus that was aged to gestational day (‘*GD*’, *hereafter*) ∼180 from the present study and (**b**) an esSDFT from a fully–developed thoroughbred equine (*or: horse; Equus caballus*), deployed in order to highlight the lack of a bimodal CFD distribution of any sort in the present tendons under study (*or: during the fetal stage*). A scale bar approximating ∼300 nanometers (‘*nm*’) was provided for image (**a**). The image denoted as (**b**) was adapted from Patterson-Kane et al. (2012)[187] as is indicated by the Creative Commons Attribution 3.0 International License (‘*CC BY 3.0*’) symbol, who reported the magnification of their image to be ×45,100. For more comprehensive copyright details regarding the adapted image, *see:* Appendix Section 8.4.

The surges in the mean CFD and abrupt increases in the breadth (*or: standard deviations*) of the fibril diameter distributions of both of the FDTs identified to occur toward the middle

of the 3rd trimester of gestation* mirror the results of previous studies[24,192] and may lend some validity to the theory of a rapid increase in mean fibril diameter perinatally, spurred by rapid lateral fibril fusion (*see: Figure 18; Unknowns About the Growth...*).[9,199,293] Particularly, adjacent collagen fibrils may be made more free to fuse with one another during the final weeks of gestation.[9,293] This sudden ability to fuse might be due to a concurrent partial or complete removal of a regulatory mechanism that otherwise inhibits lateral CFD growth during the earlier stages of gestation.[83,178,295] Further, for the esSDFT, the apparent appearance of a wide CFD distribution prior to birth (*with a relatively high SD*) plausibly resulting from uninhibited lateral fibril fusion[9,199,293] seems like a natural precursor to the subsequent, postnatal development of a bimodal CFD distribution (*Figure 16*).[207,253]

The present results suggest possible roles of regulatory proteins in: (***i***) mediating the difference in mean CFD between the esSDFT and pCDET throughout the 2nd and 3rd trimesters of fetal development, and (***ii***) restricting substantial growth of mean fibril diameter in both of the FDTs until the final weeks of gestation (*see: Figure 16*). First, the smaller mean CFD identified throughout gestation within the esSDFT relative to in the pCDET may signal a greater presence of molecules that inhibit the lateral growth of collagen fibrils in the developing esSDFT (*Figure 18*).[9,178,295] This notion is supported by the indication of relatively high homogeneity in the diameter measurements of collagen fibrils within esSDFTs throughout the 2nd and 3rd trimesters of gestation compared to that seen in their match–paired pCDETs (*see: Figure 16 & Figure 19*). On this, some examples of proteins with inhibitory effects on collagen fibril growth include:

the surge in mean diameter and abrupt increase in the breadth of diameter distribution occurred between GDs: 200 and 231

the small leucine–rich proteoglycans ('SLRPs', *of class I*)†,[78,178,256,292] COMP,[9,83] and collagen types: (***i***) III (*or:* '*COL3*') and (***ii***) XIV (*14*);[133,295] with both COMP and COL3 being of particular interest given the high expression of each protein in the esSDFT over the pCDET in tissue maturity.[21,229,295] In added support of a high presence of at least one of these inhibitory proteins in developing esSDFTs during gestation is the curious finding of a presence of visible material coating the surfaces of collagen fibrils seen more consistently in developing esSDFTs than in their pCDET counterparts (*see: Figure 24*). Conversely, the relatively low homogeneity in diameter measurements indicated among the collagen fibrils within pCDETs compared to those of their match–paired esSDFTs throughout the 2nd and 3rd trimesters of gestation could alternatively be explained by a greater presence of proteins documented to instead facilitate rather than inhibit lateral fibril growth within the developing pCDET than in the developing esSDFT (*Figure 19*). A pertinent example of such a protein could be 'fibromodulin' from the SLRPs of class II SLRPs.[38,68,241] Fibromodulin is of special interest because it was previously suggested to be more highly expressed in the fully–developed pCDET than in the fully–developed esSDFT of mature equines.[248] In a similar way, the dramatic surge of mean CFD seen in both FDTs during the 3rd trimester of gestation could result from a sudden change in the expression of any of those inhibitory or facilitatory proteins highlighted (*Figure 16*).[68,178,295] Accordingly, a more comprehensive molecular analysis of the two FDTs throughout fetal development could serve to elucidate much about the mechanisms that govern the prenatal growth of collagen fibrils.

† *and particularly the class I SLRPs:* (***i***) *decorin and* (***ii***) *biglycan*

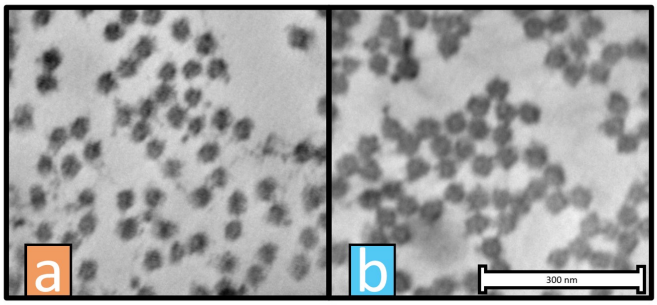

Figure 24: Transmission electron microscopy (‘*TEM*’) images of cross sections of (**a**) an energy storing superficial digital flexor tendon (‘*esSDFT*’) and (**b**) a positional common digital extensor tendon (‘*pCDET*’) of a female fetus that was aged to gestational day (‘*GD*’) ∼100; showing a clear presence of non–collagenous molecules that coated the surface of collagen fibrils in the esSDFT but not that of fibrils in the pCDET. A scale bar approximating ∼300 nanometers (‘*nm*’) was provided. These images were obtained via TEM analysis at 100,000× magnification.

5.3 Ordered and Regular Collagen Fibril Crimp in Perinatal esSDFTs Serves as a Natural Precursor to That Seen in Tissue Maturity

The steady increase in mean collagen fibril crimp ('*CFC*', *hereafter*) wavelength seen as gestation progresses is reinforced by previous studies (*see:* Figure 22)‡.[97,215,290] Perhaps counterintuitively, fibril crimp has previously been found to 'loosen' over the course of gestation and during early postnatal life,[97,102] and as such has been proposed to take form early on in fetal development.[97,215] Thereafter, the well documented reduction in the cellularity of tendon tissue from early to late gestation[155,156,212] makes a synchronous increase in mean CFC wavelength (*or: a parallel decrease in crimp tightness*) logical, in consideration of the theory that fibril crimp originates from cooperative tenocyte contraction[102] mediated by extensive intercellular actin networks (*see:* Figure 22*; Unknowns About the Formation...*).[178,215] Applied to the present analysis, a steady decrease in tissue cellularity during gestation[155,156,212] may gradually confer comparatively little cooperative tenocyte contraction and thereby induce fibril crimp of lesser tightness.[102,178,215]

The indication of consistently looser CFC in the developing esSDFT than in the developing pCDET during the 2nd and 3rd trimesters of fetal development is curious given that the opposite relationship has previously been found[104] to exist between the crimp formations of the two FDTs in tissue maturity (Figure 22).[21,76,104,232,249] In particular, Herod et al. (2016) reported a shorter

‡*from a low of: 24.64 micrometers ('µm') ± 0.61 standard deviation ('SD') in the GD 106 pCDET to a high of: 72.61 µm ± 2.13 SD in the GD 247 esSDFT; both of which were representative of a gradual decrease in crimp tightness (see:* Figure 22*)*

mean crimp wavelength[§] among the collagen fibrils of the fully–developed bovine esSDFT than those of its pCDET counterpart;[104] while Birch et al. (2013) identified larger: (***i***) mean crimp length and (***ii***) mean crimp angle among the fibrils of the fully–developed equine esSDFT than among the fibrils of its pCDET counterpart (*see: Figure 25*).[21] These findings may highlight the sole consideration of the first of these three metrics (*crimp 'wavelength'*) as a limitation of the present work. Indeed, the qualitative, visual evidence of disparity in crimp ordering and regularity seen between the esSDFT and pCDET samples of late 3rd trimester fetuses might suggest a difference in crimp length or angle between the two FDTs to arise toward the final stages of fetal development (*see: Figure 21*).

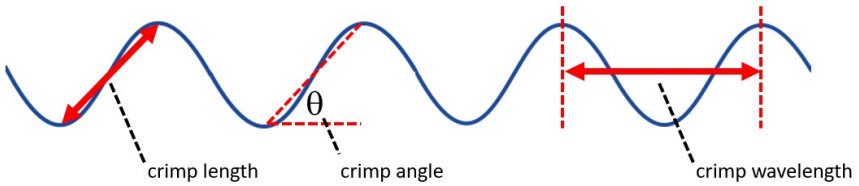

Figure 25: A diagrammatic representation of (***i***) crimp *length*, (***ii***) crimp *angle*, and (***iii***) crimp *wavelength*. Crimp angle was denoted by theta (θ). *N.B.* that crimp length has occasionally alternatively been used to instead describe a measurement exactly half of crimp wavelength. This illustration was adapted from Patterson-Kane et al. (1997).[189]

Limited evidence of tighter or more substantial fibril crimp in the esSDFT than in the pCDET for almost all of gestation may otherwise suggest the notable: (***i***) cellularity[10,20] or (***ii***) elasticity[17,184,263] of the fully–developed esSDFT over the fully–developed pCDET to exist exclusively postnatally in the present bovine model. Though the literature has posited a positive

[§] *(for a diagrammatic representation of this metric, see: Figure 25)*

relationship between: (***i***) tissue cellularity and (***ii***) the tightness of fibril crimp[¶][102,142,273] it remains difficult to rationalize that the relatively loose crimp seen within the current fetal esSDFT samples resulted from comparatively low cellularity within the developing esSDFT in relation to that within the developing pCDET (*Figure 22*). In particular, lower cellularity in the esSDFT than in its pCDET counterpart during gestation would contrast the relatively high cellularity of the esSDFT over the pCDET in tissue maturity,[10,17,20] and be even more remarkable given the comparatively early emergence of the esSDFT relative to the pCDET during the initial stages of fetal development.[50] In a similar vein, a previous study[290] reported little difference between the elasticities of a comparable set of FDTs during fetal development.[290] Applied presently, this result may suggest the collagen fibrils within the FDTs to be equally receptive to the contractile stimuli proposed to be responsible for the formation of crimp during gestation.[103]

Zamboulis et al. (2020) recently extended their analysis of equine tendons to fetal development: finding the equine esSDFT to have: (***i***) a greater mean CFC angle (*indicating tighter crimp; Figure 25*) alongside (***ii***) greater cellularity than its pCDET counterpart during the 3rd trimester of equine gestation.[290] Together, these traits are indicative of at least partial adoption of the fully–developed characteristics of the FDTs, prenatally.[290] This notion aligns with the present indication of both better ordered and more regular crimp in perinatal esSDFTs over their pCDET counterparts (*see: Figure 21*). However, the current result pertaining to mean CFC wavelength contrasts those results presented by Zamboulis et al. (2020) (*Figure 22.b*).[290] In fact, the current work's suggestion of an apparent specialization of fibril crimp in a manner opposite to that which has been documented

[¶] *a positive relationship between tissue cellularity and the tightness of fibril crimp has allegedly been realized within the fully–developed esSDFT relative to within its pCDET counterpart*[76,104,249]

to exist in tissue maturity (*Figure 22*)‖ [104] may instead suggest the existence of a determinative postnatal stimulus that bears the potential to override any preexisting configuration that should have existed between the 'crimp–like undulations' of the FDTs prenatally (*Figure 21*). For the esSDFT, an increase in cumulative tenocyte contraction as a result of cell proliferation induced by a high degree of postnatal mechanical stimulation (*as in: 'mechanoregulation'*) could serve as one possible explanation.[266]

The discordance between: (***i***) the comparatively loose CFC visualized within the esSDFT relative to that seen in the pCDET (*Figure 22*) and (***ii***) the tight and prominent fibril crimp that has previously been identified to exist within the esSDFT over the pCDET in tissue maturity [21,76,232,249] could alternatively be taken as evidence to dismiss the prenatal undulations or 'crimp–like patterning' seen in the present work as a direct precursor of the crimp previously visualized within the fully–developed FDTs in maturity.[75] Indeed, smooth 'crimp like patterning' that lacks the knots and regions of local deformation often associated with the crimp of fully–developed tendon [78,205] has been identified among the fibrils of a wide variety of collagenous tissues — *from: arterial walls,*[77] *to corneas,*[86,221] *to skin.*[221] So, the prenatal patterning seen in the present investigation may be of little relation to the prominent fibril crimp found within fully–developed tendon. In support of this dissociation, the mean wavelengths of fibril crimp in the bovine esSDFT and pCDET under present study were previously identified as being: 57 micrometers ('*μm*') ± 10 standard deviation ('*SD*') and 124 μm ± 7 SD in tissue maturity, respectively [104] — both of which were considerably different from those values identified within the two FDTs toward the end of

‖*the CFC viewed in the present work was suggested to be looser within the developing esSDFT than in its pCDET counterpart*

gestation by the present work (*Figure 22*).** Most glaringly, the mean CFC wavelength in the fully–developed esSDFT (*at: 57 µm ± 10 SD*) would represent a tightening of 'crimp' after birth, following the opposite (*a gradual loosening*) throughout the 2nd and 3rd trimesters of gestation (*Figure 22*). Resultantly, the orderly and regular undulations visualized exclusively among the collagen fibrils of perinatal esSDFTs†† may be the only true predecessor of the fibril crimp seen within fully–developed tendon that was viewed in the present work (*Figure 21*).

** *in a fetus that was aged to 247 GD, the mean wavelengths of fibril crimp in the bovine esSDFT and pCDET were found to be 73 µm ± 7 SD and 63 µm ± 7 SD, respectively (Figure 22)*

†† *the orderly and regular undulations that were seen within the esSDFT of a fetus aged to 247 GD were not present to the same degree in any other tendon analyzed — including its 247 GD pCDET counterpart (see: Figure 19)*

6 Future Directions

6.1 The Pressing Need for Molecular Biology Analysis

The results presented in this work could be built upon in numerous ways. The next logical step in building on the numerous structural differences this study uncovered — from intermolecular characteristics to features of the tendons on the macroscale — is a similar analysis of the molecular biologies of each of the FDTs during the 2nd and 3rd trimesters of gestation. Indeed, with consideration of the substantial evidence of plausible disparity in molecular signalling between ESTs and PTs during fetal development‡‡, there is good reason to believe that select proteins critical to the regulation of key tendon properties may differ in their expression during gestation between the esSDFT and pCDET. These proteins were, in order of interest for their ability to explain the identified structural disparities, (***i***) cartilage oligomeric matrix protein (*or:* 'COMP'), (***ii***) type III collagen ('COL3'), (***iii***) scleraxis ('Scx'), (***iv***) vascular endothelial growth factor ('VEGF'), and (***v***) transforming growth factor beta-2 ('TGF–β2'). The hypotheses pertaining to these five proteins that naturally follow from the work of previous studies are presented below:

6.1.1 Hypotheses Associated With Disparities in Molecular Signalling Anticipated Between the esSDFT & pCDET During Fetal Development

(***i***) That cartilage oligomeric matrix protein (*or:* '*COMP*') expression will be higher in esSDFTs than in their match–paired pCDETs throughout fetal development. This will reflect the result of a study[92] on a comparable large mammalian model that

‡‡*the considerable evidence of plausible disparity in molecular signalling between FDTs was gleaned from previous literature and presented earlier (within 'The High Potential...')*

showed tenoblasts taken from esSDFTs at the fetal stage of development have a higher capacity for COMP production than did otherwise comparable tenoblasts taken from pCDETs.[92] High COMP expression in esSDFTs relative to their PT counterparts during gestation will also align with the notable COMP found within the esSDFT over the pCDET in tissue maturity,[21,229] along with the multiple changes COMP has been proposed to effect on tendon structure.[83,295]

(***ii***) That type III collagen (*or:* '*COL3*') will be expressed to a greater degree in esSDFTs than in pCDETs throughout gestation. This will align with the high presence of COL3 in esSDFTs over pCDETs in tissue maturity[21,295] and serve to restrict lateral fibril growth in the esSDFT relative to in the pCDET gestationally.[23,133,268] It will also reinforce the result of a previous study[92] on a comparable large mammalian model that showed tenoblasts of developing esSDFTs to have a greater propensity for COL3 production than did tenoblasts of pCDETs.[92]

(***iii***) That scleraxis (*or:* '*Scx*') will be expressed more consistently throughout the prenatal development of esSDFTs than during that of pCDETs. This will reinforce the result of a Scx knockout mutation study[175] that found an absence of Scx function to effectively eliminate forelimb flexor tendons (*energy storing*) whilst having comparatively little effect on forelimb extensor tendons (*positional*).[175] However, while this differential effect may suggest a more critical role for Scx in flexor tendon development, it is important to note that genetic compensation may occur in knockout studies. Nevertheless, prolonged Scx function in esSDFTs relative to in their pCDET counterparts during fetal development will be intuitive given (***i***) the role of Scx in tenocyte recruitment[108] and (***ii***) the comparatively high expression of tenogenic factors like: COMP,[11] tenomodulin,[26] and type XIV (*or: 14*) collagen[178] in ESTs over PTs.

(***iv***) That vascular endothelial growth factor (*or:* '*VEGF*') will be expressed throughout the fetal development of esSDFTs but only until the approximate midpoint of gestation in pCDETs. This will align with the timeline of VEGF expression found in a previous study[186] of functionally comparable Achilles tendons and tibialis posterior tendons.[186] Ubiquitous VEGF expression throughout gestation will eventually confer esSDFTs with high vascularization[246,254] relative to their pCDET counterparts whilst also contributing to the notable abilities of the esSDFT to: (***i***) sustain large tenocyte populations[10,17,20] and (***ii***) regenerate from damage[10,89,253] over the pCDET in tissue maturity.

(***v***) That transforming growth factor beta–2 (*or:* '*TGF–β2*') will be expressed during the fetal development of pCDETs but not during that of esSDFTs. This will support the result of a TGF–β2 knockout study,[200] in which an absence of TGF–β2 signaling was found to result in the complete loss of developing forelimb extensor tendons (*positional*) whilst having comparatively negligible impact on (*energy storing flexor tendons*).[200] This will suggest an exclusive role of TGF–β2 in the development of the forelimb PT under present study and also help characterize the presently lacking characterization of –β2 isoform function.[246] However, similar to that hypothesis that was associated with Scx, while this study may suggest a critical role for TGF-β2 in extensor tendon development, the possibility of compensatory mechanisms in flexor tendons should also be considered.

6.1.2 Relevant Information to Molecular Biology Analysis

The current study attempted to examine potential disparity in molecular signalling between the esSDFT and pCDET during fetal development. The initial steps of two–step reverse transcription

real time quantitative polymerase chain reaction (‘*RT–qPCR*’)[34,209] were deployed with the aim of evaluating the relative mRNA expressions of: (***i***) COMP, (***ii***) COL3, (***iii***) Scx, (***iv***) VEGF, and (***v***) TGF–β2 in samples from a total of six fetuses that spanned two distinct gestational age ranges that were representative of the 2nd and 3rd trimesters. The partly completed RT–qPCR work was successful in creating primers (*or: nucleotide sequences that anneal to target mRNA*) for VEGF and TGF–β2, which are potentially of use to future investigations. Moreover, primers initially conceived by Wang et al. 2022 (*corresponding to β-Glucuronidase, abbreviated to ‘GUSB’, and TATA-Box Binding Protein, or ‘TBP’*) were validated as suitable housekeeping genes. These primers are presented in the table below. Primers were designed using Primer-BLAST® software from the National Centre for Biotechnology Information. Primers were created with default software settings with the exceptions of: (***i***) ‘PCR product size Max’ changed to 200, (***ii***) ‘Primer melting temperatures (T_m)’ changed to ‘Min’ 59, ‘Opt’ 62, ‘Max’ 65, (***iii***) ‘Exon junction span’ changed to ‘Primer must span an exon-exon junction’, and (***iv***) ‘Intron length range’ ‘Min’ changed to 200. Both forward (‘*fwd*’) and reverse (‘*rev*’) sequences are provided (*adapted from: Giffin & Franz-Odendaal 2020*[88]).

Gene	Accession Number	Strand	Sequence (5’ to 3’)	Size (bp)	Reference
VEGF	NM_174216.2	Fwd	ACATTGGAGCCTTGCCTTGC	87	This study
		Rev	TGGGGTTTCTGCCCTCCTTC		
TGF-β2	NM_001113252.1	Fwd	GCGGAGCGACGAGGAATACT	83	This study
		Rev	GCGGGATGGCATTTTCCGAG		
GUS	NM_173979.3	Fwd	CATCGGCAATGAGCGGTTCC	102	Wang et al. 2022[269]
		Rev	ACCGTGTTGGCGTAGAGGTC		
TBP	NM_001037443.2	Fwd	TCAGCCCTAGATTTGATGTGC	102	Wang et al. 2022[269]

7 In Closing

This investigation found structural idiosyncrasies pertaining to: (***i***) intermolecular cross–linking, (***ii***) collagen fibril diameter, and (***iii***) collagen fibril crimp, between the bovine energy storing superficial digital flexor tendon ('*esSDFT*') and positional common digital extensor tendon ('*pCDET*') during the 2nd and 3rd trimesters of fetal development. The presence of these architectural idiosyncrasies together suggest the combined effect of differences in other early developmental cues — rather than mechanoregulation — to be the principal catalyst for the divergence of multiple characteristics that ultimately become fine tuned for the distinct mechanical roles each of the two FDTs possess in life. Accordingly, this work suggests prenatal tendon development to be a rich area for future study of the control mechanisms responsible for the structure of collagenous tissues.

8 Appendix

8.1 Full Protocol for HIT Testing

8.1.1 Full Protocol for Standard HIT Testing

Hydrothermal isometric tension ('*HIT*') testing used to elucidate section 'T_d', 'T_{Fmax}', and '$t_{1/2}$' values was conducted using a custom–built six–section tester and JMP software via the following protocol:

1. Bisect the tendon sample longitudinally to 1–to–2 millimeters ('mm') width to stay within the 1000–gram ('g') load constraint of each load cell.
2. Section the length of each sample to 6–to–8 mm.
3. Isometrically constrain the section by clamping 2.5 mm of tissue from each end in steel grips and mounting the section vertically between a load cell and fixed support.
4. Submerge the section in a 4–liter ('L') beaker of 20–to–22 °C distilled, deionized water.
5. Apply a tensile preload of approximately ∼15 g (∼0.15 newtons) to the section.[2,104,260,262]
6. Let the section relax for 10 minutes.
7. Bring the system holding the section from room temperature to 90 °C (*at 1.5 °C per minute to 75 °C and 0.7 °C per minute thereafter*) using a computer–controlled hotplate.[104,262]
8. Maintain the temperature of the system at 90 °C for 3–to–5 hours.[2,104,275]
9. Continuously catalogue temperature–time–load data at 0.2 hertz ('Hz') using load cells.
10. Evaluate force–temperature data using Microsoft Excel.[231,262]
11. Note T_d, T_{Fmax}, and $t_{1/2}$ values.[104,262]

    To calculate $t_{1/2}$ value, first create a plot of ln(load/maximum load) vs. time.[104] Then, fit a linear line to the 3000 second data interval starting at 1000 seconds.[104] The slope of this line is used to calculate $t_{1/2}$ value as per Equation (A4).[2,195]

    Equation (A4): $t_{1/2} = log\frac{(1/2)}{-k}$

8.1.2 Full Protocol for HIT Testing with $NaBH_4$ Reduction

HIT testing also involved analysis of '$t_{1/2}$' values following sodium borohydride ('$NaBH_4$') treatment of sections as per the following protocol:

1. Follow Steps 1–2 outlined in Full Protocol for HIT Testing with two replicate sections of each sample.
2. Assign each replicate to a *CONTROL* or *TREATMENT* group.
3. Prepare a 200–milliliter ('mL') beaker containing 100 mL of borate buffer solution, pH = 9 for the *CONTROL* group via the following protocol:
    - Prepare Solution A of 0.1 M sodium hydroxide ($NaOH$) by dissolving 2 g of $NaOH$ in 500 mL of distilled water in a 1–L graduated cylinder.
    - Prepare Solution B by dissolving 7.46 g of potassium chloride (KCl) and 6.18 g of boric acid (H_3BO_3) in 1 L of distilled water in a 2–L graduated cylinder.
    - Add Solution A to Solution B until the resulting borate buffer solution has a pH of approximately 9.0.
    - Add distilled water to bring the volume of the borate buffer solution to 2 L.
    - Maintain the borate buffer solution in a 2–L plastic jar at 4 °C for continued use.
    - Transfer 100 mL of borate buffer solution from the 2–L plastic jar to a 200–mL beaker immediately prior to sample treatment.
4. Prepare a 200–mL beaker containing 100 mL of borate buffer solution and 0.1 milligrams ('mg') per mL $NaBH_4$, pH = 9 for the *TREATMENT* group via the following protocol:
    - Prepare a stock solution three minutes before sample treatment by adding 0.2 g of $NaBH_4$ to 20 mL of borate buffer solution in a 50–mL beaker.
    - Keep the stock solution at 4°C.
    - Pipette 1 mL of stock solution into a 100–mL graduated cylinder.
    - Add 99 mL of the borate buffer solution prepared in 3 to the 100–mL graduated cylinder containing 1 mL of stock solution.
    - Cover the 100–mL graduated cylinder with stock solution.
    - Shake the 100–mL graduated cylinder well.
    - Transfer the contents of the 100–mL graduated cylinder into a 200–mL beaker.

5. Place the section replicates assigned to the *CONTROL* and *TREATMENT* groups into the 200–mL beakers prepared in 3 and 4, respectively.

6. Shake the section replicates in their respective beakers at 4 °C for 15 minutes.

7. Prepare two new 200–mL beakers containing (i) 100 mL of borate buffer solution, pH = 9 and (ii) 100 mL of borate buffer solution and 0.1–mg–per–mL $NaBH_4$, pH = 9 as in 3 and 4.

8. Transfer the section replicates to the new beakers prepared in 7.

9. Shake the section replicates in their respective beakers at 4 °C for 15 minutes.

10. Repeat 7 through 9 two more times for a total of four shaking periods.

11. Prepare two new 200–mL beakers containing 50 mL of phosphate buffered saline.

12. Transfer the section replicates to the new beakers prepared in 10.

13. Shake the section replicates in the beakers containing phosphate buffered saline at 4 °C for 10 minutes.

14. Transfer the section replicates into capped Falcon tubes containing 10 mL of phosphate buffered saline such that the section replicates are submerged for transportation to the HIT Testing apparatus.

15. Perform Steps 3 through 11 as outlined in Protocol for Standard HIT Testing.

8.2 Full Protocol for TEM Analysis

Transmission electron microscopy ('*TEM*') analysis was conducted via the following protocol adapted from protocol provided by Ms. Mary Ann Trevors from Dalhousie University's Electron Microscope Core Facility:

1. Fix the sample in 2.5% glutaraldehyde diluted with 0.1 M sodium cacodylate buffer for via the following protocol:
    - Rinse the sample in distilled, deionized water thrice for ten minutes under constant agitation each time.
    - Transfer the sample in 2.5% glutaraldehyde in 0.1 M cacodylate buffer for two hours under constant agitation.
    - Rinse the sample in distilled, deionized water thrice for ten minutes under constant agitation each time.
    - Cut the sample in half longitudinally.
    - Rinse the sample in 30% ethanol in distilled, deionized water for ten minutes.
    - Store samples in 70% ethanol in distilled, deionized water at 4 °C.
2. Rinse the sample in 0.1 M sodium cacodylate buffer thrice for 10 minutes each time.
3. Fix the sample in 1% osmium tetroxide for 2 hours.
4. Quickly rinse the sample with distilled water.
5. Place the sample in 0.25% uranyl acetate at 4 °C for 12 hours.
6. Dehydrate the sample with a graduated series of acetone (50% acetone — 10 minutes; 70% acetone — 10 minutes x 2; 95% acetone — 10 minutes x 2; 100% acetone — 10 minutes x 2; Dried 100% acetone — 10 minutes).
7. Infiltrate the sample with epon araldite resin (3:1 ratio ... 3 parts dried 100% acetone: 1 part resin for 3 hours; 1:3 ratio ... 1 part dried 100% acetone: 3 parts resin for 12 hours; 100% epon araldite resin for twice for 3 hours).
8. Embed the sample in 100% epon araldite resin.
9. Place the sample in an oven at 60°C for 48 hours.
10. Section the sample to a thickness of approximately 100 nanometers ('nm') using a Reichert — Jung Ultracut E Ultramicrotome with a diamond knife.
11. Place the resulting sections on a 300–mesh copper grid.

12. Stain the sections as follows: 2% aqueous uranyl acetate — 10 minutes, 2 x 5 minutes distilled water rinse, lead citrate — 4 minutes, quick rinse with distilled water, air dry.

13. View the sections using a JEOL JEM 1230 Transmission Electron Microscope at 80 kilovolts.

14. Capture images of the sections using a Hamamatsu ORCA–HR digital camera.

15. Evaluate CFD at 10,000× to 150,000× magnification.[90,121,208] In quantification of FD, measure 500 fibrils areas per developmental time point per tendon class.[121] Analyse 960–nm–by–1280–nm imaging fields using the Fiji release of ImageJ software (*see:* Figure 26).[95,121,122]

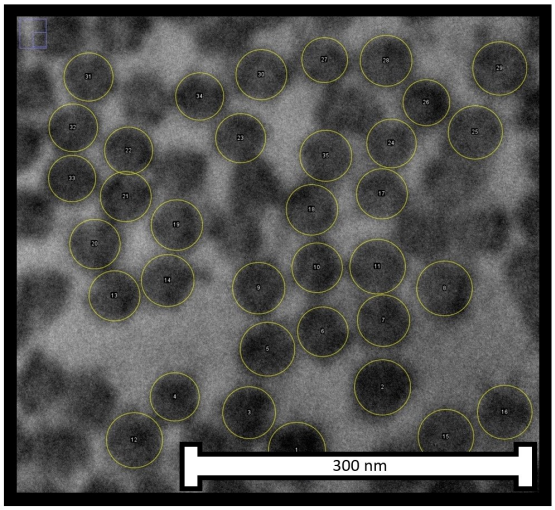

Figure 26: An image depicting the Fiji ('*Fiji Is Just ImageJ*') protocol that was associated with the determination of CFD. Perfect circles were first drawn within the utmost bounds of each fibril such that each circle never extended beyond the circumference of its associated fibril. Following this, CFD was determined using $A = \pi r^2$. This image was obtained via transmission electron microscopy ('TEM') analysis of tendons at 100,000× magnification.

8.3 Full Protocol for PLM Analysis

Polarized light microscopy (‘*PLM*’) analysis was conducted via the following protocol:

1. Fix the sample in 2.5% glutaraldehyde diluted with 0.1 M sodium cacodylate buffer for 2 hours (as described in Step 1 of Structural Assessment via TEM).
2. Cryosection three sections of the sample longitudinally to 30 micrometers (‘µm’).
3. Mount the resulting sections on a microscope slide using Hydromount^{TM}.
4. Evaluate the slide using a Nikon Eclipse E600 light microscope equipped with a polarizer.
5. Image the slide with a 10–megapixel AmScope digital camera (*see: Figure 27*).
6. Assess the images using ImageJ.[194,196]

   Obtain three clear images from different regions of each section.

   Draw a line normal to the to the principal crimp direction that is at least 600 µm in length (*∼633 to 635 µm lines were used in the present work*) and divide the distance of the line by the number of discernible crimps it encompasses for a measure of mean collagen fibril crimp (‘*CFC*’, *hereafter*) wavelength (*Figure 27*).[102,153,194,195]

   Repeat this process three times in the top, middle, and bottom regions of each image.

   Average measurements made over three images of each of the three 30–µm–sections to obtain a final measurement of mean CFC wavelength.

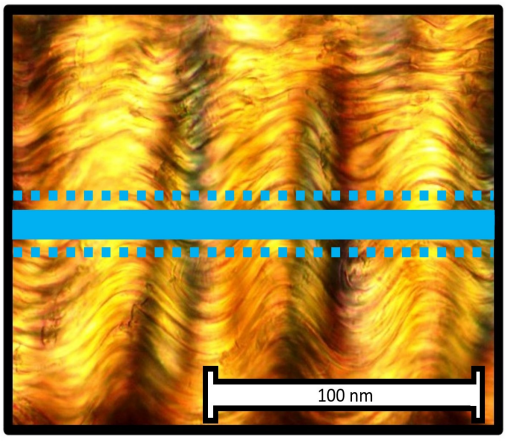

Figure 27: An image depicting the Fiji (‘*Fiji Is Just ImageJ*’) protocol that was associated with the determination of mean CFC wavelength. A line was first drawn down the center of each image normal to the principal creep direction. The mean CFC wavelength was then determined by dividing the length of this line by the number of discernible crimp peaks it encompassed. A scale bar approximating ∼300 nanometers (‘*nm*’) was provided. This image was obtained via polarized light microscopy (‘*PLM*’) analysis of tendons at 10× magnification.

8.4 Image Copyright Information

8.4.1 Modified Image #1: '*The Hierarchical Structure of Tendon*'

Original Image Title: '*Hierarchical arrangement of the structure of tendons*'.

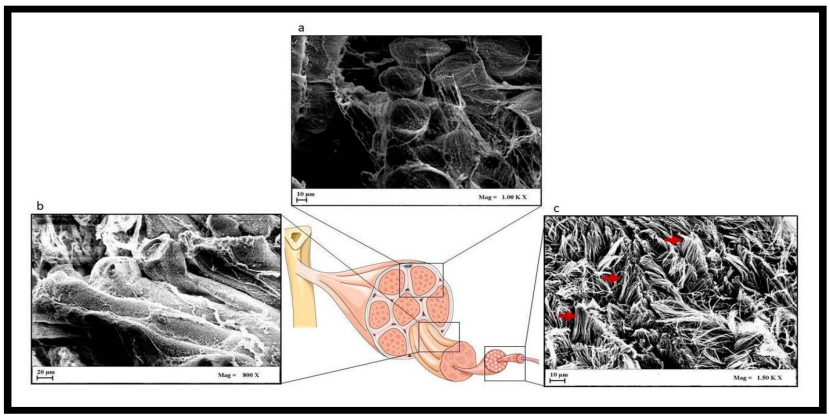

Description: This image was taken and modified from a scientific article titled: '*In Vitro Innovation of Tendon Tissue Engineering Strategies*'. This article was published under the terms of the Creative Commons Attribution 4.0 International License (*CC BY 4.0*). The image depicts a mock–up of tendon hierarchical structure with three 'scanning electron microscopy' (SEM) images deployed to highlight the varying architecture between regions. In this thesis, this image was modified for Figure 1, titled: '*The Hierarchical Structure of Tendon*'. To access the article and complete image caption, *see:* Citeroni et al. (2020) [44].

License: This image is licensed under the Creative Commons Attribution 4.0 International License (CC BY 4.0).

Attribution: Citeroni MR, Ciardulli MC, Russo V, Porta GD, Mauro A, El Khatib M, Mattia MD, Galesso D, Barbera C, Forsyth NR, Maffulli N, Barboni B. 2020. *In Vitro Innovation of Tendon Tissue Engineering Strategies*. Int. J. Mol. Sci. 21(18): 6726, doi: 10.3390/ijms21186726.

8.4.2 Modified Image #2: '*The Molecular Structure of Collagen...*'

Original Image Titles: (a) '*Fig 4.1 Reaction of telopeptide*'... and (b) '*Fig 4.2 Reaction of telopeptide*'....

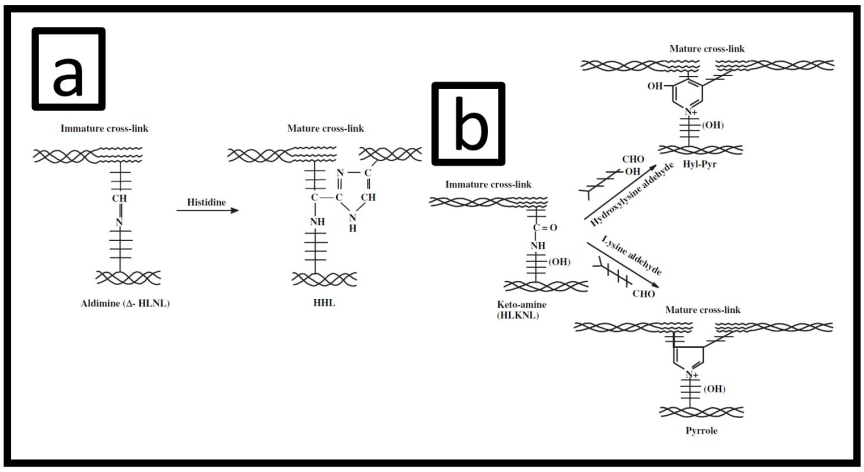

Description: This image was taken and modified from: '*Chapter 4: Restraining Cross-Links Responsible for the Mechanical Properties of Collagen Fibers: Natural and Artificial*' in *Collagen: Structure and Mechanics (2008)*. This book was published under the copyright terms set out by Springer Nature. The two figures depict diagrams of multiple types of enzymatic intermolecular cross–links found between collagen molecules. In this thesis, these figures were modified for Figures 2, 3, and 4, titled: '*The Molecular Structure of Collagen*', '*The Creation of a Collagen Intermolecular Cross–Link*', and '*Representative Intermolecular Cross–Links of Tendon*', respectively. To access this book and the complete caption for each figure, *see: Collagen: Structure and Mechanics (2008)*[6].

License: This image is licensed under an agreement between Mr. Theodore Lownie (author) and Springer Nature (*"Springer Nature"; License Number: 5736640838808, License date: Feb 26, 2024*). Further details are provided in the image below.

SPRINGER NATURE LICENSE
TERMS AND CONDITIONS

Feb 26, 2024

This Agreement between Mr. Theodore Lownie ("You") and Springer Nature ("Springer Nature") consists of your license details and the terms and conditions provided by Springer Nature and Copyright Clearance Center.

License Number	5736640838808
License date	Feb 26, 2024
Licensed Content Publisher	Springer Nature
Licensed Content Publication	Springer eBook
Licensed Content Title	Restraining Cross-Links Responsible for the Mechanical Properties of Collagen Fibers: Natural and Artificial
Licensed Content Author	N.C. Avery, A.J. Bailey
Licensed Content Date	Jan 1, 2008
Type of Use	Thesis/Dissertation
Requestor type	academic/university or research institute
Format	print and electronic
Portion	figures/tables/illustrations
Number of figures/tables/illustrations	2
Will you be translating?	no
Circulation/distribution	1 - 29
Author of this Springer Nature content	no
Title of new work	Developmental Divergence of Tendon
Institution name	Saint Mary's University
Expected presentation date	Jun 2024
Order reference number	14972024
Portions	Fig. 4.1, Page 84. Fig 4.2, Page 85.
Requestor Location	Mr. Theodore Lownie 6095 Coburg Road Unit 304 Halifax, NS B3H4K1 Canada Attn: Mr. Theodore Lownie
Total	0.00 CAD

Attribution: Avery NC, Bailey AJ. 2008. *Chapter 4: Restraining Cross-Links Responsible for the Mechanical Properties of Collagen Fibers: Natural and Artificial in P. Fratzl (ed.), Collagen: Structure and Mechanics (2008)*. Available from: *Collagen: Structure and Mechanics (2008)*[6].

8.4.3 Modified Image #3: '*The Bovine SDFT and CDET*'.

Original Image Title: '*Fig 1 Experimental procedure used...*'.

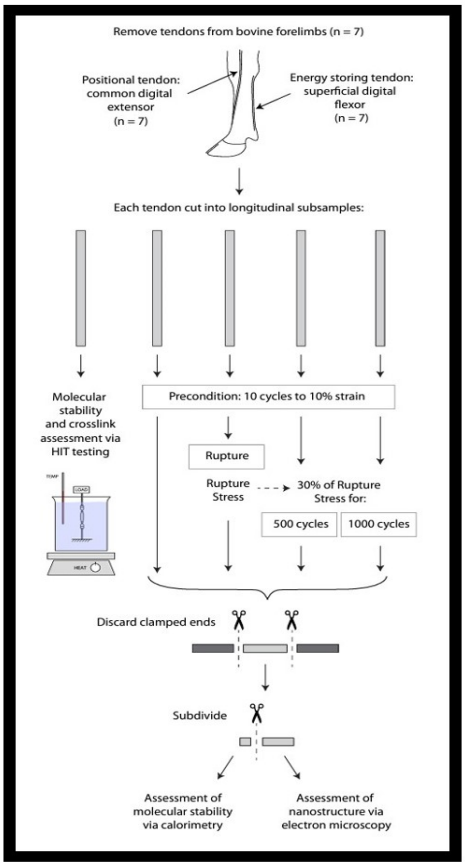

Description: This image was taken and modified from: '*Collagen fibrils in functionally distinct tendons have differing structural responses to tendon rupture and fatigue loading*'. This article was published under the copyright terms set out by Elsevier. The figure depicts a diagram illustrating tendon excision from a bovine forelimb and subsequent (i) hydrothermal isometric tension– ('HIT') and (ii) mechanical testing. In this thesis, this figure was modified for Figure 6, titled:'*The Bovine SDFT and CDET*'. To access this article and the complete caption for the figure, *see: Herod et al. (2016)*[104].

License: This image is licensed under an agreement between Mr. Theodore Lownie (author) and Elsevier (*"Elsevier"; License Number: 5737380401486, License date: Feb 27, 2024*). Further details are provided in the image below.

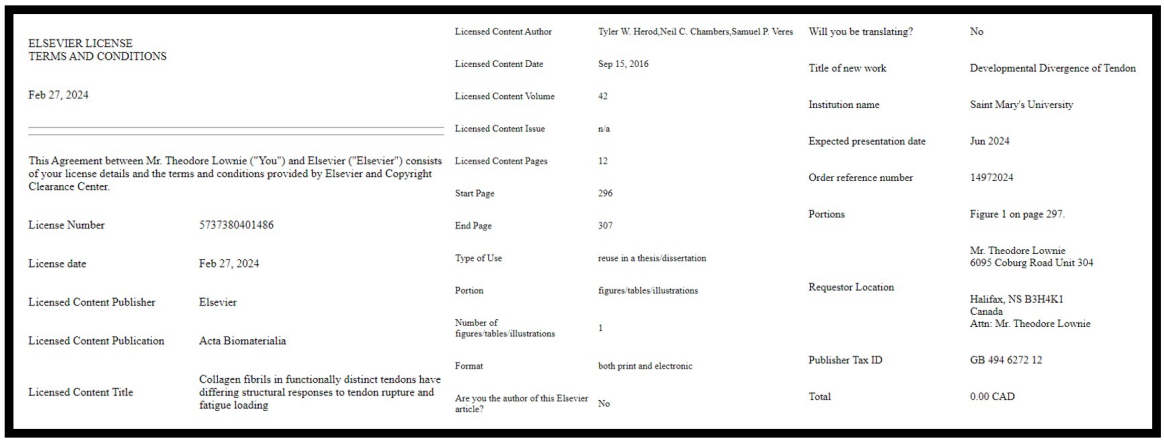

ELSEVIER LICENSE
TERMS AND CONDITIONS

Feb 27, 2024

This Agreement between Mr. Theodore Lownie ("You") and Elsevier ("Elsevier") consists of your license details and the terms and conditions provided by Elsevier and Copyright Clearance Center.

License Number	5737380401486
License date	Feb 27, 2024
Licensed Content Publisher	Elsevier
Licensed Content Publication	Acta Biomaterialia
Licensed Content Title	Collagen fibrils in functionally distinct tendons have differing structural responses to tendon rupture and fatigue loading
Licensed Content Author	Tyler W. Herod,Neil C. Chambers,Samuel P. Veres
Licensed Content Date	Sep 15, 2016
Licensed Content Volume	42
Licensed Content Issue	n/a
Licensed Content Pages	12
Start Page	296
End Page	307
Type of Use	reuse in a thesis/dissertation
Portion	figures/tables/illustrations
Number of figures/tables/illustrations	1
Format	both print and electronic
Are you the author of this Elsevier article?	No
Will you be translating?	No
Title of new work	Developmental Divergence of Tendon
Institution name	Saint Mary's University
Expected presentation date	Jun 2024
Order reference number	14972024
Portions	Figure 1 on page 297.
Requestor Location	Mr. Theodore Lownie 6095 Coburg Road Unit 304 Halifax, NS B3H4K1 Canada Attn: Mr. Theodore Lownie
Publisher Tax ID	GB 494 6272 12
Total	0.00 CAD

Attribution: Herod TW, Chambers NC, Veres SP. 2016. *Collagen fibrils in functionally distinct tendons have differing structural responses to tendon rupture and fatigue loading*. Acta Biomater. 42: 296-307. doi: 10.1016/j.actbio.2016.06.017.

8.4.4 Modified Image #4: '*A Depiction of a Tendon Cell*'

Original Image Title: '*Figure 5: TEM image of cross–sectioned collagen fibrils and a tenocyte...*'.

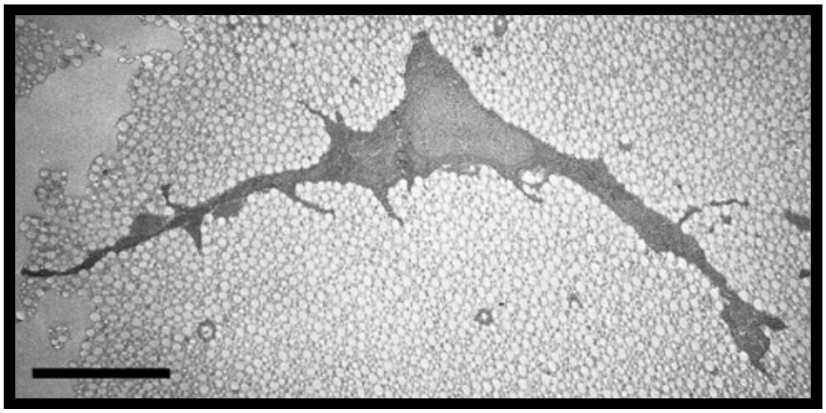

Description: This image was taken and modified from a scientific article titled: '*Collagen Structure of Tendon Relates to Function*'. This article was published under the terms of the Creative Commons Attribution 3.0 International License (*CC BY 3.0*). The image depicts a transmission electron microscope ('TEM') capture of a cross–sectioned tendon cell (*commonly referred to as a 'fibroblast', 'tenoblast', or 'tenocyte'*) and the abundance of collagen fibrils that surround it. In this thesis, this image was modified for Figure 7, titled: '*A Depiction of a Tendon Cell*'. To access the article and complete image caption, *see:* Franchi et al. (2007)[78].

License: This image is licensed under the Creative Commons Attribution 3.0 International License (CC BY 3.0).

Attribution: Marco F, Trirè A, Quaranta M, Orsini E, Ottani V. 2007. *Collagen Structure of Tendon Relates to Function*. Sci. World J. 7: 404-420, doi: 10.1100/tsw.2007.92.

8.4.5 Modified Image #5: '*TEM Discussion: A Comparison of Collagen...*'

Original Image Title: '*Fig. 2. Transmission electron micrograph of a SDFT...*'.

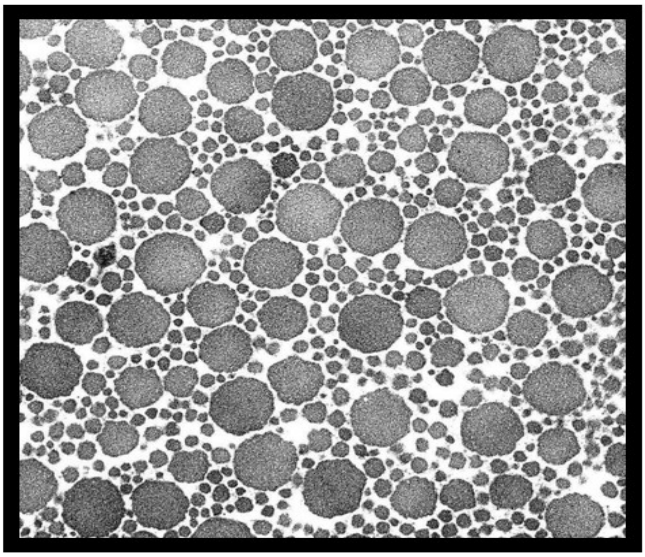

Description: This image was taken and modified from a scientific article titled: '*The Pathogenesis of Tendon Microdamage in Athletes: the Horse as a Natural Model for Basic Cellular Research*'. This article was published under the terms of the Creative Commons Attribution 3.0 International License (*CC BY 3.0*). The image depicts a transmission electron microscope ('TEM') capture of cross–sectioned collagen fibrils from a thoroughbred horse (*equine*; *Equus caballus*). In this thesis, this image was modified for Figure 20, titled: '*TEM Discussion: A Comparison of Collagen...*'. To access the article and complete image caption, *see:* Patterson-Kane et al. (2012)[188].

License: This image is licensed under the Creative Commons Attribution 3.0 International License (CC BY 3.0).

Attribution: Patterson-Kane JC, Becker DL, Rich T. 2012. *The Pathogenesis of Tendon Microdamage in Athletes: the Horse as a Natural Model for Basic Cellular Research*. J. Comp. Pathol. 147(2-3): 227-247, doi: 10.1016/j.jcpa.2012.05.010.

Bibliography

[1] **Aldous IG**. Thermomechanical stability of heart valve collagen: Differences with valve type and age, and implications for remodelling. *Doctorate Thesis: Dalhousie University*, 2008.

[2] **Aldous IG, Veres SP, Jahangir A, Lee MJ**. Differences in collagen cross-linking between the four valves of the bovine heart: a possible role in adaptation to mechanical fatigue. *Am. J. Physiol. – Heart Circ. Physiol.*, 296(6):1898–1906, 2009. doi:10.1152/ajpheart.01173.2008.

[3] **Alshomer F, Chaeves C, Kalaskar DM**. Advances in tendon and ligament tissue engineering: materials perspective. *J. Mater.*, 9868151, 2018. doi:10.1155/2018/9868151.

[4] **Asgari M, Latifi N, Heris HK, Vali H, Mongeau L**. In vitro fibrillogenesis of tropocollagen type iii in collagen type i affects its relative fibrillar topology and mechanics. *Sci. Rep.*, 7:1392, 2017. doi:10.1038/s41598-017-01476-y.

[5] **Ashenhurst J**. Carboxylic Acid Derivatives: Why Is Hydrolysis of Amides So Difficult Compared To Acid Halides and Esters? Two Reasons. Master Organic Chemistry. URL: https://www.masterorganicchemistry.com/2019/10/07/amide-hydrolysis/#two, 2022.

[6] **Avery AC & Bailey AJ**. Restraining cross-links responsible for the mechanical properties of collagen fibers: Natural and artificial. In Peter Fratzl, editor, *Collagen Structure and Mechanics*, chapter 4, pages 81–110. Springer Science+Business Media, LLC, Springer Science+Business Media, LLC, 233 Spring Street, New York, NY 10013, USA, 2008.

[7] **Avery NC & Bailey AJ**. Enzymatic and non-enzymatic cross-linking mechanisms in

relation to turnover of collagen: relevance to aging and exercise. *Scand. J. Med. Sci. Sports*, 15(4):231–240, 2005. doi:10.1111/j.1600-0838.2005.00464.x.

[8] **Backman C, Boquist L, Fridén J, Lorentzon R, Toolanen G**. Chronic achilles paratenonitis with tendinosis: An experimental model in the rabbit. *J. Orthop. Res.*, 8(4):541–547, 1990. doi:10.1002/jor.1100080410.

[9] **Banos CC, Thomas AH, Kuo CK**. Collagen fibrillogenesis in tendon development: current models and regulation of fibril assembly. *Birth Defects Res. C Embryo Today*, 84(3):228–244, 2008. doi:10.1002/bdrc.20130.

[10] **Batson EL, Paramour RJ, Smith TJ, Birch HL, Patterson-Kane JC, Goodship AE**. Are the material properties and matrix composition of equine flexor and extensor tendons determined by their functions? *Equine Vet. J.*, 35(3):314–318, 2003. doi:10.2746/042516403776148327.

[11] **Bavin EP, Atkinson F, Barsby T, Guest DJ**. Scleraxis is essential for tendon differentiation by equine embryonic stem cells and in equine fetal tenocytes. *Stem Cells Dev.*, 26(6):441–450, 2017. doi:10.1089/scd.2016.0279.

[12] **Bayer ML, Yeung CYC, Kadler KE, Qvortrup K, Baar K, Svensson RB, Magnusson PS, Krogsgaard M, Koch M, Kjaer M**. The initiation of embryonic-like collagen fibrillogenesis by adult human tendon fibroblasts when cultured under tendon. *Biomater.*, 31(18):4889–4897, 2010. doi:10.1016/j.biomaterials.2010.02.062.

[13] **Benedict JV, Walker LB, Harris EH**. Stress-strain characteristics and tensile strength of unembalmed human tendon. *J. Biomech.*, 1(1):53–56, 1968. doi:10.1016/0021-9290(68)90038-9.

[14] **Benjamin M, Kaiser E, Milz S**. Structure-function relationships in tendons: a review. *J. Anat.*, 212(3):211–228, 2008. doi:10.1111/j.1469-7580.2008.00864.x.

[15] **Biewener AA**. Tendons and ligaments: Structure, mechanical behavior and biological function. In Peter Fratzl, editor, *Collagen Structure and Mechanics*, chapter 10, pages 269–284. Springer Science+Business Media, LLC, Springer Science+Business Media, LLC, 233 Spring Street, New York, NY 10013, USA, 2008.

[16] **Billette JM & Janz T** Injuries in Canada: Insights from the Canadian Community Health Survey. *Statistics Canada Catalogue*, no. 82-624-X, 2011.

[17] **Birch HL**. Tendon matrix composition and turnover in relation to functional requirements. *Int. J. Exp. Pathol.*, 88:241–248, 2007. doi:10.1111/j.1365-2613.2007.00552.x.

[18] **Birch HL, Bailey AJ, Goodship AE**. Macroscopic 'degeneration' of equine superficial digital flexor tendon is accompanied by a change in extracellular matrix composition. *Equine Vet. J.*, 30(6):534–539, 1998. doi:10.1111/j.2042-3306.1998.tb04530.x.

[19] **Birch HL, Smith TJ, Draper ER, Bailey AJ, Avery NC, Goodship AE**. Collagen crosslink profile relates to tendon mechanical properties. *Matrix Biol.*, 25:S74, 2006.

[20] **Birch HL, Smith TJ, Tasker T, Goodship AE**. Age related changes to mechanical and matrix properties in human achilles tendon. *Transactions of the 47th Annual Meeting of the Orthopaedic Research Society, San Francisco, California*, 2001.

[21] **Birch HL, Thorpe CT, Rumian AP**. Specialisation of extracellular matrix for tendons and ligaments. *Muscles Ligaments Tendons J.*, 3(1):12–22, 2013. doi:10.11138/mltj/2013.3.1.012.

[22] **Birch HL, Worboys S, Eissa S, Jackson B, Strassburg S, Clegg PD**. Matrix metabolism rate differs in functionally distinct tendons. *Matrix Biol.*, 27:182–189, 2008. doi:10.1016/j.matbio.2007.10.004.

[23] **Birk DE & Mayne R**. Localization of collagen types i, iii and v during tendon development. changes in collagen types i and iii are correlated with changes in fibril diameter. *Eur. J. Cell Biol.*, 72:352–361, 1997.

[24] **Birk DE, Nurminskaya MV, Zycband EI**. Collagen fibrillogenesis in situ: fibril segments undergo post-depositional modifications resulting in linear and lateral growth during matrix development. *Dev. Dyn.*, 202:229–243, 1995. doi:10.1002/aja.1002020303.

[25] **Blitz E, Viukov S, Sharir A, Schwartz Y, Galloway JL, Pryce BA, Johnson RL, Tabin CJ, Schweitzer R, Zelzer E**. Bone ridge patterning during musculoskeletal assembly is mediated through scx regulation of bmp4 at the tendon-skeleton junction. *Dev. Cell*, 17:861–873, 2009. doi:10.1016/j.devcel.2009.10.010.

[26] **Bobzin L, Hoberts RR, Chen HJ, Crump JG, Merrill AE**. Development and maintenance of tendons and ligaments. *Development*, 148(8):186916, 2021. doi:10.1242/dev.186916.

[27] **Bordoni B & Varacallo M** Anatomy: Tendons. In: StatPearls [Internet]. Treasure Island (FL): StatPearls Publishing. URL: https://www.ncbi.nlm.nih.gov/books/NBK513237/, 2022.

[28] **Brown JP, Finley VG, Kuo CK**. Embryonic mechanical and soluble cues regulate tendon progenitor cell gene expression as a function of developmental stage and anatomical origin. *J. Biomech.*, 47(1):214–222, 2014. doi:10.1016/j.jbiomech.2013.09.018.

[29] **Brown NAT, Pandy MG, Kawak CE, McIllwraith CW**. Force- and moment-generating capacities of muscles in the distal forelimb of the horse. *J. Anat.*, 203:101–113, 2003. doi:10.1046/j.1469-7580.2003.00206.x.

[30] **Brumitt J & Cudderford T**. Current concepts of muscle and tendon adaptation to strength and conditioning. *Int. J. Sports Phys. Ther.*, 10(6):748–759, 2015.

[31] **Buckley MR, Evans E, Satchel LN, Matuszewski PE, Chen YL, Elliott DM, Soslowsky LJ, Dodge GR**. Distributions of types i, ii and iii collagen by region in the human supraspinatus tendon. *Connect. Tissue Res.*, 54(6):374–379, 2013. doi:10.3109/03008207.2013.847096.

[32] **Budras KD, Habel RE, Wünsche A, Buda S**. Bovine anatomy: An illustrated text. first edition. *Die Deutsche Bibliothek. Printed in Germany.*, 2003.

[33] **Burton B, Willet T, Marc G**. Improving the mechanical properties of irradiation-sterilized bone. *Master's Thesis: University of Toronto*, 2013.

[34] **Bustin SA, Benes V, Garson JA, Hellemans J, Huggett J, Kubista M, Mueller R, Nolan T, Pfaffl MW, Shipley GL, Vandesompele J, Wittwer CT**. The miqe guidelines: minimum information for publication of quantitative real-time pcr experiments. *Clin. Chem.*, 55(4):611–622, 2009. doi:10.1373/clinchem.2008.112797.

[35] **Caceres MD, Pfeifer CG, Docheva D**. Understanding tendons: lessons from transgenic mouse models. *Stem Cells Dev.*, 27(17):1161–1174, 2018. doi:10.1089/scd.2018.0121.

[36] **Canty-Laird E & Kadler K**. Procollagen trafficking, processing and fibrillogenesis. *J. Cell Sci.*, 118:1341–1353, 2005. doi:10.1242/jcs.01731.

[37] **Carlton RA**. Pharmaceutical Microscopy Chapter 2: Polarized Light Microscopy / pp. 7-64. URL: https://link.springer.com/book/10.1007/978-1-4419-8831-7, last accessed on 2022-10-06, 2011.

[38] **Chakravarti S**. Functions of lumican and fibromodulin: lessons from knockout mice. *Glycoconj. J.*, 19:287–293, 2003.

[39] **Chakravarti S, Magnuson T, Lass JH, Jepsen KJ, LaMantia C, Carroll H**. Lumican regulates collagen fibril assembly: skin fragility and corneal opacity in the absence of lumican. *J. Cell Biol.*, 141:1277–1286, 1998. doi:10.1083/jcb.141.5.1277.

[40] **Chambers NC, Herod TW, Veres SP**. Ultrastructure of tendon rupture depends on strain rate and tendon type. *J. Orthop. Res.*, 35(1):96–102, 2018. doi:10.1002/jor.24067.

[41] **Chang SW & Buehler MJ**. Molecular biomechanics of collagen molecules. *Mater. Today Commun.*, 17(2):70–76, 2014. doi:10.1016/j.mattod.2014.01.019.

[42] **Chen X, Yin Z, Chen J, Liu H, Shen W, Fang Z, Zhu T, Ji J, Ouyang HW, Zou XH**. Scleraxis-overexpressed human embryonic stem cell-derived mesenchymal stem cells for tendon tissue engineering with knitted silk-collagen scaffold. *Tissue Eng. Part A*, 20:11–12, 2014. doi:10.1089/ten.tea.2012.0656.

[43] **Choi R, Smith M, Clarke E, Little C**. Cellular, matrix, and mechano-biological differences in load-bearing versus positional tendons throughout development and aging: a narrative review. *Connect. Tissue Res.*, 59:367–375, 2018. doi:10.1080/03008207.2018.1504929.

[44] **Citeroni MR, Ciardulli MC, Russo V, Porta GD, Mauro A, El Khatib M, Mattia MD, Galesso D, Barbera C, Forsyth NR, Maffulli N, Barboni B**. In

vitro innovation of tendon tissue engineering strategies. *Int. J. Mol. Sci.*, 21(18):6726, 2020. doi:10.3390/ijms21186726.

[45] **Collier TA, Nash A, Birch HL, de Leeuw NH**. Effect on the mechanical properties of type i collagen of intra-molecular lysine-arginine derived advanced glycation end-product cross-linking. *J. Biomech.*, 67:55–61, 2018. doi:10.1016/j.jbiomech.2017.11.021.

[46] **Connizzo BK, Yannascoli SM, Soslowsky LJ**. Structure-function relationships of postnatal tendon development: a parallel to healing. *Matrix Biol.*, 32(2):106–116, 2013. doi:10.1016/j.matbio.2013.01.007.

[47] **Couppé C, Hansen P, Kongsgaard M, Kovanen V, Suetta C, Aagaard P, Kjær M, Magnusson SP**. Mechanical properties and collagen cross-linking of the patellar tendon in old and young men. *J. Appl. Physiol.*, 107(3):880–886, 2009. doi:10.1152/japplphysiol.00291.2009.

[48] **Cserjesi P, Brown D, Ligon KL, Lyons GE, Copeland NG, Gilbert DJ, Jenkins NA, Olson EN**. Scleraxis: a basic helix-loop-helix protein that prefigures skeletal formation during mouse embryogenesis. *Development*, 121:1099–1110, 1995. doi:10.1242/dev.121.4.1099.

[49] Clark T **CVM Large Animal Anatomy**. Distal Limb. URL: https://pressbooks.umn.edu/largeanimalanatomy/chapter/distal-limb/, last accessed on 2024-09-01, 2024.

[50] **Dahners LE. Ed: Maffulli N, Renström P, Leadbetter WB**. Tendon injuries: basic science and clinical medicine. *Springer*, 3:22–24, 2005. doi:10.1007/1-84628-050-8_3.

[51] **Davies PF, Manduchi E, Jiménez JM, Jiang YZ**. Biofluids, cell mechanics and

epigenetics: Flow-induced epigenetic mechanisms of endothelial gene expression. *J. Biomech.*, 50:3–10, 2018. doi:10.1016/j.jbiomech.2016.11.017.

[52] **Denoix JM**. Functional anatomy of tendons and ligaments in the distal limbs (manus and pes). *Tendon and Ligament Injuries: Part 1*, 10(2):273–322, 1994.

[53] **Denoix JM**. Essentials of clinical anatomy of the equine locomotor system. *Taylor Francis Group*, 2019.

[54] **Depalle B, Qin Z, Shefelbine SJ, Buehler MJ**. Influence of cross-link structure, density and mechanical properties in the mesoscale deformation mechanisms of collagen fibrils. *J. Mech. Behav. Biomed. Mater.*, 52:1–13, 2015. doi:10.1016/j.jmbbm.2014.07.008.

[55] **Dienes B, Bazsó T, Szabó L, Csernoch L**. The role of the piezo1 mechanosensitive channel in the musculoskeletal system. *Int J Mol Sci.*, 24(7):6513, 2023. doi:10.3390/ijms24076513.

[56] **Do I Qualify for Long-Term Disability Benefits if I have Carpal Tunnel Syndrome or Tendonitis?**. Ertl Lawyers. URL: https://www.ertl-lawyers.com/disability-law/disabling-conditions/carpal-tunnel-tendonitis/, last accessed on 2022-07-03, 2020.

[57] **Dunkman AA, Buckley MR, Mienaltowski MJ, Adams SM, Thomas SJ, Satchell L, Kumar A, Pathmanathan L, Beason DP, Iozzo RV, Birk DE, Soslowsky LJ**. Decorin expression is important for age-related changes in tendon structure and mechanical properties. *Matrix Biol.*, 32(1):3–13, 2012. doi:10.1016/j.matbio.2012.11.005.

[58] **D'Souza D & Patel K**. Involvement of long- and short-range signalling during early tendon development. *Anat. Embryol.*, 200:367–375, 1999. doi:10.1007/s004290050286.

[59] **Edom-Vovard F & Duprez D**. Signals regulating tendon formation during chick embryonic development. *Dev. Dyn.*, 229(3):449–457, 2004. doi:10.1002/dvdy.10481.

[60] **Eekhoff JD, Fang F, Lake SP**. Multiscale mechanical effects of native collagen cross-linking in tendon. *Connect. Tiss. Res.*, 59(5):410–422, 2018. doi:10.1080/03008207.2018.1449837.

[61] **Electron Microscopy Tutorial**. Advanced Microscopy: The University of Utah. URL: https://advanced-microscopy.utah.edu/education/electron-micro/index.html, last accessed on 2022-10-03, 2011.

[62] **Ellingson AJ, Pancheri NM, Schiele NR**. Regulators of collagen crosslinking in developing and adult tendons. *Eur. Cells. Mater.*, 43:130–152, 2022. doi:10.22203/eCM.v043a11.

[63] **Engle J**. Versatile collagens in invertebrates. *Science*, 277:1785–1786, 1997. doi:10.1126/science.277.5333.1785.

[64] **Ergonomics in the Workplace**. Injuries in Canada: Insights from the Canadian Community Health Survey. Ministry of Labour Training and Skills Development. Government of Ontario. URL: https://www.ontario.ca/page/ergonomics-workplace, last accessed on 2022-07-03, 2021.

[65] **Eriksen HA, Pajala A, Leppilahti J, Risteli J**. Increased content of type iii collagen at the rupture site of human achilles tendon. *J. Orthop. Res*, 20:1352–1357, 2002. doi:10.1016/S0736-0266(02)00064-5.

[66] **Eyre DR & Oguchi H**. The hydroxypyridinolinium cross-links of skeletal collagen: their

measurement, properties and proposed pathway of formation. *Biophys. Res. Commun.*, 92:403–410, 1980.

[67] **Eyre DR & Wu JJ**. Collagen cross-links. *Top. Curr. Chem.*, 247:207–229, 2005. doi:10.1007/b103828.

[68] **Ezura Y, Chakravarti S, Oldberg A, Chervoneva I, Birk DE**. Differential expression of lumican and fibromodulin regulate collagen fibrillogenesis in developing mouse tendons. *J. Cell Biol.*, 151(4):779–788, 2000. doi:10.1083/jcb.151.4.779.

[69] **Favata M, Beredjiklian PK, Zgonis MH, Beason DP, Crombleholme TM, Jawad AF, Soslowsky LJ**. Regenerative properties of fetal sheep tendon are not adversely affected by transplantation into an adult environment. *J. Orthop. Res.*, 11:2124–2132, 2006. doi:10.1002/jor.20271.

[70] **Feniyanos E**. Age-, sex-, and diabetes-determined changes in the structure and mechanics of human sartorius tendon collagen. *Master's Thesis: Dalhousie University*, 2019.

[71] **Fessel G, Gerber C, Snedeker JG**. Potential of collagen cross-linking therapies to mediate tendon mechanical properties. *J. Shoulder Elbow Surg.*, 21(2):209–217, 2012. doi:10.1016/j.jse.2011.10.002.

[72] **Fleischhacker V, Klatte-Schulz F, Minkwitz S, Schmock A, Rummler M, Seliger A, Willie BM, Wildemann B**. In vivo and in vitro mechanical loading of mouse achilles tendons and tenocytes—a pilot study. *Int. J. Mol. Sci.*, 21(4):1313, 2020. doi:10.3390/ijms21041313.

[73] **Fleischmajer R, Timpl R, Tuderman L, Rausger L, Wuestner M, Perlish JS,**

Graves PN. Ultrastructural identification of extension aminopropeptides of type i and iii collagens in human skin. *Proc. Natl. Acad. Sci. USA*, 78:7360–7364, 1981.

[74] **Flory PJ, Spurr Jr. OK**. Melting equilibrium for collagne fiberes under stress. elasticity in the amorphous state. *J. Am. Chem. Soc.*, 83(6), 1961.

[75] **Franchi M, Ottani V, Stagni R, Ruggeri A**. Tendon and ligament fibrillar crimp give rise to left-handed helices of collagen fibrils in both planar and helical crimps. *J. Anat.*, 216(3):301–309, 2010. doi:10.1111/j.1469-7580.2009.01188.x.

[76] **Franchi M, Quaranta M, Macciocca M, De Pasquale V, Ottani V, Ruggeri A**. Structure relates to elastic recoil and functional role in quadriceps tendon and patellar ligament. *Micron.*, 40(3):370–377, 2009. doi:10.1016/j.micron.2008.10.004.

[77] **Franchi M, Raspanti M, Dell'Orbo C, Quaranta M, De Pasquale V, Ottani V, Ruggeri A**. Different crimp patterns in collagen fibrils relate to the subfibrillar arrangement. *Connect. Tissue Res.*, 49(2):85–91, 2008. doi:10.1080/03008200801913635.

[78] **Franchi M, Trirè A, Quaranta M, Orsini E, Ottani V**. Collagen structure of tendon relates to function. *Sci. World J.*, 7:404–420, 2007. doi:10.1100/tsw.2007.92.

[79] **Frandsen AF**. Polarized Light Microscopy. NASA Kennedy Space Center. URL: https://ntrs.nasa.gov/api/citations/20170000349/downloads/20170000349.pdf, last accessed on 2022-10-06, 2016.

[80] **Franken LE, Grünewald K, Boekema EJ, Stuart MCA**. A technical introduction to transmission electron microscopy for soft-matter: imaging, possibilities, choices, and technical developments. *Small*, 16(14):1906198, 2020. doi:10.1002/smll.201906198.

[81] **Frankewycz B, Bell R, Chatterjee M, Andarawis-Puri N**. The superior healing capacity of mrl tendons is minimally influenced by the systemic environment of the mrl mouse. *Sci. Rep.*, 13:17242, 2023. doi:10.1038/s41598-023-42449-8.

[82] **Fratzl P**. Collagen structure and mechanics, an introduction. In Peter Fratzl, editor, *Collagen Structure and Mechanics*, chapter 1, pages 1–13. Springer Science+Business Media, LLC, Springer Science+Business Media, LLC, 233 Spring Street, New York, NY 10013, USA, 2008.

[83] **Frolova EG, Drazba J, Krukovets I, Kostenko V, Blech L, Harry C, Vasanji A, Drumm C, Sul P, Jenniskens GJ, Plow EF, Stenina-Adognravi O**. Control of organization and function of muscle and tendon by thrombospondin-4. *Matrix Biol.*, 37:35–48, 2014. doi:10.1016/j.matbio.2014.02.003.

[84] **Gao J, Guo Z, Zhang Y, Liu Y, Xing F, Wang J, Luo X, Kong Y, Zhang G**. Age-related changes in the ratio of type i/iii collagen and fibril diameter in mouse skin. *Regen. Biomater.*, 10:rbac110, 2022. doi:10.1093/rb/rbac110.

[85] **Garnero P**. The contribution of collagen crosslinks to bone strength. *Bonekey Rep.*, 1:182, 2012. doi:10.1038/bonekey.2012.182.

[86] **Gathercole LJ & Keller A**. Crimp morphology in the fibre-forming collagens. *Matrix*, 11:214–234, 1991. doi:10.1016/S0934-8832(11)80161-7.

[87] **Gaut L & Duprez D**. Tendon development and diseases. *Wiley Interdiscip. Rev. Dev. Biol.*, 5(1):5–23, 2015. doi:10.1002/wdev.201.

[88] **Giffin JL. Franz-Odendaal TA**. Quantitative gene expression dynamics of key placode

signalling factors in the embryonic chicken scleral ossicle system. *Gene Expr. Patterns*, 38:119131, 2020. doi:10.1016/j.gep.2020.119131.

[89] **Godinho MSC, Thorpe CT, Greenwald SE, Screen HRC**. Elastin is localised to the interfascicular matrix of energy storing tendons and becomes increasingly disorganized with ageing. *Sci. Rep.*, 7:9713, 2017. doi:10.1038/s41598-017-09995-4.

[90] **Goh KL, Holmes DF, Lu Y, Purslow PP, Kadler KE, Bechet D, Wess TJ**. Bimodal collagen fibril diameter distributions direct age-related variations in tendon resilience and resistance to rupture. *J. Appl. Physiol.*, 113(6):878–888, 2012. doi:10.1152/japplphysiol.00258.2012.

[91] **Goldberga I, Li R, Duer MJ**. Collagen structure-function relationships from solid-state nmr spectroscopy. *Acc. Chem. Res.*, 51(7):1621–1629, 2018. doi:10.1021/acs.accounts.8b00092.

[92] **Goodman SA, May SA, Heinegård D, Smith RKW**. Tenocyte response to cyclical strain and transforming growth factor beta is dependent upon age and site of origin. *Biorheology*, 41:613–628, 2004.

[93] **Graham L & Orenstein JM**. Processing tissue and cells for transmission electron microscopy in diagnostic pathology and research. *Nat. Protoc.*, 2:2439–2450, 2007. doi:10.1038/nprot.2007.304.

[94] **Graudejus O, Wong RDP, Varghese N, Wagner S, Morrison B**. Bridging the gap between in vivo and in vitro research: Reproducing in vitro the mechanical and electrical environment of cells in vivo. *MEA Meeting 2018 — 11th International Meeting on Substrate Integrated Microelectrode Arrays*, 2019.

[95] **Grol MW, Haelterman NA, Lim J, Munivez EM, Archer M, Hudson DM, Tufa SF, Keene DR, Lei K**. Tendon and motor phenotypes in the crtap-/- mouse model of recessive osteogenesis imperfecta. *eLife*, 10:e63488, 2021. doi:10.7554/eLife.63488.

[96] **Gumucio JP, Schonk MM, Kharaz YA, Comerford E, Mendias CL**. Scleraxis is required for the growth of adult tendons in response to mechanical loading. *JCI Insight*, 5(13):e138295, 2020. doi:10.1172/jci.insight.138295.

[97] **Hadraba D, Janacek J, Filova E, Lopot F, Paesen R, Fanta O, Jarman A, Necas A, Ameloot M, Jelen K**. Calcaneal tendon collagen fiber morphometry and aging. *Microsc Microanal.*, 23(5):1040–1047, 2017. doi:10.1017/S1431927617012569.

[98] **Hansen KA, Weiss JA, Barton JK**. Recruitment of tendon crimp with applied tensile strain. *J. Biomech. Eng.*, 124:72–77, 2002. doi:10.1115/1.1427698.

[99] **Harrison SM, Whitton RC, Kawcak CE, Stover SM, Pandy MG**. Relationship between muscle forces, joint loading and utilization of elastic strain energy in equine locomotion. *J. Exp. Biol.*, 213(23):3998–4009, 2010. doi:10.1242/jeb.044545.

[100] **Haut RC**. The effect of a lathyritic diet on the sensitivity of tendon to strain rate. *J. Biomed. Eng.*, 107:166–174, 1985.

[101] **He P, Ruan D, Huang Z, Wang C, Xu Y, Cai H, Liu H, Fei Y, Heng BC, Chen W, Shen W**. Comparison of tendon development versus tendon healing and regeneration. *Front. Cell Dev. Biol.*, 10:821667, 2022. doi:10.3389/fcell.2022.821667.

[102] **Herchenhan A, Kalson NS, Holmes DF, Hill P, Kadler KE, Margetts L**. Tendon contraction induces crimp formation in tendon-like tissue. *Biomech. Model Mechanobiol.*, 11:449–459, 2012. doi:10.1007/s10237-011-0324-0.

[103] **Herchenhan A, Uhlenbrock F, Eliasson P, Weis M, Eyre D, Kadler KE, Magnusson SP, Kjaer M**. Lysyl oxidase activity is required for ordered collagen fibrillogenesis by tendon cells. *J. Biol. Chem.*, 290:16440–16450, 2015. doi:10.1074/jbc.M115.641670.

[104] **Herod TW, Chambers NC, Veres SP**. Collagen fibrils in functionally distinct tendons have differing structural responses to tendon rupture and fatigue loading. *Acta Biomater.*, 42:296–307, 2016. doi:10.1016/j.actbio.2016.06.017.

[105] **Holmes DF, Graham HK, Kadler KE**. Collagen fibrils forming in developing tendon show an early and abrupt limitation in diameter at the growing tips. *J. Mol. Biol.*, 283(5):1049–1058, 1998. doi:10.1006/jmbi.1998.2153.

[106] **Holmes R, Kirk S, Tronci G, Yang X, Wood D**. Influence of telopeptides on the structural and physical properties of polymeric and monomeric acid-soluble type i collagen. *Mater. Sci. Eng. C Mater. Biol. Appl.*, 77:823–827, 2017. doi:10.1016/j.msec.2017.03.267.

[107] **Huang AH, Lu HH, Schweitzer R**. Molecular regulation of tendon cell fate during development. *J. Orthop. Res.*, 33:800–812, 2015. doi:10.1002/jor.22834.

[108] **Huang AH, Watson SS, Wang L, Baker BM, Akiyama H, Brigande JV, Schweitzer R**. Requirement for scleraxis in the recruitment of mesenchymal progenitors during embryonic tendon elongation. *Development*, 146(20):182782, 2019. doi:10.1242/dev.182782.

[109] **Hudson DM, Archer M, King KB, Eyre DR**. Glycation of type i collagen selectively targets the same helical domain lysine sites as lysyl oxidase–mediated cross-linking. *J. Biol. Chem.*, 80:15620–15627, 2018. doi:10.1074/jbc.RA118.004829.

[110] **Huisman E, Lu A, McCormack RG, Scott A**. Enhanced collagen type i synthesis by human tenocytes subjected to periodic in vitro mechanical stimulation. *BMC Musculoskelet Disord.*, 15:386, 2014. doi:10.1186/1471-2474-15-386.

[111] **Hulmes DJS**. Collagen diversity, synthesis and assembly. In Peter Fratzl, editor, *Collagen Structure and Mechanics*, chapter 2, pages 15–48. Springer Science+Business Media, LLC, Springer Science+Business Media, LLC, 233 Spring Street, New York, NY 10013, USA, 2008.

[112] **Hulmes DJS**. Collagen diversity, synthesis and assembly. In Peter Fratzl, editor, *Collagen Structure and Mechanics*, chapter 2, pages 15–48. Springer Science+Business Media, LLC, Springer Science+Business Media, LLC, 233 Spring Street, New York, NY 10013, USA, 2008.

[113] **Imaging**. Gatan: Ametek. URL: https://www.gatan.com/techniques/imaging, last accessed on 2024-08-31, 2020.

[114] **Iranmanesh F & Willet TL**. A linear systems model of the hydrothermal isometric tension test for assessing collagenous tissue quality. *J. Mech. Behav. Biomed. Mater.*, 125:104916, 2022. doi:10.1016/j.jmbbm.2021.104916.

[115] **Jarvinen TA, Jozsa L, Kannus P, Jarvinen TL, Kvist M, Hurme T, Isola J, Kalimo H, Jarvinen M**. Mechanical loading regulates tenascin-c expression in the osteotendinous junction. *J. Cell Sci.*, 112(18):3157–3166, 1999. doi:10.1242/jcs.112.18.3157.

[116] **Jepsen KJ, Wu F, Pergallo JH, Paul J, Roberts L, Ezura Y, Oldberg A, Birk DE, Chakravarti S**. A syndrome of joint laxity and impaired tendon integrity in lumican-

and fibromodulin-deficient mice. *J. Biol. Chem.*, 227:35532–35540, 2002. doi:10.1074/jbc.M205398200.

[117] **Jones ER, Jones GC, Legerlotz K, Riley GP**. Cyclical strain modulates metalloprotease and matrix gene expression in human tenocytes via activation of tgfβ. *Biochim. Biophys. Acta*, 12:2596–2607, 2013. doi:10.1016/j.bbamcr.2013.06.019.

[118] **Jukic AM, Baird DD, Weinberg CR, McConnaughey DR, Wilcox AJ**. Length of human pregnancy and contributors to its natural variation. *Hum. Reprod.*, 28(10):2848–2855, 2013. doi:10.1093/humrep/det297.

[119] **Józsa L & Kannus P**. *Human Tendons: Anatomy, Physiology, and Pathology. Champaign, IL: Human Kinetics.*, 1997.

[120] **Kaku M, Rosales Rocabado JM, Kitami M, Ida T, Akiba Y, Yamauchi M, Uoshima K**. Mechanical loading stimulates expression of collagen crosslinking associated enzymes in periodontal ligament: mechanical stress stimulates cross-linking in pdl. *J. Cell Physiol.*, 231:926–933, 2016. doi:10.1002/jcp.25184.

[121] **Kalson NS, Lu Y, Taylor SH, Starborg T, Holmes DF, Kadler KE**. A structure-based extracellular matrix expansion mechanism of fibrous tissue growth. *eLife*, 4:05958, 2015. doi:10.7554/eLife.05958.

[122] **Kataoka K, Kurimoto R, Tsutsumi H, Chiba T, Kato T, Shishido K, Kato M, Ito Y, Cho Y, Hoshi O, Mimata A, Sakamaki Y, Nakamichi R, Lotz MK, Naruse K, Asahara H**. In vitro neo-genesis of tendon/ligament-like tissue by combination of mohawk and a three-dimensional cyclic mechanical stretch culture system. *Front. Cell Dev. Biol.*, 8:307, 2020. doi:10.3389/fcell.2020.00307.

[123] **Kaya M, Karahan N, Yilmaz B**. Tendon structure and classification. *In (Ed.), Tendons. IntechOpen*, 2019. doi:10.5772/intechopen.84622.

[124] **Keene DR, Sakai LY, Bachinger HP, Burgeson RE**. Type iii collagen can be present on banded collagen fibrils regardless of fibril diameter. *J. Cell. Bio.*, 105:2393–2402, 1987.

[125] **Kent MJC, Light ND, Bailey AJ**. Evidence for glucose-mediated covalent cross-linking of collagen after glycosylation in vitro. *Biochem. J.*, 225:745–752, 1985. doi:10.1042/bj2250745.

[126] **Kerr RF, Alexander R, Bennett MB**. Why are mammalian tendons so thick? *J. Zool.*, 216(2):309–324, 1998. doi:10.1111/j.1469-7998.1988.tb02432.x.

[127] **Klemm KM, Klein MJ, Zhang Y**. Biochemical markers of bone metabolism. In McPherson RA Pincus MR, editor, *Henry's Clinical Diagnosis and Management by Laboratory Methods,*, chapter 16, pages 208–224. Elsevier, Elsevier, 2022.

[128] **Knobloch K, Yoon U, Vogt PM**. Acute and overuse injuries correlated to hours of training in master running athletes. *Foot Ankle Int.*, 29(7):671–676, 2008. doi:10.3113/FAI.2008.0671.

[129] **Knott L& Bailey AJ**. Collagen cross-links in mineralising tissue: a review of their chemistry, function and clinical relevance. *Bone*, 22:181–187, 1998. doi:10.1016/s8756-3282(97)00279-2.

[130] **Koike-Tani M, Tani T, Mehta SB, Verma A, Oldenbourg R**. Polarized light microscopy in reproductive and developmental biology. *Mol. Reprod. Dev.*, 82(7-8):548–562, 2015. doi:10.1002/mrd.22221.

[131] **Kostrominova TY, Calve S, Arruda EM, Larkin LM**. Ultrastructure of myotendinous junctions in tendon-skeletal muscle constructs engineered in vitro. *Histol. Histopathol.*, 24(5):541–550, 2009. doi:10.14670/HH-24.541.

[132] **Kuivaniemi H Tromp G**. Type iii collagen (col3a1): Gene and protein structure, tissue distribution, and associated diseases. *Gene*, 707:151–171, 1993. doi:10.1016/j.gene.2019.05.003.

[133] **Kuo CK, Petersen BC, Tuan RS**. Spatiotemporal protein distribution of tgf-betas, their receptors, and extracellular matrix molecules during embryonic tendon development. *Dev. Dyn.*, 237(5):1477–1489, 2008. doi:10.1002/dvdy.21547.

[134] **Kupyers R, Tyler M, Kurth LB, Jenkins ID, Horgan DJ**. Identification of the loci of the collagen associated ehrlich chromogen in type i collagen confirms its role as a trivalent cross-link. *Biochem J.*, 283:129–136, 1992. doi:10.1042/bj2830129.

[135] **Lanthanum and Cerium Hexaboride (LaB6 and CeB6) Cathodes**. Electron Microscopy Services. URL: https://www.emsdiasum.com/lanthanum-and-cerium-hexaboride-lab6-and-ceb6-cathodes, last accessed on 2024-08-31, 2020.

[136] **Latorre ME, Velàquez DE, Purslow PP**. The thermal shrinkage force in perimysium from different beef muscles is not affected by post-mortem aging. *Meat Sci.*, 135:109–114, 2018. doi:10.1016/j.meatsci.2017.09.003.

[137] **Lavagnino M, Wall ME, Little D, Banes AJ, Guilak F, Arnoczky SP**. Tendon mechanobiology: Current knowledge and future research opportunities. *J. Orthop. Res.*, 33(6):813–822, 2015. doi:10.1002/jor.22871.

[138] **Lazarczuk SL, Maniar N, Opar DA, Duhig SJ, Shield A, Barrett RS, Bourne MA**. Mechanical, material and morphological adaptations of healthy lower limb tendons to mechanical loading: a systematic review and meta–analysis. *Sports Med.*, 52:2405–2429, 2022. doi:10.1007/s40279-022-01695-y.

[139] **Le Lous M, Allain JC, Cohen-solal L, Maroteaux P**. Hydrothermal isometric tension curves from different connective tissues. role of collagen genetic types and noncollagenous components. *Connect Tissue Res.*, 11(2-3):199–206, 1983. doi:10.3109/03008208309004856.

[140] **Leading Through Change: WCB Nova Scotia 2015 Annual Report**. URL: https://www.wcb.ns.ca//Portals/wcb/Annual%20Reports/2015%20Annual%20Report%20Final.pdf, last accessed on 2022-07-03, 2015.

[141] **Lee JM, Pereira CA, Abdulla D, Naimark WA, Crawford I**. A multi-sample denaturation temperature tester for collagenous biomaterials. *Med. Eng. Phys.*, 17:115–121, 1995. doi:10.1016/1350-4533(95)91882-H.

[142] **Legerlotz K, Dorn J, Richter J, Rausch M, Leupin O**. Age-dependent regulation of tendon crimp structure, cell length and gap width with strain. *Acta. Biomater.*, 10(10):4447–4455, 2014. doi:10.1016/j.actbio.2014.05.029.

[143] **Leighton MP, Kreplak L, Rutenberg AD**. Non-equilibrium growth and twist of cross-linked collagen fibrils. *Soft Matter*, 17:1415–1427, 2021. doi:10.1039/d0sm01830a.

[144] **Lejard V, Blais F, Guerquin MJ, Bonnet A, Bonnin MA, Havis E, Malbouyres M, Bidaud CB, Maro G, Gilardi-Hebenstreit P, Rossert J, Ruggiero F, Duprez D**. Egr1 and egr2 involvement in vertebrate tendon differentiation. *J. Biol. Chem.*, 286(7):5855–5867, 2011. doi:10.1074/jbc.M110.153106.

[145] **Leppilahti J, Puranen J, Orava S**. Incidence of achilles tendon rupture. *Acta. Orthop. Scand.*, 67:277–279, 1996. doi:10.3109/17453679608994688.

[146] **Li Y, Wu T, Liu S**. Identification and distinction of tenocytes and tendon-derived stem cells. *Front. Cell Dev. Biol.*, 9:629515, 2021. doi:10.3389/fcell.2021.629515.

[147] **Lim J, Munivez E, Jiang MM, Song IW, Gannon F, Keene DR, Schweitzer R, Lee BH, Jeong KS**. mtorc1 signaling is a critical regulator of postnatal tendon development. *Sci. Rep.*, 7:17175, 2017. doi:10.1038/s41598-017-17384-0.

[148] **Linsenmayer TF, Gibney E, Igoe F, Gordon MK, Fitch JM, Fessler LI, Birk DE**. Type v collagen: molecular structure and fibrillar organization of the chicken alpha 1(v) nh2-terminal domain, a putative regulator of corneal fibrillogenesis. *J. Cell Biol.*, 121(5):1181–1189, 1993. doi:10.1083/jcb.121.5.1181.

[149] **Liu J, Xu M, Wu J, Zhang H, Yang L, Lun D, Hu Y, Liu B**. Picosirius-polarization method for collagen fiber detection in tendons: a mini-review. *Orthop. Surg.*, 13(3):701–707, 2021. doi:10.1111/os.12627.

[150] **Liu JF & He JH**. Hierarchical structure and fractal dimension of tendon. *Mater. Sci. Technol.*, 26(11):1317, 2010. doi:10.1179/026708310X12798718274232.

[151] **Liu SH, Yang RS, al-Shaikh R, Lane JM**. Collagen in tendon, ligament, and bone healing: a current review. *Clin. Orthop. Relat. Res.*, 318:265–278, 1995.

[152] **Liu X, Wu H, Byrne M, Krane S, Jaenisch R**. Type iii collagen is crucial for collagen i fibrillogenesis and for normal cardiovasculardevelopment. *Proc. Natl. Acad. Sci.*, 94(5):1852–1856, 1997. doi:10.1073/pnas.94.5.1852.

[153] **Liu X, Zhu B, Li Y, Liu X, Guo S, Wang C, Li S, Wang D**. The role of vascular endothelial growth factor in tendon healing. *Front. Physiol.*, 12:766080, 2021. doi:10.3389/fphys.2021.766080.

[154] **Liu Y, Xuan R, He Y, Ren F, Gu Y**. Computation of fetal kicking in various fetal health examinations: A systematic review. *Int. J. Environ. Res. Public Health*, 19(7):4366, 2022. doi:10.3390/ijerph19074366.

[155] **Lui PPY & Wong CM**. Biology of tendon stem cells and tendon in aging. *Front. Genet. Sec. Stem Cell Research*, 10:1338, 2020. doi:10.3389/fgene.2019.01338.

[156] **Macedo RS, Teodoro WR, Capellozzi VL, Rosemberg DV, Sposeto RB, Netto CC, Deland JT, Maffulli N, Ellis SJ, Godoy-Santos AL**. Histoarchitecture of the fibrillary matrix of human fetal posterior tibial tendons. *Sci. Rep.*, 12:17922, 2022. doi:10.1038/s41598-022-19695-3.

[157] **Maeda T, Sakabe T, Sunaga A, et al.** Conversion of mechanical force into tgf-β-mediated biochemical signals. *Curr. Biol.*, 21(11):933–941, 2011. doi:10.1016/j.cub.2011.04.007.

[158] **Maffulli N, Cuozzo F, Migliorini F, Oliva F**. The tendon unit: biochemical, biomechanical, hormonal influences. *J. Orthop. Surg. Res.*, 18(1):311, 2023. doi:10.1186/s13018-023-03796-4.

[159] **Makris EA, Responte DJ, Paschos NK, Hu JC, Athanasiou KA**. Developing functional musculoskeletal tissues through hypoxia and lysyl oxidase-induced collagen cross-linking. *Proc. Natl. Acad. Sci. U.S.A.*, 111:E4832–E4841, 2014. doi:10.1073/pnas.1414271111.

[160] **Marini JC, Forlino A, Cabral WA, Barnes AM, San Antonio JD, Milgrom S, Hyland JC, Körkkö J, Prockop DJ, De Paepe A, Coucke P, Symoens S, Glorieux FH, Roughley PJ, Lund AM, Kuurila-Svahn K, Hartikka H, Cohn DH, Krakow D, Mottes M, Schwarze U, Chen D, Yang K, Kuslich C, Troendle J, Dalgleish R, Byers PH**. Consortium for osteogenesis imperfecta mutations in the helical domain of type i collagen: regions rich in lethal mutations align with collagen binding sites for integrins and proteoglycans. *Hum. Mutat.*, 28(3):209–21, 2007. doi:10.1002/humu.20429.

[161] **Marturano JE, Arena JD, Schiller ZA, Georgakoudi I, Kuo CK**. Characterization of mechanical and biochemical properties of developing embryonic tendon. *Proc. Natl. Acad. Sci.*, 110(16):6370–6375, 2013. doi:10.1073/pnas.1300135110.

[162] **Marturano JE, Xylas JF, Sridharan GV, Georgakoudi I, Kuo CK**. Lysyl oxidase-mediated collagen crosslinks may be assessed as markers of functional properties of tendon tissue formation. *Acta Biomater.*, 10(3):1370–1379, 2014. doi:10.1016/j.actbio.2013.11.024.

[163] **Matuszewski PE, Chen YL, Szczensy SE, Lake SP, Elliott DM, Soslowsky LJ, Dodge GR**. Regional variation in human supraspinatus tendon proteoglycans: decorin, biglycan, and aggrecan. *Connect. Tiss. Res.*, 53(5):343–348, 2011. doi:10.3109/03008207.2012.654866.

[164] **Maul TM, Chew DW, Nieponice A, Vorp DA**. Mechanical stimuli differentially control stem cell behavior: morphology, proliferation, and differentiation. *Biomech. Model Mechanobiol.*, 10(6):939–953, 2011. doi:10.1007/s10237-010-0285-8.

[165] **McCormick RJ Thomas PD**. Collagen crosslinking in the heart: relationship to development and function. *Basic Appl. Myol.*, 8(2):143–150, 1998.

[166] **McLain PE**. Chemistry of collagen crosslinking. *29th Annual Reciprocal Meat Conference of the American Meat Science Association*, 29, 1976. doi:https://meatscience.org/docs/default-source/publications-resources/rmc/1976/chemistry-of-collagen-crosslinking.pdf?sfvrsn=2.

[167] **Miles CA & Bailey AJ**. Thermally labile domains in the collagen molecule. *Micron*, 32:325–332, 2001. doi:10.1016/s0968-4328(00)00034-2.

[168] **Miles CA & Burjanadze TV**. Thermal stability of collagen fibers in ethylene glycol. *Biophys. J.*, 80:1480–1486, 2001. doi:10.1016/S0006-3495(01)76120-6.

[169] **Miles CA, Avery NC, Rodin V and Bailey AJ**. The increase in denaturation temperature following cross-linking is caused by dehydration of the fibres. *J. Mol. Biol.*, 346:551–556, 2005. doi:10.1016/j.jmb.2004.12.001.

[170] **Miles CA, Ghelashvili M**. Polymer-in-a-box mechanism for the thermal stabilization of collagen molecules in fibers. *Biophys. J.*, 76:3243–3252, 1999.

[171] **Moore MJ De Beaux A**. A quantitative ultrastructural study of rat tendon from birth to maturity. *J. Anat.*, 153:163–169, 1987.

[172] **Moore S**. What is Polarized Light Microscopy Used For? AZO Optics: Editorial Feature. URL: https://www.azooptics.com/Article.aspx?ArticleID=1945, last accessed on 2022-10-06, 2021.

[173] **Mosler E, Folkhard W, Knörzer E, Nemetschek-Gansler H, Nemetschek T, Koch MH**. Stress-induced molecular rearrangement in tendon collagen. *J. Mol. Biol.*, 182(4):589–596, 1985. doi:10.1016/0022-2836(85)90244-x.

[174] **Mowa CN**. Bovine prenatal development: a comparative study of ultrasonography and radiography techniques. *Submitted for the degree of Master in Veterinary Medicine. University of Glasgow, Veterinary School, Department of Veterinary Anatomy.*, 1994.

[175] **Murchison ND, Price BA, Conner DA, Keene DR, Olson EN, Tabin CJ, Schweitzer R**. Regulation of tendon differentiation by scleraxis distinguishes force-transmitting tendons from muscle-anchoring tendons. *Development*, 134(14):2697–2708, 2007. doi:10.1242/dev.001933.

[176] **Naomi R, Ridzuan PM, Bahari H**. Current insights into collagen type i. *Polymers (Basel)*, 13(16):2642, 2021. doi:10.3390/polym13162642.

[177] **Navarro J, Korcari A, Nguyen P, Bah I, AlKhalifa A, Fink S, Buckley M, Kuo CK**. Method development and characterization of chick embryo tendon mechanical properties. *J. Biomech.*, 133:110970, 2022. doi:10.1016/j.jbiomech.2022.110970.

[178] **Nguyen PK, Pan XS, Li J, Kuo CK**. Roadmap of molecular, compositional, and functional markers during embryonic tendon development. *Connect. Tiss. Res.*, 59(5):495–508, 2018. doi:10.1080/03008207.2018.1511710.

[179] **O'Brien C, Marr N, Thorpe C**. Microdamage in the equine superficial digital flexor tendon. *Equine Vet. J*, 53(3):417–430, 2020. doi:10.1111/evj.13331.

[180] **Oliver G, Wehr R, Jenkins NA, Copeland NG, Cheyette BN, Hartenstein V, Zipursky SL, Gruss P**. Homeobox genes and connective tissue patterning. *Development*, 121(3):693–705, 1995. doi:10.1242/dev.121.3.693.

[181] **Oryan A Shoushtari AH**. Histology and ultrastructure of the developing superficial

digital flexor tendon in rabbits. *J. Anat.*, 37(2):134–140, 2007. doi:10.1111/j.1439-0264.2007.00811.x.

[182] **Pan XS, Li J, Brown EB, Kuo CK**. Embryo movements regulate tendon mechanical property development. *Philos. Trans. R. Soc. Lond. B*, 373:20170325, 2018. doi:10.1098/rstb.2017.0325.

[183] **Parry DA, Barnes GR, Craig AS**. A comparison of the size distribution of collagen fibrils in connective tissues as a function of age and a possible relation between fibril size distribution and mechanical properties. *Proc. R. Soc. Lond. B. Biol. Sci.*, 203:305–321, 1978.

[184] **Patel D, Zamboulis DE, Spiesz EM, Birch HL, Clegg PD, Thorpe CT, Screen HRC**. Structure-function specialisation of the interfascicular matrix in the human achilles tendon. *Acta Biomater.*, 131:381–390, 2021. doi:10.1016/j.actbio.2021.07.019.

[185] **Paterlini MG, Nemethy G, Scheraga HA**. The energy of formation of internal loops in triple-helical collagen polypeptides. *Biopolymers*, 35:607–619, 1995. doi:10.1002/bip.360350607.

[186] **Paterson YZ, Cribbs A, Espenel M, Smith EJ, Henson FMD, Guest DJ**. Genome-wide transcriptome analysis reveals equine embryonic stem cell-derived tenocytes resemble fetal, not adult tenocytes. *Stem Cell Res. Ther.*, 11:184, 2020. doi:10.1186/s13287-020-01692-w.

[187] **Patterson-Kane JC & Rich T**. Achilles tendon injuries in elite athletes: lessons in pathophysiology from their equine counterparts. *ILAR J.*, 55(1):86–99, 2014. doi:10.1093/ilar/ilu004.

[188] **Patterson-Kane JC, Becker DL, Rich T**. The pathogenesis of tendon microdamage in athletes: the horse as a natural model for basic cellular research. *J. Comp. Pathol.*, 147(2-3):227–247, 2012. doi:10.1016/j.jcpa.2012.05.010.

[189] **Patterson-Kane JC, Firth EC, Goodship AE, Parry DA**. Age-related differences in collagen crimp patterns in the superficial digital flexor tendon core region of untrained horses. *Aust. Vet. J.*, 75:39–44, 1997. doi:10.1111/j.1751-0813.1997.tb13829.x.

[190] **Paul GR & Bailey AJ**. Chemical stabilisation of collagen as a biomimetic. *Sci. World J.*, 3:138–155, 2003. doi:10.1100/tsw.2003.13.

[191] **Petersen W, Pufe T, Kurz B, Mentlein R, Tillmann B**. Angiogenesis in fetal tendon development: spatial and temporal expression of the angiogenic peptide vascular endothelial cell growth factor. *Anat. Embryol.*, 205(4):263–270, 2002. doi:10.1007/s00429-002-0241-1.

[192] **Peterson BE, Rolfe RA, Kunselman A, Murphy P, Szczesny SE**. Mechanical stimulation via muscule activity is necessary for the maturation of tendon multiscale mechanics during embryonic development. *Front. Cell. Dev. Biol.*, 9:725563, 2021. doi:10.3389/fcell.2021.725563.

[193] **Peuch P-H, Bongrand P**. Mechanotransduction as a major driver of cell behaviour: mechanisms, and relevance to cell organization and future research. *Biomech. Model Mechanobiol.*, 11(11):210256, 2021. doi:10.1098/rsob.210256.

[194] **Pierlot CM, Lee JM, Amini R, Sacks MS, Wells SM**. Pregnancy-induced remodeling of collagen architecture and content in the mitral valve. *Ann. Biomed. Eng.*, 42:2058–2071, 2014. doi:10.1007/s10439-014-1077-6.

[195] **Pierlot CM, Lee JM, Amini R, Sacks MS, Wells SM**. Biaxial creep resistance and structural remodeling of the aortic and mitral valves in pregnancy. *Ann. Biomed. Eng.*, 43:1772–1785, 2015. doi:10.1007/s10439-014-1230-2.

[196] **Pierlot CM, Moeller D, Lee JM, Wells SM**. Pregnancy-induced remodeling of heart valves. *Am. J. Physiol. Heart Circ. Physiol.*, 309:H1565–H1578, 2015. doi:10.1152/ajpheart.00816.2014.

[197] **Polarized Light Microscopy**. MicroscopyU: The Source for Microscopy Education. URL: https://www.microscopyu.com/techniques/polarized-light, last accessed on 2022-10-06, 2022.

[198] **Proske U & Morgan DL**. Tendon stiffness: methods of measurement and significance for the control of movement. a review. *J. Biomech.*, 20(1):75–82, 1987. doi:10.1016/0021-9290(87)90269-7.

[199] **Provenzano PP & Vanderby Jr. R**. Collagen fibril morphology and organization: implications for force transmission in ligament and tendon. *Matrix Biol.*, 25(2):71–84, 2006. doi:10.1016/j.matbio.2005.09.005.

[200] **Pryce BA, Watson SS, Murchison ND, Staverosky JA, Dunker N, Schweitzer R**. Recruitment and maintenance of tendon progenitors by tgf signaling are essential for tendon formation. *Development*, 136(8):1351–1361, 2009. doi:10.1242/dev.027342.

[201] **Puxkandl R, Zizak I, Paris O, Keckes J, Tesch W, Bernstorff S, Purslow P, Fratzl P**. Viscoelastic properties of collagen: synchrotron radiation investigations and structural model. *Philos. Trans. R. Soc. Lond. B Biol. Sci.*, 357(1418):191–197, 2002. doi:10.1098/rstb.2001.1033.

[202] **Qi F, Deng Z, Ma Y, Wang S, Liu C, Lyu F, Wang T, Zheng Q**. From the perspective of embryonic tendon development: various cells applied to tendon tissue engineering. *Ann. Transl. Med.*, 8(4):131, 2020. doi:10.21037/atm.2019.12.78.

[203] **Quigley AS, Bancelin S, Deska-Gauthier D, Légaré F, Kreplak L, Veres SP**. In tendons, differing physiological requirements lead to functionally distinct nanostructures. *Sci. Rep.*, 8:4409, 2018. doi:10.1038/s41598-018-22741-8.

[204] **Raisat K, Bardell D, Goljanek-Whysall K, Clegg PD, Peffers MJ**. Epigenetic mechanisms in tendon ageing. *Br. Med. Bull.*, 135(1):90–107, 2020. doi:10.1093/bmb/ldaa023.

[205] **Raspanti M, Manelli A, Franchi M, Ruggeri A**. The 3d structure of crimps in the rat achilles tendon. *Matrix Biol.*, 24(7):503–507, 2005. doi:10.1016/j.matbio.2005.07.006.

[206] **Ribitsch I, Bileck A, Aldoshin AD, Kanula MM, Mayer RP, Egerbacher M, Gabner S, Auer U, Gultekin S, Huber J, Kreil DP, Gerner C, Jenner F**. Molecular mechanisms of fetal tendon regeneration versus adult fibrous repair. *Int. J. Mol. Sci.*, 22:5619, 2021. doi:10.3390/ijms22115619.

[207] **Ribitsch I, Gueltekin S, Keith MF, Minichmair K, Peham C, Jenner F, Egerbacher M**. Age-related changes of tendon fibril micro-morphology and gene expression. *J. Anat.*, 236(4):688–700, 2020. doi:10.1111/joa.13125.

[208] **Rigozzi S, Müller R, Snedeker JG**. Collagen fibril morphology and mechanical properties of the achilles tendon in two inbred mouse strains. *J. Anat.*, 216(6):724–731, 2010. doi:10.1111/j.1469-7580.2010.01225.x.

[209] **RNeasy® Plus Micro Handbook**. Qiagen. URL: https://www.qiagen.com/us/resources/download.aspx?id=1961e574-091d-42cc-8b51-1bc3747da874&lang=en, last accessed on 2022-07-15, 2020.

[210] **Robins SP, Shimokomaki M, and Bailey AJ**. The chemistry of the collagen cross-links. age-related changes in the reducible components of intact bovine collagen fibres. *Biochem. J.*, 131:771–780, 1973. doi:10.1042/bj1310771.

[211] **Robinson PS, Huang TF, Kazam E, Iozzo RV, Birk DE, Soslowsky LJ**. Influence of decorin and biglycan on mechanical properties of multiple tendons in knockout mice. *J. Biomech. Eng.*, 127(1):181–185, 2005. doi:10.1115/1.1835363.

[212] **Russo V, Mauro A, Martelli A, Di Giacinto O, Di Marcantonio L, Nardinocchi D, Berardinelli P, Barboni B**. Cellular and molecular maturation in fetal and adult ovine calcaneal tendons. *J. Anat.*, 216(6):724–731, 2015. doi:10.1111/j.1469-7580.2010.01225.x.

[213] **Saito M Marumo K**. Collagen cross-links as a determinant of bone quality: a possible explanation for bone fragility in aging, osteoporosis, and diabetes mellitus. *Osteoporos. Int*, 21:195–214, 2010. doi:10.1007/s00198-009-1066-z.

[214] **Schiele NR, Marturano JE, Kuo CK**. Mechanical factors in embryonic tendon development: potential cues for stem cell tenogenesis. *Curr. Opin. Biotechnol.*, 24(5):834–840, 2013. doi:10.1016/j.copbio.2013.07.003.

[215] **Schiele NR, von Flotow F, Tochka ZL, Hockaday LA, Marturano JE, Thibodeau JJ, Kuo CK**. Actin cytoskeleton contributes to the elastic modulus of embryonic tendon during early development. *J. Orthop. Res.*, 33(6):874–881, 2015. doi:10.1002/jor.22880.

[216] **Scott A, Cook JL, Hart DA, Walker DC, Duronio V, Khan KM**. Tenocyte responses to mechanical loading in vivo: A role for local insulin-like growth factor 1 signaling in early tendinosis in rats. *Arthritis Rheum.*, 56(3):871–881, 2007. doi:10.1002/art.22426.

[217] **Scott JE, Orford CR, Hughes EW**. Proteoglycan–collagen arrangements in developing rat tail tendon. an electron microscopical and biochemical investigation. *Biochem. J.*, 195:573–581, 1981. doi:10.1042/bj1950573.

[218] **Screen HRC, Shleton JC, Chhaya VH, Kayser MV, Bader DL, Lee DA**. The influence of noncollagenous matrix components on the micromechanical environment of tendon fascicles. *Ann. Biomed. Eng.*, 33:1090–1099, 2005. doi:10.1007/s10439-005-5777-9.

[219] **Sensini A, Massafra G, Gotti C, Zucchelli A, Crisofolini L**. Tissue engineering for the insertions of tendons and ligaments: an overview of electrospun biomaterials and structures. *Front. Bioeng. Biotechnol.*, 9:645544, 2021. doi:10.3389/fbioe.2021.645544.

[220] **Shah JS, Palacios E, Palacios L**. Development of crimp morphology and cellular changes in chick tendons. *Dev. Biol.*, 94:499–504, 1982. doi:10.1016/0012-1606(82)90366-9.

[221] **Sharabi M**. Structural mechanisms in soft fibrous tissues: a review. *Front. Mater.*, 2022. doi:10.3389/fmats.2021.793647.

[222] **Shearer T, Thorpe CT, Screen HRC**. The relative compliance of energy-storing tendons may be due to the helical fibril arrangement of their fascicles. *J. R. Soc. Interface*, 14(133):20170261, 2017. doi:10.1098/rsif.2017.0261.

[223] **Shepherd JH, Legerlotz K, Demirci T, Klemt C, Riley GP, Screen HRC**. Functionally distinct tendon fascicles exhibit different creep and stress relaxation behaviour. *Proc. Inst. Mech. Eng. H.*, 228:49–59, 2014. doi:10.1177/0954411913509977.

[224] **Shoulders MD & Raines RT**. Collagen structure and stability. *Annu. Rev. Biochem.*, 78:929–958, 2009. doi:10.1146/annurev.biochem.77.032207.120833.

[225] **Silver FH, Freeman JW, Seehra GP**. Collagen self-assembly and the development of tendon mechanical properties. *J. Biomech.*, 36:1529–1553, 2003. doi:10.1016/s0021-9290(03)00135-0.

[226] **Silver FH, Horvath I, Foran DJ**. Mechanical implications of the domain structure of fibril forming collagens: comparison of the molecular and fibrillar flexibilities of the alpha1-chains found in types i-iii collagen. *J. Theor. Biol.*, 216:243–254, 2002. doi:10.1006/jtbi.2002.2542.

[227] **Silverstein BA, Bao SS, Fan ZJ, Howard N, Smith C, Spielholz P, Bonauto D, Viikari-Juntura E**. Rotator cuff syndrome: personal, work-related psychosocial and physical load factors. *J. Occup. Environ. Med.*, 50(9):1062–1076, 2008. doi:10.1097/JOM.0b013e31817e7bdd.

[228] **Skjong CC, Meininger AK, Ho SSW**. Tendinopathy treatment: where is the evidence? *Clin. Sports Med.*, 31:329–350, 2012. doi:10.1016/j.csm.2011.11.003.

[229] **Smith RKW, Zunino L, Webbon PM, Heinegård D**. The distribution of cartilage oligomeric matrix protein (comp) in tendon and its variation with tendon site, age and load. *Matrix Biol.*, 16(5):255–271, 1997. doi:10.1016/s0945-053x(97)90014-7.

[230] **Snedeker J & Gautieri A**. The role of collagen crosslinks in ageing and diabetes - the good, the bad, and the ugly. *Muscle Ligaments Tendons J.*, 4(3):303–308, 2014. doi:10.11138/mltj/2014.4.3.303.

[231] **Sparavalo S, Bray CAM, Brock-Fisher TM, Easton NM, Guinard CA, Wells SM, Lee JM, Veres SP**. Structural differences between distinct tendon types arise during fetal development. *Biomedical Engineering Society 2015 Annual Meeting, Tampa, Florida, USA*, 2015.

[232] **Spiesz EM, Thorpe CT, Thurner PJ, Screen HRC**. Structure and collagen crimp patterns of functionally distinct equine tendons, revealed by quantitative polarised light microscopy (qplm). *Acta Biomater.*, 70:281–292, 2018. doi:10.1016/j.actbio.2018.01.034.

[233] **Sprains and Strains**: Preventing musculoskeletal injury through workplace design. URL: https://www.wcb.ns.ca/Portals/wcb/Sprains_and_Strains_Preventing_MSI_through_work_design.pdf, last accessed on 2022-07-03, 2018.

[234] **Stammers M, Ivanova IM, Niewczas IS, Segonds-Pichon A, Streeter M, Spiegel DA, Clark J**. Age-related changes in the physical properties, cross-linking, and glycation of collagen from mouse tail tendon. *J. Biol. Chem.*, 295:10562–10571, 2020. doi:10.1074/jbc.RA119.011031.

[235] **Stanley RL, Fleck RA, Becker DL, Goodship AE, Ralphs JR, Patterson-Kane JC**. Gap junction protein expression and cellularity: comparison of immature and adult equine digital tendons. *J. Anat.*, 211:325–334, 2007. doi:10.1111/j.1469-7580.2007.00781.x.

[236] **Stephens PR, Nunamaker DM, Butterweck DM**. Application of a hall-effect transducer for measurement of tendon strains in horses. *Am. J. Vet. Res.*, 50(7):1089–1095, 1989.

[237] **Stevenson K, Kucich U, Whitbeck C, Levin RM, Howard PS**. Functional changes

in bladder tissue from type iii collagen-deficient mice. *Mol. Cell. Biochem.*, 283:107–114, 2006. doi:10.1007/s11010-006-2388-1.

[238] **Subramanian A Schilling TF**. Thrombospondin-4 controls matrix assembly during development and repair of myotendinous junctions. *eLife*, 3:e02372, 2014. doi:10.7554/eLife.02372.

[239] **Subramanian A & Schilling TF**. Tendon development and musculoskeletal assembly: emerging roles for the extracellular matrix. *Development*, 142(24):4191–4204, 2015. doi:10.1242/dev.114777.

[240] **Subramanian A, Kanzaki LF, Galloway JL, Schilling TF**. Mechanical force regulates tendon extracellular matrix organization and tenocyte morphogenesis through tgfbeta signaling. *eLife*, 7:e38069, 2018. doi:10.7554/eLife.38069.

[241] **Svensson L, Aszodi A, Reinholt FP, Fassler R, Heinegård D, Oldberg .** Fibromodulin-null mice have abnormal collagen fibrils, tissue organization, and altered lumican deposition in tendon. *Cell Biol. Met.*, 274(14):9636–9647, 1999. doi:10.1074/jbc.274.14.9636.

[242] **Svensson RB, Smith ST, Moyer PJ, Magnusson SP**. Effects of maturation and advanced glycation on tensile mechanics of collagen fibrils from rat tail and achilles tendons. *Acta. Biomater.*, 70:270–280, 2018. doi:10.1016/j.actbio.2018.02.005.

[243] **Södersten F, Ekman S, Eloranta ML, Heinegård D, Dudhia J, Hultenby K**. Ultrastructural immunolocalization of cartilage oligomeric matrix protein (comp) in relation to collagen fibrils in the equine tendon. *Matrix Biol.*, 24(5):376–385, 2005. doi:10.1016/j.matbio.2005.06.003.

[244] **Taye N, Karoulias SZ, Hubmacher D**. The "other" 15-40%: the role of non-collagenous extracellular matrix proteins and minor collagens in tendon. *J. Orthop.*, 38(1):23–35, 2020. doi:10.1002/jor.24440.

[245] **Tendon**. Cleveland Clinic. URL: https://my.clevelandclinic.org/health/body/21738-tendon, 2021.

[246] **Theodossiou SK & Schiele NR**. Models of tendon development and injury. *BMC Biomed. Eng.*, 1:32, 2019. doi:10.1186/s42490-019-0029-5.

[247] **Thomopoulos S, Genin GM, Galatz LM**. The development and morphogenesis of the tendon-to-bone insertion - what development can teach us about healing. *J. Musculoskelet. Neuronal Interact.*, 10(1):35–45, 2013.

[248] **Thorpe CT, Karunaseelan KJ, Ng Chieng Hin J, Riley GP, Birch HL, Clegg PD, Screen HRC**. Distribution of proteins within different compartments of tendon varies according to tendon type. *J. Anat.*, 229:450–458, 2016. doi:10.1111/joa.12485.

[249] **Thorpe CT, Klemt C, Riley GP, Birch HL, Clegg PD, Screen HRC**. Helical sub-structures in energy-storing tendons provide a possible mechanism for efficient energy storage and return. *Acta Biomater.*, 9:7948–7956, 2013. doi:10.1016/j.actbio.2013.05.004.

[250] **Thorpe CT, Riley GP, Birch HL, Clegg PD, Screen HRC**. Fascicles from energy-storing tendons show an age-specific response to cyclic fatigue loading. *J. R. Soc. Interface.*, 11(92):20131058, 2014. doi:10.1098/rsif.2013.1058.

[251] **Thorpe CT, Stark RJF, Goodship AE, Birch HL**. Mechanical properties of the equine superficial digital flexor tendon relate to specific collagen cross-link levels. *Equine Vet. J.*, 42(38):538–543, 2010. doi:10.1111/j.2042-3306.2010.00175.x.

[252] **Thorpe CT, Streeter I, Pinchbeck GL, Goodship AE, Clegg PD, Birch HL**. Aspartic acid racemization and collagen degradation markers reveal an accumulation of damage in tendon collagen that is enhanced with aging. *J. Biol. Chem.*, 285(21):15674–15681, 2010. doi:10.1074/jbc.M109.077503.

[253] **Thorpe CT, Udeze CP, Birch HL, Clegg PD, Screen HRC**. Capacity for sliding between tendon fascicles decreases with aging in injury prone equine tendons: A possible mechanism for age-related tendinopathy? *Eur. Cells Mater.*, 25:48–60, 2012. doi:10.22203/ecm.v025a04.

[254] **Titan AL, Foster DS, Chang J, Longaker M**. Flexor tendon: development, healing, adhesion, formation, and contributing growth factors. *Plast. Reconstr. Surg.*, 144(4):639e–647e, 2019. doi:10.1097/PRS.0000000000006048.

[255] **Toroian D, Lim JE, Price PA**. The size exclusion characteristics of type i collagen. *J. Biol. Chem.*, 282:22437–22447, 2007. doi:10.1074/jbc.M700591200.

[256] **Toser S & Duprez D**. Tendon and ligament: development, repair and disease. *Birth Defects Res. C Embryo Today*, 75(3), 2005. doi:10.1002/bdrc.20049.

[257] **Tresoldi I, Oliva F, Benvenuto M, Fantini M, Masuelli L, Bei R, Modesti A**. Tendon's ultrastructure. *Muscles Ligaments Tendons J.*, 21;3(1):2–6, 2013. doi:10.11138/mltj/2013.3.1.002.

[258] **Tsang AS, Dart AJ, Biasutti SA, Jeffcott LB, Smith MM, Little CB**. Effects of tendon injury on uninjured regional tendons in the distal limb: An in-vivo study using an ovine tendinopathy model. *PLoS One*, 14(4):e0215830, 2019. doi:10.1371/journal.pone.0215830.

[259] **Tsutsumi H, Kurimoto R, Nakamichi R, Chiba T, Matsushima T, Fujii Y, Sanada R, Kato T, Shishido K, Sakamaki Y, Kimura T, Kishida A, Asahara H**. Generation of a tendon-like tissue from human ips cells. *J. Tissue Eng.*, 13:20417314221074018, 2022. doi:10.1177/20417314221074018.

[260] **Ventre M, Padovani M, Covington AD, Netti PA**. Composition, structure and physical properties of foetal calf skin. *IULTCS II, Eurocongress Istanbul*, 2006.

[261] **Veres SP, Harrison JM, Lee JM**. Repeated subrupture overload causes progression of nanoscaled discrete plasticity damage in tendon collagen fibrils. *J. Orthop. Res.*, 31:731–737, 2012. doi:10.1002/jor.22292.

[262] **Veres SP, Harrison JM, Lee JM**. Cross-link stabilization does not affect the response of collagen molecules, fibrils, or tendons to tensile overload. *J. Orthop. Res.*, 12:1907–1913, 2013. doi:10.1002/jor.22460.

[263] **Veres SP, Harrison JM, Lee JM**. Mechanically overloading collagen fibrils uncoils collagen molecules, placing them in a stable, denatured state. *Matrix Biol.*, 33:54–59, 2014. doi:10.1016/j.matbio.2013.07.003.

[264] **Viidik A**. The effect of training on the tensile strength of isolated rabbit tendons. *Scand. J. Plast. Reconstr. Surg. Hand Surg.*, 1:141–147, 1967. doi:10.3109/02844316709022844.

[265] **Vitagliano L, Némethy G, Zagari A, Scheraga HA**. Structure of the type i collagen molecule based on conformational energy computations: the triple-stranded helix and the n-terminal telopeptide. *J Mol Biol.*, 247(1):69–80, 1995. doi:10.1006/jmbi.1994.0123.

[266] **Wahlsten A, Rutsche D, Nanni M, Giampierto C, Biedermann T, Reichmann E, Mazza E**. Mechanical stimulation induces rapid fibroblast proliferation and accelerates the

early maturation of human skin substitutes. *Biomater.*, 273:120779, 2021. doi:10.1016/j.biomaterials.2021.120779.

[267] **Walden G, Liao X, Donell S, Raxworthy MJ, Riley GP, Saeed A**. A clinical, biological, and biomaterials perspective into tendon injuries and regeneration. *Tissue Eng. Part B Rev.*, 23:44–58, 2017. doi:10.1089/ten.TEB.2016.0181.

[268] **Wang C, Brisson BK, Terajima M, Li Q, Hoxha K, Han B, Goldberg AM, Sherry Liu X, Marcolongo MS, Enomoto-Iwamoto M, Yamauchi M, Volk SW, Han L**. Type iii collagen is a key regulator of the collagen fibrillar structure and biomechanics of articular cartilage and meniscus. *Matrix Biol.*, 85-86:47–67, 2020. doi:10.1016/j.matbio.2019.10.001.

[269] **Wang GH, Liang CC, Li BZ, Zhang WZ, Cheng G, Zan LS**. Screening and validation of reference genes for qrt pcr of bovine skeletal muscle derived satellite cells. *Sci. Rep.*, 12:5653, 2022. doi:10.1038/s41598-022-09476-3.

[270] **Wang JH, Thampatty BP, Lin JS, Im HJ**. Mechanoregulation of gene expression in fibroblasts. *Gene*, 391(1-2):503–507, 2007. doi:10.1016/j.gene.2007.01.014.

[271] **Watson SS, Riordan TJ, Pryce A, Schweitzer R**. Tendons and muscles of the mouse forelimb during embryonic development. *Dev. Dyn.*, 283(3):693–700, 2009. doi:10.1002/dvdy.21866.

[272] **Weinreb JH, Sheth C, Apostolakos J, McCarthy MB, Barden B, Cote MP, Mazzocca AD**. Tendon structure, disease, and imaging. *Muscles Ligaments Tendon J.*, 4(1):66–73, 2020. doi:10.1016/j.matbio.2019.10.001.

[273] **Weiss M, Unterhauser FN, Weiler A**. Crimp frequency is strongly correlated to myofibroblast density in the human anterior cruciate ligament and its autologous tendon grafts. *Knee Surg. Sports Traumatol. Arthrosc.*, 20:889–895, 2012. doi:10.1007/s00167-011-1644-4.

[274] **Wells SM**. Structural-mechanical relations in the developing ovine thoracic aorta. *Doctorate Thesis: University of Toronto*, 1999.

[275] **Wells SM, Adamson SL, Langille BL, Lee MJ**. Thermomechanical analysis of collagen crosslinking in the developing ovine thoracic aorta. *Biorheology*, 35(6):399–414, 1998. doi:10.1016/S0006-355X(99)80019-5.

[276] **Willet TL, Dapaah DY, Uppuganti S, Granke M, Nyman JS**. Bone collagen network integrity and transverse fracture toughness of human cortical bone. *Bone*, 120:187–193, 2019. doi:10.1016/j.bone.2018.10.024.

[277] **Williams S**. Pathology of equine extensor tendons: Can they function without them? *Equine Vet. Educ.*, 31(6):315–317, 2019. doi:10.1111/eve.12997.

[278] **Winey M, Meehl JB, O'Toole ET, Giddings Jr. TH**. Conventional transmission electron microscopy. *Mol. Biol. Cell*, 25(3):319–323, 2014. doi:10.1091/mbc.E12-12-0863.

[279] **Winey M, Meehl JB, O'Toole E, Giddings TH**. Conventional transmission electron microscopy. *Mol. Biol. Cell*, 25(3):319–426, 2017. doi:10.1091/mbc.e12-12-0863.

[280] **Winters LM, Green WW, Comstock RE**. Prenatal development of the bovine. *University of Minnestota, Agricultural Experiment Station.*, 345, 2012.

[281] **Workers' Compensation Board Statistical Report**: Workers' Compensation Board of Nova Scotia. URL: https://www.wcb.ns.ca/Portals/wcb/Annual%20Reports/WCB%20Statistical%20Report%202021-Oct%205.pdf?ver=2021-10-05-090411-260, last accessed on 2022-07-03, 2021.

[282] **Wu F, Nerlich M, Docheva D**. Tendon injuries: Basic science and new repair proposals. *EFORT Open Reviews*, 2(7):332–342, 2017. doi:10.1302/2058-5241.2.160075.

[283] **Wunderli SL, Blanche U, Snedeker JG**. Tendon explant models for physiologically relevant study of tissue biology: a perspective. *Connect. Tis. Res.*, 61(3-4):262–277, 2019. doi:10.1080/03008207.2019.1700962.

[284] **Xu PX, Cheng J, Epstein JA, Maas RL**. Eya genes are expressed during limb tendon development and encode a transcriptional activation function. *Proc. Natl. Acad. Sci.*, 94:11974–11979, 1997. doi:10.1073/pnas.94.22.11974.

[285] **Yamauchi M, London RE, Guenat C, Hashimoto F, Mechanic GL**. Structure and formation of a stable histidine-based trifunctional cross-link in skin. *J. Biol. Chem.*, 262:11428–11434, 1987. doi:10.1016/S0021-9258(18)60824-5.

[286] **Yamauchi M, Taga Y, Hattori S, Shiiba M, Terajima M**. Analysis of collagen and elastin cross-links. *Methods Cell Biol.*, 143:115–132, 2018. doi:10.1016/bs.mcb.2017.08.006.

[287] **Yan Z, Yin H, Nerlich M, Pfeifer CG, Docheva D**. Boosting tendon repair: interplay of cells, growth factors and scaffold-free and gel-based carriers. *J. Exp. Orthop.*, 5(1), 2018. doi:10.1186/s40634-017-0117-1.

[288] **Yoon JH & Halper J**. Tendon proteoglycans: biochemistry and function. *J. Musculoskelet. Neuronal Interact.*, 5(1):22–34, 2005.

[289] **Young RD, Lawrence PA, Duance VC, Aigner T, Monaghan P**. Immunolocalization of collagen types ii and iii in single fibrils of human articular cartilage. *J. Histochem. Cytochem.*, 48(3):423–432, 2000. doi:10.1177/002215540004800312.

[290] **Zamboulis DE, Thorpe CT, Kharaz YA, Birch HL, Screen HRC, Clegg PD**. Postnatal mechanical loading drives adaptation primarily through modulation of the non-collagenous matrix. *eLife*, 9:e58075, 2020. doi:10.7554/eLife.58075.

[291] **Zelzer E, Blitz E, Killian ML, Thomopoulos S**. Tendon to bone attachment: from development to maturity. *Birth Defects Res. C Embryo Today*, 102(1):101–112, 2014. doi:10.1002/bdrc.21056.

[292] **Zhang G, Ezura Y, Chervoneva I, Robinson PS, Beason DP, Carine ET, Soslowsky LJ, Iozzo RV, Birk DE**. Decorin regulates assembly of collagen fibrils and acquisition of biomechanical properties during tendon development. *J. Cell. Biochem.*, 98(6):1436–1449, 2006. doi:10.1002/jcb.20776.

[293] **Zhang G, Young BB, Ezura Y, Favata M, Soslowsky LJ, Chakravarti S, Birk DE**. Development of tendon structure and function: regulation of collagen fibrillogenesis. *J. Musculoskelet. Neuronal Interact.*, 5(1):5–21, 2005.

[294] **Zhang J, Wang JH**. The effects of mechanical loading on tendons – an in vivo and in vitro model study. *PLoS One*, 8(8):e71740, 2013. doi:10.1371/journal.pone.0071740.

[295] **Zhang S, Ju W, Chen X, Zhao Y, Feng Y, Yin Z, Chen X**. Hierarchical ultrastructure:

an overview of what is known about tendons and future perspective for tendon engineering. *Bioact. Mater.*, 8:124–139, 2022. doi:10.1016/j.bioactmat.2021.06.007.

[296] **Zioupos P, Currey JD, Hamer AJ**. The role of collagen in the declining mechanical properties of aging human cortical bone. *J. Biomed. Mater. Res.*, 45(2):108–116, 1999. doi:10.1002/(SICI)1097-4636(199905)45:2<108::AID-JBM5>3.0.CO;2-A.